



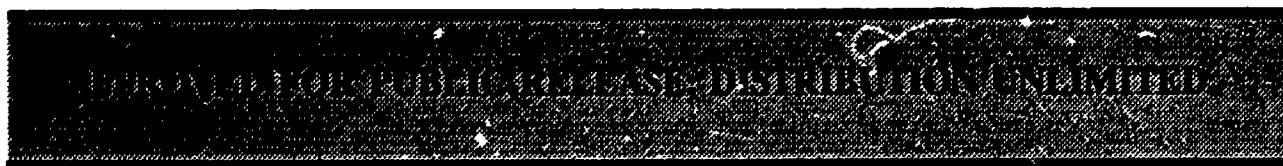
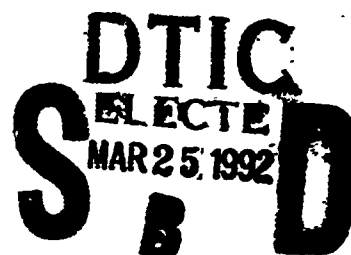
ENGINEERING CONSIDERATIONS FOR THE SELF-ENERGIZING MAGNETOPLASMADYNAMIC (MPD) - TYPE FUSION PLASMA THRUSTER

Professor Chan K. Choi

School of Nuclear Engineering
Purdue University
West Lafayette IN 47907

February 1992

Final Report



92-07616



PHILLIPS LABORATORY
Propulsion Directorate
AIR FORCE SYSTEMS COMMAND
EDWARDS AIR FORCE BASE CA 93523-5000

92 3 25 060

**Best
Available
Copy**


NOTICE

When U.S. Government drawings, specifications, or other data are used for any purpose other than a definitely related Government procurement operation, the fact that the Government may have formulated, furnished, or in any way supplied the said drawings, specifications, or other data, is not to be regarded by implication or otherwise, or in any way licensing the holder or any other person or corporation, or conveying any rights or permission to manufacture, use or sell any patented invention that may be related thereto.

FOREWORD

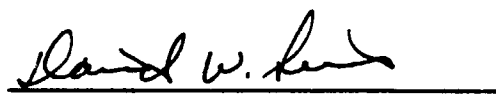
This annual report was prepared The School of Nuclear Engineering, Purdue University, West Lafayette, IN under contract F4611-90-K-0054 for Operating Location AC, Phillips Laboratory (AFSC), Edwards AFB CA 93523-5000. OLAC PL Project Manager was Frank Mead.

This report has been reviewed and is approved for release and distribution in accordance with the distribution statement on the cover and on the SF Form 298.


FRANKLIN B. MEAD, JR.
Project Manager


STEPHEN L. RODGERS
Chief, Emerging Technologies Branch

FOR THE COMMANDER

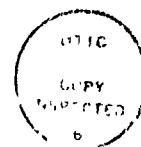

DAVID W. LEWIS, Major, USAF
Acting Director,
Fundamental Technologies Division


RANNEY G. ADAMS
Public Affairs Director

REPORT DOCUMENTATION PAGE			Form Approved OMB No. 0704-0128	
<small>Public reporting burden for this collection of information is estimated to average 1 hour per response, including the time for reviewing instructions, searching existing data sources, gathering and maintaining the data needed, and completing and reviewing the collection of information. Send comments regarding this burden estimate or any other aspect of this collection of information, including suggestions for reducing the burden, to Washington Headquarters Service, Directorate for Information Operations and Reports, 1215 Jefferson Davis Highway, Suite 1204, Arlington, VA 22202-4302, and to the Office of Management and Budget, Paperwork Reduction Project (0704-0128), Washington, DC 20503.</small>				
1. AGENCY USE ONLY (Leave blank)		2. REPORT DATE February 1992		3. REPORT TYPE AND DATES COVERED Annual Progress Report 900608-910712
4. TITLE AND SUBTITLE Engineering Considerations for the Self-Energizing Magnetoplasmadynamic (MPD) - Type Fusion Plasma Thruster			5. FUNDING NUMBERS PE: 62302F PR: 3058 TA: 00AF C: F04611-90-K-0054 WU: 345249	
6. AUTHOR(S) Chan K. Choi, Professor				
7. PERFORMING ORGANIZATION NAME(S) AND ADDRESS(ES) School of Nuclear Engineering Purdue University West Lafayette, IN 47907			8. PERFORMING ORGANIZATION REPORT NUMBER PL/PU-91007	
9. SPONSORING/MONITORING AGENCY NAME(S) AND ADDRESS(ES) Phillips Laboratory Propulsion Directorate Edwards AFB CA 93523-5000			10. SPONSORING/MONITORING AGENCY REPORT NUMBER PL-TR-91-3087	
11. SUPPLEMENTARY NOTES COSATI CODES: 21/06; 22/05.				
12a. DISTRIBUTION/AVAILABILITY STATEMENT Approved for Public Release; Distribution is Unlimited.			12b. DISTRIBUTION CODE	
13. ABSTRACT (Maximum 200 words) Feasibility studies of dense plasma focus (DPF) device as a fusion propulsion thruster have been performed. Both conventional and spin-polarized D- ³ He fuels were used. Three modes of operation were identified and each was investigated for its usefulness in space travel with special attention paid to a manned Mars mission. Using fusion products to directly produce thrust resulted in specific impulse, I _{sp} (i.e., the ratio of the rocket thrust to the propellant weight flow rate), around 10 ⁶ sec, but produced system thrust-to-weight ratios (F/W) less than 10 ⁻⁵ . This F/W is many orders of magnitude less than a typical value of 0.2 for a manned Mars mission which is presently possible with chemical and nuclear thermal rockets. Using large quantities of propellant to burn "impulsively" gave I _{sp} 's of 4,000 sec with F/W equal to 0.05 for one thruster and 0.132 if five thrusters are used. The spin-polarized D- ³ He studies provided increased values of F/W and I _{sp} over conventional D- ³ He fuel which was due to the increased fusion power and decreased radiation losses for the spin-polarized case. Thus, the DPF provides attractive plasma conditions as a space propulsion thruster, though uncertainties remain in the validity of scaling laws on capacitor mass at high current beyond 1 MA.				
14. SUBJECT TERMS Fusion Propulsion, Dense Plasma Focus, Magnetoplasmadynamic Thruster, Advanced Fuel, D- ³ He Fusion, Spin-Polarized Fusion			15. NUMBER OF PAGES 108	
			16. PRICE CODE	
17. SECURITY CLASSIFICATION OF REPORT UNCLASSIFIED	18. SECURITY CLASSIFICATION OF THIS PAGE UNCLASSIFIED	19. SECURITY CLASSIFICATION OF ABSTRACT UNCLASSIFIED	20. LIMITATION OF ABSTRACT SAR	

TABLE OF CONTENTS

Section	Page
I. INTRODUCTION	1
II. FEASIBILITY STUDIES OF DENSE PLASMA FOCUS AS A PROPUSION THRUSTER	13
II. 1. PARAMETRIC STUDIES OF DENSE PLASMA FOCUS WITH D- ³ He FUEL	13
II. 1.1 DPF COMBUSTOR MODEL	13
II. 1.2 DPF PROPULSION MODEL	18
II. 2 PARAMETRIC STUDIES OF DPF WITH SPIN-POLARIZED D- ³ He FUEL	43
III. CONCLUSIONS AND RECOMMENDATIONS	64
REFERENCES	66
APPENDIX A	75
APPENDIX B	87



Accession For	
NTIS GRA&I	<input checked="" type="checkbox"/>
DTIC TAB	<input type="checkbox"/>
Unannounced	<input type="checkbox"/>
Justification	
By _____	
Distribution/	
Availability Codes	
Dist	Avail and/or Special
A-1	

LIST OF TABLES

Section	Page
Table 1. Ranges of Typical Performance Parameters for Several Different Rocket Engine Types	2
Table 2. Yield From Various Energy Sources	3
Table 3. Livermore-I Dense Plasma Focus Parameters	16
Table 4. Assumed Parameters of DPF Propulsion System	46
Table 5.1. Propulsion Parameters for Base Case and Spin-Polarized Case	60
Table 5.2. Propulsion Parameters for Base Case and Spin-Polarized Case	61

LIST OF FIGURES

Section	Page
Figure 1. Propulsion System Specific Mass (kg/kWj)	4
Figure 2. The MPD Thruster Diagram	6
Figure 3. Coaxial Electrode Configuration	8
Figure 4. Phase of the DPF Cycle	9
Figure 5. Neutron Yield as Functions of Pinch Current and Stored Energy	11
Figure 6. Reaction Rate Parameters for Various Fuels	17
Figure 7. Plasma Focus Fusion Propulsion System	19
Figure 8. Axial Variation of Fluid Variables for a quasi-1D Meridional Magnetic Nozzle	23
Figure 9. Plasma Pinch Temperature vs. Current	26
Figure 10. Propellant Temperature vs. Current	27
Figure 11. Specific Impulse vs. Current	28
Figure 12. Thrust-to-Weight Ratio vs. Current	29
Figure 13. Thrust-to-Weight Ratio vs. Current	31
Figure 14. Thrust-to-Weight Ratio vs. Firing Time	32
Figure 15. Δv Capability vs. Payload Mass Fraction	34
Figure 16. Vehicle F/W vs. Propellant Mass Flow Rate for $\Delta v=5$ km/s	35
Figure 17. Vehicle F/W vs. Propellant Mass Flow Rate for $\Delta v=10$ km/s	36
Figure 18. Vehicle F/W vs. Propellant Mass Flow Rate for $\Delta v=20$ km/s	37
Figure 19. Vehicle F/W vs. Propellant Mass Flow Rate for $\Delta v=30$ km/s	38
Figure 20. Vehicle F/W vs. Propellant Mass Flow Rate for $\Delta v=40$ km/s	39

Figure 21. Specific Impulse vs. Propellant Mass Flow Rate (for any Δv)	40
Figure 22. F/W Ratio vs. Propellant Mass Flow Rate and Number of Thrusters for $\Delta v = 10\text{km/s}$	41
Figure 23. F/W Ratio vs. Propellant Mass Flow Rate and Number of Thrusters for $\Delta v = 40\text{km/s}$	42
Figure 24. Vehicle F/W vs. Propellant Mass Flow Rate for $I = 20 \text{ MA}$ and $\Delta v = 10\text{km/s}$	44
Figure 25. Vehicle F/W vs. Propellant Mass Flow Rate for $I = 20 \text{ MA}$ and $\Delta v = 40\text{km/s}$	45
Figure 26. Specific Impulse vs. Propellant Mass Flow Rate	48
Figure 27. Vehicle F/W vs. Propellant Mass Flow Rate for $\Delta v = 10\text{km/s}$ (I^2 Scaling)	49
Figure 28. Vehicle F/W vs. Specific Impulse for $\Delta v = \text{km/s}$ (I^2 Scaling)	50
Figure 29. Vehicle F/W vs. Propellant Mass Flow Rate for $\Delta v = 40\text{km/s}$ (I^2 Scaling)	51
Figure 30. Vehicle F/W vs. Specific Impulse for $\Delta v = 40\text{km/s}$ (I^2 Scaling)	52
Figure 31. Vehicle F/W vs. Propellant Mass Flow Rate for $\Delta v = 10\text{km/s}$ ($I^{8/3}$ Scaling)	54
Figure 32. Vehicle F/W vs. Specific Impulse for Δv (I^2 Scaling)	55
Figure 33. Vehicle F/W vs. Propellant Mass Flow Rate for $\Delta v = 10\text{km/s}$ ($I^{8/3}$ Scaling)	56
Figure 34. Vehicle F/W vs. Specific Impulse for $\Delta v = 10\text{km/s}$ ($I^{8/3}$ Scaling)	57
Figure 35. Vehicle F/W vs. Propellant Mass Flow for $\Delta v = 40\text{km/s}$ ($I^{8/3}$ Scaling)	58
Figure 36. Vehicle F/W vs. Specific Impulse for $\Delta v = 40\text{km/s}$ ($I^{8/3}$ Scaling)	59
Figure 37. Vehicle F/W vs. Propellant Mass Flow Rate for $\Delta v = 5\text{km/s}$ ($I^{8/3}$ Scaling)	77
Figure 38. Vehicle F/W vs. Propellant Mass Flow Rate for $\Delta v = 10\text{km/s}$ ($I^{8/3}$ Scaling)	78
Figure 39. Vehicle F/W vs. Propellant Mass Flow Rate for $\Delta v = 20\text{km/s}$ ($I^{8/3}$ Scaling)	79
Figure 40. Vehicle F/W vs. Propellant Mass Flow Rate for $\Delta v = 30\text{km/s}$ ($I^{8/3}$ Scaling)	80
Figure 41. Vehicle F/W vs. Propellant Mass Flow Rate for $\Delta v = 40\text{km/s}$ ($I^{8/3}$ Scaling)	81
Figure 42. F/W Ratio vs. Propellant Mass Flow Rate and Number of Thrusters for $\Delta v = 10\text{km/s}$ ($I^{8/3}$ Scaling)	82

Figure 43. F/W Ratio vs. Propellant Mass Flow Rate and Number of Thrusters for $\Delta v = 40\text{km/s}$ ($I^{8/3}$ Scaling)	83
Figure 44. F/W Ratio vs. Propellant Mass Flow Rate for $I = 20\text{ MA}$ and $\Delta v = 10\text{km/s}$ ($I^{8/3}$ Scaling)	84
Figure 45. F/W Ratio vs. Propellant Mass Flow Rate for $I = 20\text{ MA}$ and $\Delta v = 40\text{km/s}$ ($I^{8/3}$ Scaling)	85

ENGINEERING CONSIDERATIONS ON THE SELF-ENERGIZING MAGNETOPLASMA DYNAMIC (MPD)-TYPE FUSION PLASMA THRUSTER

I. INTRODUCTION

During this initial period of the three-year project, various fusion propulsion concepts, and in particular a plasma focus device and its analysis, have been studied. Based on the identified key operating parameters (e. g., capacitor voltage, capacitance, inductance, electrode dimensions, plasma pinch current and temperature, etc.) of existing plasma focus devices, feasibility studies of the dense plasma focus (DPF) device as a fusion propulsion thruster have been performed. The initial findings indicate that the dense plasma focus device provides attractive plasma conditions leading to the ignition for DPF as a space propulsion thruster, though uncertainties remain in the validity of scaling laws on capacitor mass at high current beyond 1 MA. Both conventional and spin-polarized D-³He fuels were studied for parametric analysis of DPF as a propulsion system. The major portion of this report consists of the parametric study.

Ever since Robert Goddard, Theodor von Karman, and Werner von Braun proposed concepts of rocketry, various rocket engines have been promoted as the main vehicle for space exploration. On July 20, 1989, President Bush announced the new Space Exploration Initiative to return to the Moon and then to put a manned presence on Mars. The goal of this current project is consistent with the Earth-Mars mission, with the emphasis placed on a fusion-powered propulsion device.

Conventional propulsion devices based on chemical energy have been used successfully for early space explorations with firing duration ranging from seconds to a few hours. Chemical propulsion has been used for the Saturn 5 (the same rocket that was used successfully for the Moon Mission in 1969), the space shuttle, interplanetary probes, and the missile defense system. The best current chemical engines can provide specific impulse values, I_{sp} , (i.e., the ratio of the rocket thrust to the propellant weight flow rate) approaching 500 seconds [1].

The Nuclear fission engines utilize both solid- and fluid-core (liquid, gas, and plasma) reactors. Graphite solid-core reactors operating at 2000 to 2700°K have been well demonstrated, though the fluid-core reactors are still being investigated very actively. Typical specific impulse for the nuclear fission engine ranges from 600 to 1100 sec [1-2]. Other rocket engine concepts (e.g., ion, solar thermal, etc.) have also been considered. Performance of 220-W

and 10-kW class xenon ion thrusters have been investigated recently in Europe and at NASA laboratories, respectively [3]. Rare gas propellants (xenon or argon) rather than mercury are being used in ion thrusters to avoid any spacecraft surface erosion problems. Solar powered electric propulsion and solar-pumped lasers for space applications are also being pursued [4]. Typical performance parameters for different rocket engine types are summarized in Table 1.

Table 1. Ranges of Typical Performance Parameters for Several Different Rocket Engine Types (Refs. 1-3)						
Engine Type	Specific Impulse (sec)	Maximum Temperature (°K)	Thrust-to- Weight ratio	Duration	Specific Power (hp/lb)	Typical Working Fluid
Chemical (liquid)	300 to 460	4,500 to 7,800	10^{-2} to 100	Seconds to a few hours	0.1 to 1,000	H ₂ to O ₂
Chemical (solid)	200 to 310	4,500 to 7,500	10^{-2} to 100	Seconds to minutes	0.1 to 1,000	fuel and oxidizer
Chemical (hybrid)	200 to 400	4,000 to 7,500	10^{-2} to 100	Seconds to minutes	0.1 to 1,000	fuel and oxidizer
Nuclear fission	600 to 1,100	5,000	10^{-2} to 30	Seconds to a few hours	0.1 to 1,000	H ₂
Radioactive Isotope Decay	400 to 700	2,200 to 3,000	10^{-5} to 10^{-3}	Days	0.001 to 0.01	H ₂
Arc Heating	400 to 2,000	10,000	10^{-4} to 10^{-2}	Days	0.001 to 1	H ₂
Ion	5,000 to 25,000	10^{-5} to 10^{-3}	Months	0.001 to 1	mercury, xenon, argon
Solar thermal	400 to 700	2,500	10^{-3} to 10^{-2}	Days	0.001 to 1	H ₂

The chemical rockets, and to some extent also the nuclear fission rockets, have relatively low values of specific impulse, relatively low engine weight, a very high thrust capability, and, therefore, high acceleration and high specific powers [2]. At the other extreme, the ion and plasma propulsion devices can have a very high specific impulse, but they must carry a heavy electrical energy source to deliver the power necessary for high ejection velocities, which results in a low thrust value [3]. Thus, the specific impulse of the advanced electrical rocket engines can be appreciably higher than those of chemical or some nuclear fission rocket engines. This means that electrical rocket engines need to carry relatively little propellant because the propellant mass is ejected at a very high velocity. The low thrust values of the electrical rocket engines imply that they are not useful in the fields of strong gravitational gradients (such as for take-offs or landings on earth) [5].

The new U.S. space mission to explore Mars initiating from the Earth orbit would require a 1400-sec I_{sp} engine and a longer duration of flight [6]. Naturally, new concepts beyond the

chemical and other conventional propulsion scenarios discussed above would be required to satisfy the higher I_{sp} and the sufficient flight duration.

Advanced concepts for non-conventional propulsion developments which include fusion energy, anti-matter energy, etc. have been proposed [7]. One of the most promising propulsion systems, which minimizes the size of the device and the total mass, is considered to be a fusion rocket. The attractive features of a fusion rocket are its capabilities to convert the kinetic energies of energetic charged particles directly to the thrust power for propulsion. As illustrated in Table 2 and Fig. 1, the yield per unit mass from chemical and nuclear fission are orders of magnitude smaller than those of nuclear fusion. Typical specific impulse for fusion rockets could range up to 10,000 sec while maintaining relatively high thrust levels.

Table 2. Yield From Various Energy Sources

<u>ENERGY SOURCES</u>	<u>REACTION PRODUCTS</u>	<u>ENERGY RELEASE(J/kg)</u>
<u>CHEMICAL</u>		
Conventional (LO_2/LH_2)	Water, Hydrogen	1.5×10^7
Recombination ($\text{H} + \text{H} = \text{H}_2$)	Hydrogen	2.18×10^8
<u>NUCLEAR FISSION</u>		
$\text{U}^{233}, \text{U}^{235}, \text{Pu}^{239}$ ($\sim 200\text{MeV} / \text{U}^{235}$ fission)	Radioactive Fission Fragments Neutrons, Gammas	8.2×10^{13}
<u>NUCLEAR FUSION</u>		
DT (0.4/0.6)	Helium, Neutrons	3.38×10^{14}
Cat DD (1.0)	Hydrogen, Helium & Neutrons	3.45×10^{14}
DHe ³ (0.4/0.6)	Hydrogen, Helium (Very Few Neutrons)	3.52×10^{14}

Recently, the Phillips Laboratory completed a fusion propulsion study [8] in which a 50-m long translating compact torus (TCT) (e.g., moving spheromak reactor), operating with $\text{D}-^3\text{He}$ fusion fuel, was shown to be a prime fusion rocket candidate. The large size of the TCT device, delivering a total payload mass of 36,000 kg for the round trip between a low Earth orbit (LEO) and the Geosynchronous Earth orbit (GEO), implied that the thrust-to-weight ratio (i.e., condition for proper acceleration) would be rather low. The ignition condition for $\text{D}-^3\text{He}$ fuel

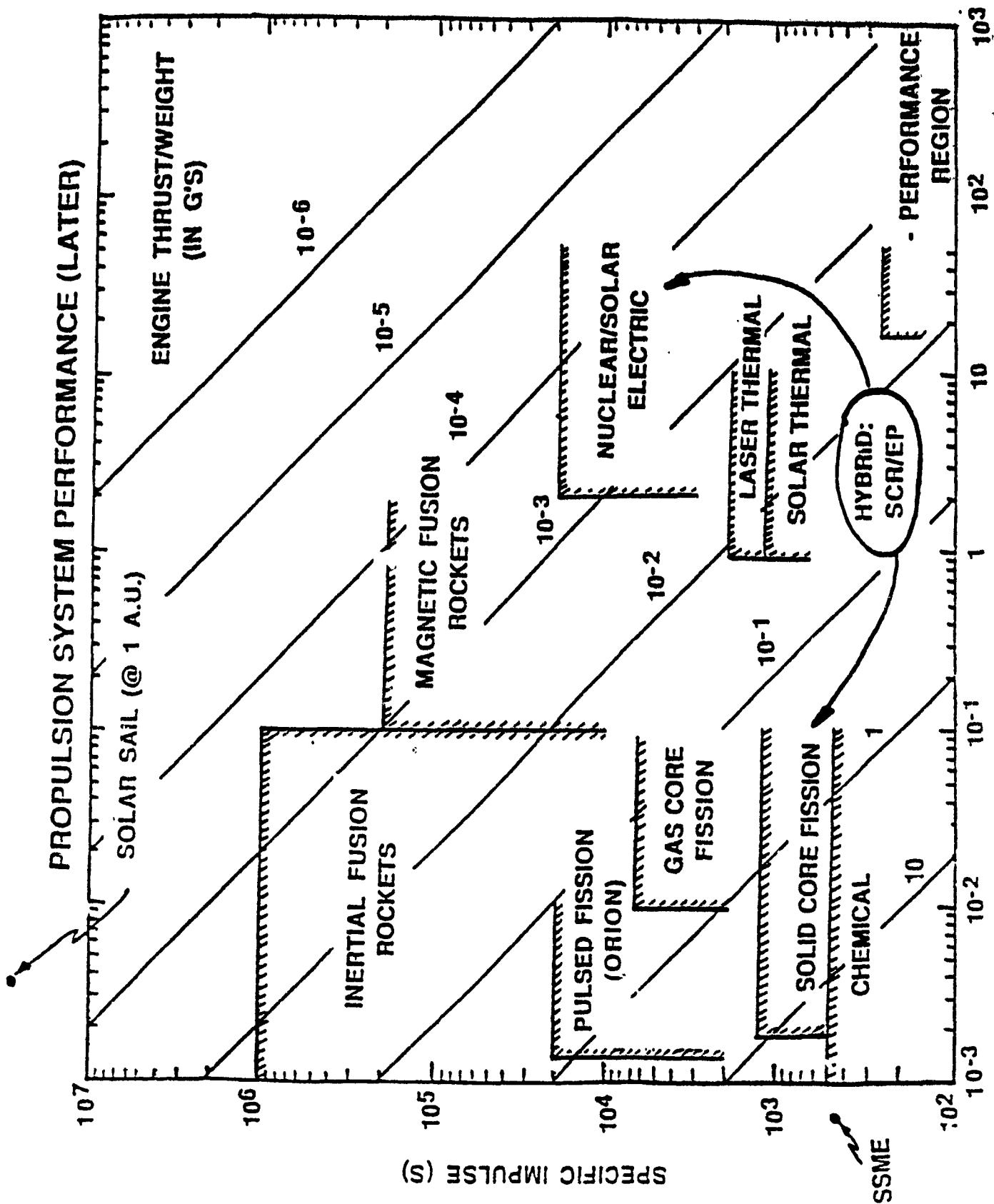


Figure 1. Propulsion System Specific Mass (kg/kWj) [29]

was later found to be marginal which makes the TCT device somewhat doubtful as an effective fusion propulsion device. NASA has also recently recommended that a D-³He fueled field-reversed configuration (FRC), another compact torus device, be their choice for fusion space propulsion since the FRC could provide both desired characteristics of high beta (90 %) (i.e., the ratio of plasma pressure to magnetic field pressure) and good conversion of energy to thrust [9]. However, the DOE's FRC experiment is no longer supported and further development of this concept would be somewhat hampered if NASA decides to pursue it.

One of the most interesting and practical plasma thruster concepts is the magneto-plasma-dynamic (MPD) arc in which plasma is being driven by magnetic fields generated by the currents in the arc [5]. The thruster geometry is coaxial, with a cylindrical cathode at the center and an annular anode around it. The two electrodes are separated at the back of the device by an insulating plate as illustrated in Fig. 2. The current from the ring anode to the cathode produces an azimuthal magnetic field which exerts a pressure against the arc plasma. Propellant from gas inlet flows through the arc where it is ionized and forced away by the magnetic field via a $\vec{J} \times \vec{B}$ interaction. The simpler illustration of the basic principle of the MPD effect is illustrated at the lower portion of Fig. 2. Efficiencies as high as 50% [10] and higher specific impulse values up to 10,000 sec were obtained at low values of propellant flow. Current MPD tests at the Phillips Laboratory operate in a 2 msec-pulse mode with the capacitor bank charged to 800 volts and delivering 40,000 amps. Instruments are used to measure the current and voltage seen by the MPD thruster during each firing. Typical range of plasma temperature in MPD is a few eV. However, in order to create fusion conditions with D-³He fuels in an MPD-type coaxial device, much higher current and plasma temperature (in keV range) are needed which necessitate a dense plasma focus device.

The dense plasma focus (DPF), one of the complementary fusion devices between low-beta tokamak and high compression inertial fusion, is a system of coaxial electrodes which allows the formation and subsequent propagation of a thin plasma sheath in the annular region between the center anode and the outer cathode. When the sheath reaches the end of the anode, magneto-hydrodynamic (MHD) instabilities develop and the sheath disconnects from the cathode and collapses toward the axis forming a very small region of high density, hot plasma like in a linear pinch device [11]. It is here where fusion reactions take place and generate the energy to be used for propulsion.

The DPF is similar in geometry to the magnetoplasma-dynamic (MPD) thruster [5] currently used in electric propulsion but differs greatly in its operation. There are two common plasma focus types: The Mather type, like a coaxial plasma gun, has the current-carrying plasma sheath

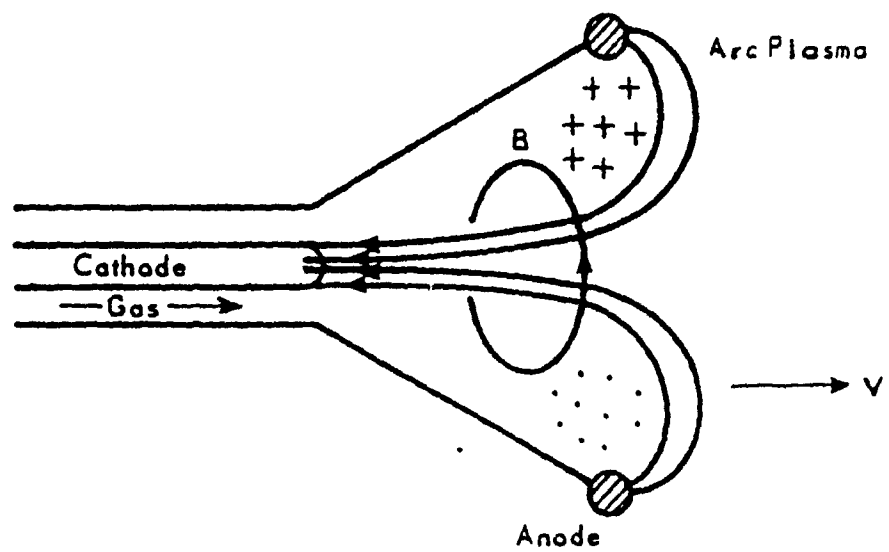
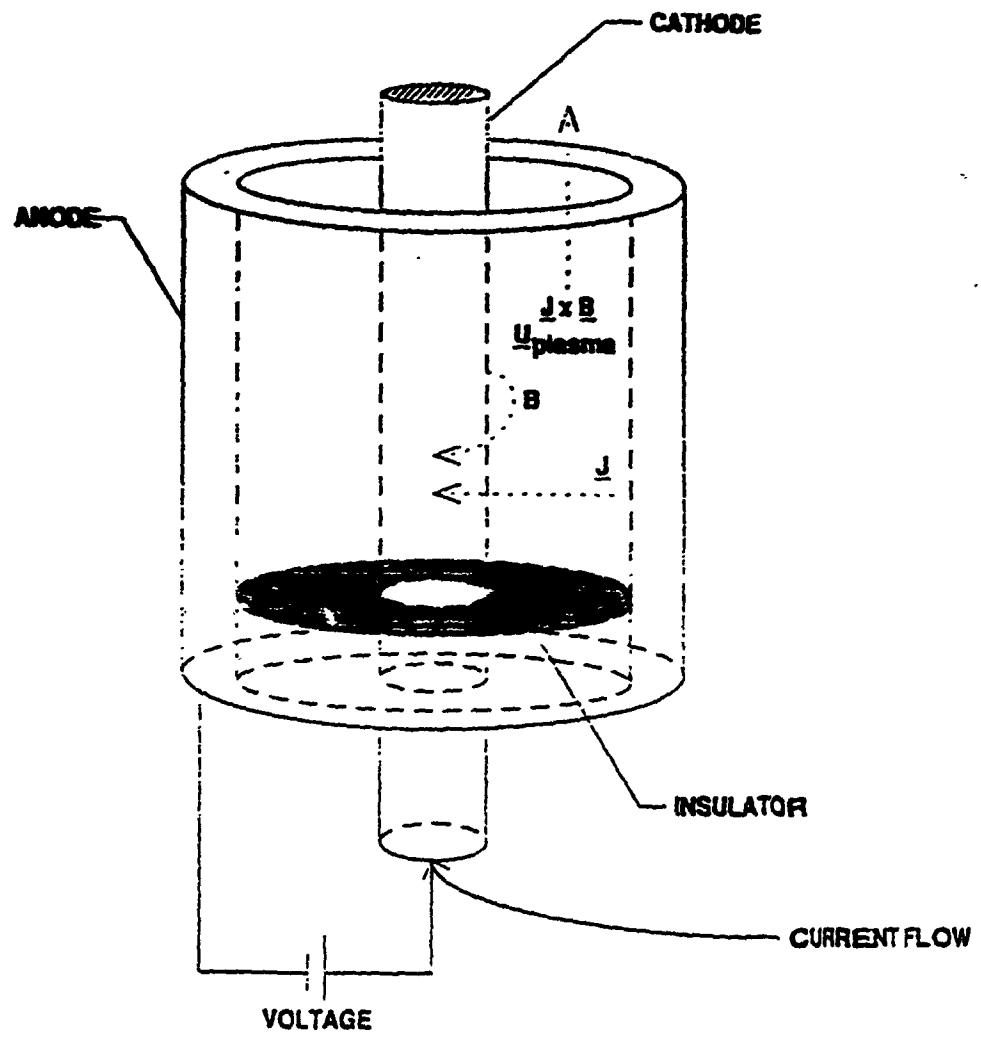


Figure 2. The MPD Thruster Diagram

accelerated axially [12], and the Filippov type with the plasma sheath accelerated radially inward [13]. The DPF typically will use currents which are about 1,000 times greater, and unlike the MPD does not currently operate in the steady-state mode. The MPD forms a stable sheath near the end of the electrode system and makes no use of a rundown phase which occurs in the DPF. However, the key distinction between the two devices is that the MPD makes no attempt to use the tremendous amounts of energy available from fusion. It is here that the DPF gains an advantage over most propulsion concepts. For example, the fusion of deuterium (D) and helium-3 (^3He) can release almost five times more energy per unit mass than the fissioning of a uranium-235 nucleus.

In the DPF, the plasma sheath is initially created when a large current is discharged through the center anode. The resulting potential difference causes the current to arc between the electrodes. In the process, the fill gas (fusion fuel) is ionized and forms an azimuthally symmetric plasma sheath in the annular region between the electrodes. The current flowing through the anode also produces an azimuthal magnetic field, B_θ , which interacts with the plasma sheath current. This results in the propagation of the sheath down the length of the anode due to the $J_r \times B_\theta$ force. Figure 3 shows the cylindrical thruster configuration as well as the directions of the current, magnetic field, and sheath propagation. During "rundown," some fraction of the fill gases is entrained in the sheath and carried down to the end of the anode. As the sheath reaches the end of the anode, it does collapse or "focus" radially inward toward the central axis of the device, forming a high density ($= 10^{26} \text{ m}^{-3}$), hot plasma where fusion reactions may take place. This number density may change depending on the fraction of initial fuel which is trapped in the pinch region.

The pinched plasma expands and contracts several times before it eventually becomes completely disrupted by plasma instabilities. It is particularly susceptible to the $m = 0$ "sausage" and $m = 1$ "kink" instabilities. Figure 4 gives a graphic representation of the different phases which occur during one cycle of the DPF. The pinch lifetime is typically very short, on the order of a microsecond [14]. However, if the pinch lifetime can be made sufficiently long to allow a good fusion burn inside the pinch, the DPF could provide enough energy to propel spacecraft at either high thrust, high specific impulse, or both. While the rundown can be predicted with reasonable accuracy, the collapse and subsequent plasma behavior are not well understood and are in great need of further study.

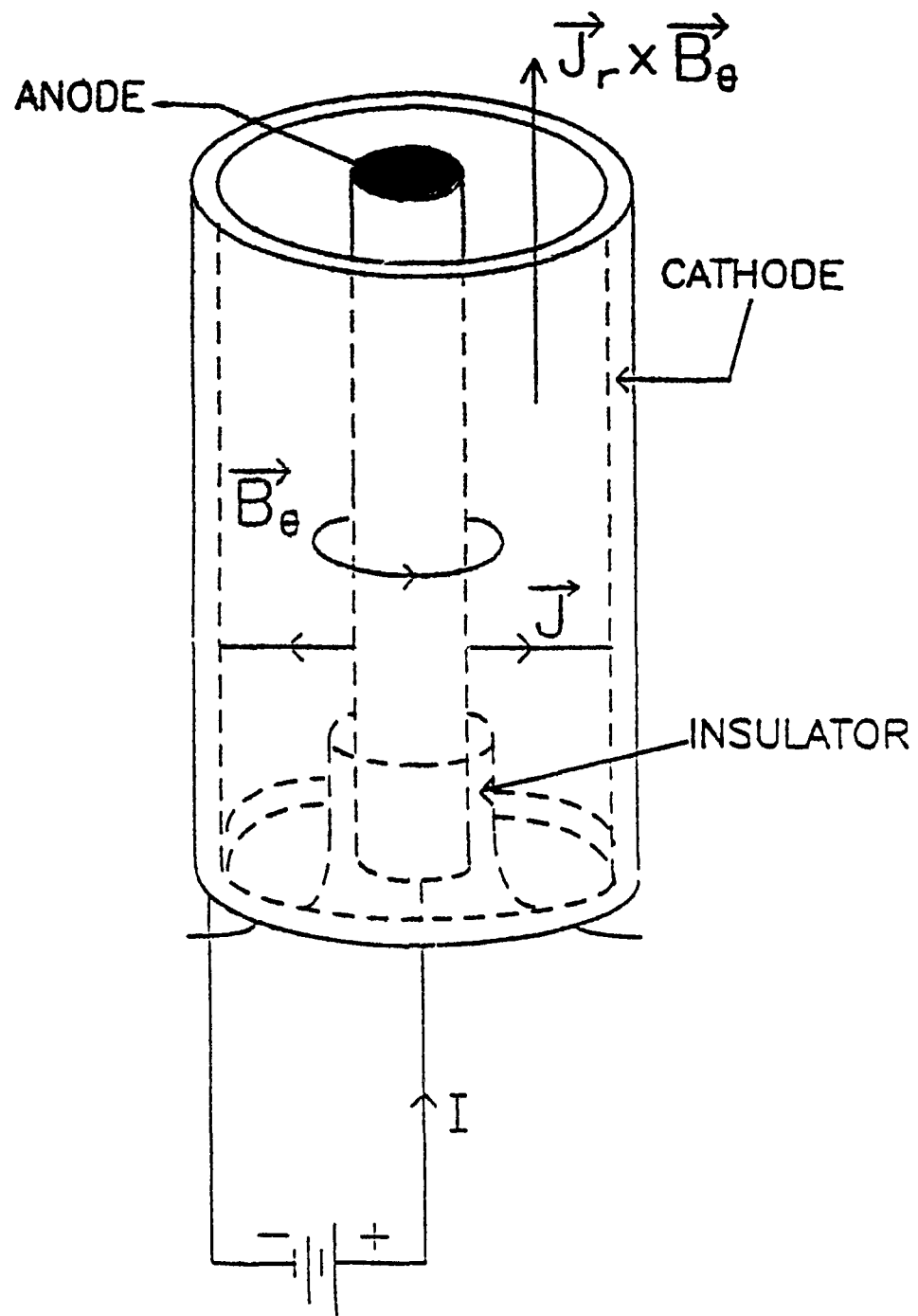
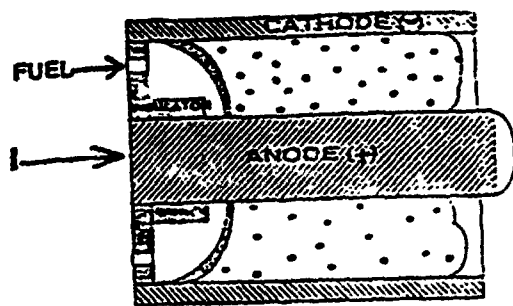
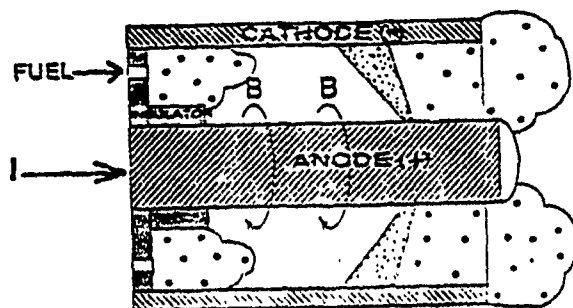


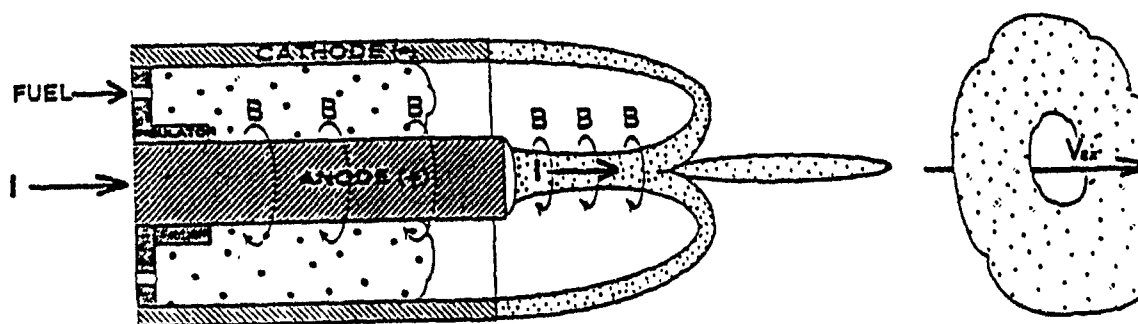
Figure 3. Coaxial Electrode Configuration



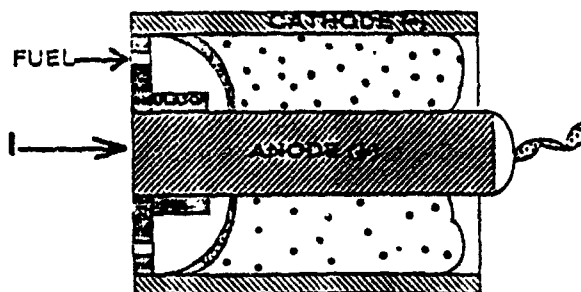
1) BREAKDOWN



2) RUNDOWN



3) FOCUS (PINCH)



1) RE-BREAKDOWN

Figure 4. Phase of the DPF Cycle

There have been numerous activities with the plasma focus experiments around the world [15-17]. A break even plasma focus reactor concept has been proposed by Herold and Hayd operating on 3.0 MJ energy at 1.8 MV voltage with 6.0 MA current. The Stuttgart group proposed a power level range of 100kW to megawatts for fusion reactions and plasma stability studies [15].

In previous experiments at the Lawrence Livermore National Laboratory, various mixtures of D_2 and 3He were used with two plasma-focus devices that operated with a stored energy of 73 kJ at 18 kV, and with 67 kJ at 20 kV [18]. Though the purpose of the experiment was to develop a diagnostic tool for determining the plasma ion temperature by evaluating the $D-D/D-^3He$ yield ratio, the significant yield of 14.6 MeV protons from the $^3He(d,p)^4He$ reaction was observed. For a 50/50 $D_2/^3He$ mixture, the $D-D/D-^3He$ yield ratio corresponded to deuterium beams with 28 to 47 keV incident upon stationary 3He ions.

Also a 1-MJ plasma focus device was used at Frascati to measure the $D-D/D-^3He$ yield ratio [19]. A new calibration of the (p,n) cross section and the ratio of fusion reaction yields resulted in the higher deuteron beam temperature at 72 keV. Filippov has also observed high energy ions emitted from his plasma focus device [13]; Gullickson and Sahlin have measured more than 10^{15} deuterons above 330 keV and 10^{12} deuterons with energy greater than 5 MeV [20]; and Mozer et al. have reported the fast deuterons with energies greater than 350 keV by using 50 kJ at 18 kV plasma focus device [21]. Quasisteady multimegawatt MPD thruster performance and some comparative analysis of large plasma focus experiments (of 360 kJ and 500 kJ devices) performed at IPF (Stuttgart) and at IPJ (Poland) were also reported [22-25]. More specific experimental component studies with a chamber magnetic nozzle provided 30% increase of the ion density with 8% addition of the electric power to the discharge chamber [26]. Small discharge chamber length yielded high extracted ion fractions [27] and the characterization of plasma flow through magnetic nozzles was also performed by Gerwin, et al. [28].

Various plasma focus experimental data were compiled in an effort to understand the scaling relations between neutron yield vs. pinch current and stored energy, and they are illustrated in Fig. 5 [30]. It is apparent from the above observations that the plasma focus device is capable of igniting $D-D$ and $D-^3He$ fuels. Hence, the goal of this study was not only to recognize the MPD-type plasma focus device but also to optimize engineering parameters including optimum capacitor bank voltage, energy, inductance, and plasma temperatures. The optimized parameters will allow the maximum energy transfer from the capacitor bank to the plasma pinch.

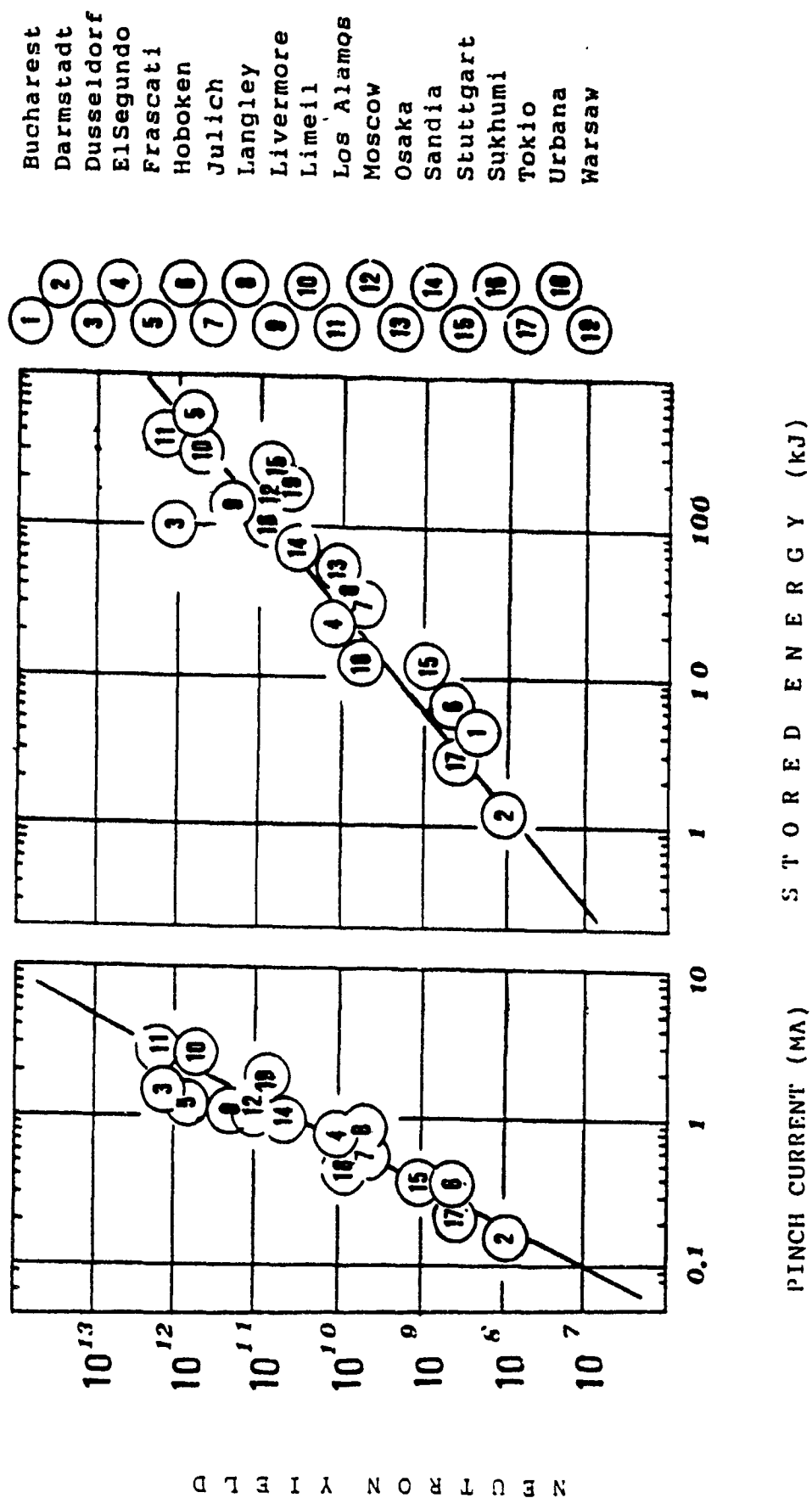


Figure 5. Neutron Yield as Functions of Pinch Current and Stored Energy [Ref. 30]

Plasma focus calculations in the literature were also compared. Typical calculational models include 1) a simple LRC circuit model in which entire plasma focus is included in the circuit equation by regarding it as contributing a variable inductance; 2) a plasma focus model in which the plasma focus is divided into three areas of i) radial lift-off region above insulator, where current is generated due to a pressure balance between magnetic field and particle pressure, ii) run-down region above anode (with snow-plow model), and iii) pinch region off the end of the anode; and 3) a 2-D MHD model in which both energy and momentum are conserved. The 2-D MHD model was developed [31] and used by Eltgroth [32] to check experimental values of the Livermore-I & -II and Frascati devices. Other related numerical studies were done for a soft x-ray experiment, high temperature pinch, current distribution, and MPD thrusters [33-38]. Various scaling relations were also studied by others using the Boltzmann equation, Maxwell equations and binary collision approximation [39]. However, the aspects of plasma scaling relations will not be included in this current report.

In general, all the calculational models are interconnected with the conservation of energy and momentum. 2-D MHD models are more rigorous and often rely on complex numerical codes. However, by developing a simple plasma focus model with, for example, a plasma snow plow driven by magnetic pressure during the run-down phase [32], one can simplify the computations analytically. The present study employs the analytical plasma focus model using the steady-state MHD momentum equation coupled with the equations for maximum attainable plasma current described in terms of capacitance, inductance, charging voltage, etc.

II. FEASIBILITY STUDIES OF DENSE PLASMA FOCUS AS A PROPULSION THRUSTER

A systems model of DPF is developed for both conventional and spin-polarized D-³He fuels to investigate the feasibilities of DPF as a propulsion thruster. Three modes of operations (i.e., two pulsed operations with and without hydrogen propellant, and one impulsive firing mode with hydrogen propellant) were studied and each was investigated for its usefulness in space travel with special attention paid to a manned Mars mission. This portion of the study with the conventional D-³He is described in Section II.1. The spin-polarized D-³He operation was also analyzed to study the effect of polarized fuels on the systems operations on, for example, thrust-to-weight ratio (F/W) and specific impulse (I_{sp}). Increased fusion power and decreased radiation losses for the spin-polarized case provided the increased values of F/W and I_{sp} which are described in Section II.2.

II. 1. PARAMETRIC STUDIES OF DENSE PLASMA FOCUS WITH D-³He FUEL*

II.1.1 DPF COMBUSTOR MODEL

The rundown velocity, U_{run}, can be predicted accurately by solving the steady-state momentum equation for the plasma sheath neglecting dissipative effects, starting with [32]

$$\rho_i \nabla \cdot (\vec{U}_{run} \vec{U}_{run}) = -\nabla P \quad (1)$$

then taking only z-components and integrating gives

$$U_{run} = \sqrt{\frac{\mu_0}{8\pi^2 r_a^2 \rho_i}} I \quad (2)$$

where I is the current discharged through the anode, r_a is the radius of the anode and ρ_i is the

* An earlier version of this section of the report has been published as PL-TR-91-3014 and the revised version has been documented as the M.S. project report by C. Leakeas as a partial requirement for the M.S. degree from Purdue University.

initial fill gas density. The sheath then reaches the end of the anode and collapses forming a small, hot plasma. (It will be shown later that the final temperature depends on many factors including the capacitor discharge current. Also, the pinch dimensions are assumed to be independent of operating conditions.) If one assumes that a fraction, f , of particles goes into the pinch, and makes a rough estimate of the dimensions of the resulting pinch formation, one can determine the number density of particles inside the pinch. To determine the temperature inside the pinch, one assumes a balance between plasma pressure and the magnetic pressure due to the external azimuthal field, B_θ , generated by the current in the pinch, as in Eq. 3.

$$n_p kT = \frac{B_\theta^2}{2\mu_0} , \quad (3)$$

where kT is the product of Boltzmann's constant and the plasma temperature (in degrees) and μ_0 is the permeability of free space.

By Ampere's Law, B_θ at the pinch surface is

$$B_\theta = \frac{\mu_0 I}{2\pi r_p} . \quad (4)$$

Solving for the pinch number density, n_p , in terms of the initial fill density and pinch and electrode dimensions, one finds

$$n_p = \frac{f \rho_i l_a (r_c^2 - r_a^2)}{l_p r_p^2 m_p} , \quad (5)$$

where f is the fraction of initial fuel which is trapped in the pinch region, l_a and l_p are the anode and pinch lengths, r_a , r_c , and r_p are the anode, cathode, and pinch radii, respectively, and m_p is the average mass of particles in the pinch. The fraction, f , is left as an independent variable during thruster evaluation, but is assumed to be about 17.5% for the baseline case. This value is arrived at by assuming that about 70% of all fuel is entrained during rundown, and of that, 25% is captured in the pinch. Substituting Eqns. 4 and 5 into Eqn. 3 gives an expression for the plasma temperature inside the pinch.

$$kT = \frac{\mu_0 I^2 m_p l_p}{8\pi^2 f \rho_i l_a (r_c^2 - r_a^2)} \quad (6)$$

This gives the plasma temperature for any current I . The maximum attainable current must now be calculated as a function of the electrical parameters of the system (e.g. capacitance, inductance, charging voltage, etc.). The maximum attainable current is given by

$$I_{\max} = 0.64 \left[\frac{W \dot{i}}{\dot{L}} \right]^{1/3} \quad (7)$$

where

$$W = \frac{1}{2} CV^2 \quad (8)$$

$$\dot{i} = \frac{V}{L_0} \quad (9)$$

$$\dot{L} = \frac{\mu_0}{2\pi} U_{\text{run}} \ln \left[\frac{r_c}{r_a} \right], \quad (10)$$

where C is the total capacitance, V is the charging potential, and L_0 is the initial circuit inductance [40]. Thus, from the initial conditions defined in Eqs. 8-10, the maximum current and resulting plasma pinch temperature can be found with Eqs. 6 and 7. It is assumed through the rest of this report that the plasma pinch temperature continues to scale as current squared as shown in Eqn. 6 and Figure 9, although this scaling seems to fail for currents above 1 MA due to saturation and degradation effects [25].

The plasma focus device analyzed in this report is assumed to be identical to the "Livermore-I" dense plasma focus. Therefore the same geometrical and electrical parameters which were used in the operation of this device will be adopted [20,32]. The parameters used can be found in Table 3 where asterisks denote assumed values. If operated at the values in Table 3, the Livermore-I focus should be capable of a maximum current of 1.245 MA and a maximum plasma temperature of about 300 eV. This plasma temperature is much too low to

produce significant amounts of fusion energy. As seen in Figure 6, one would ideally operate at kT greater than about 50 keV (depending on the fuel) in order to maximize the reaction rate parameter. Therefore the capacitor banks are assumed to be capable of delivering in excess of 20 MA. Using the values in Table 3, the DPF performance can be modeled for a wide range of currents using the simple scaling laws found in Eqs. 4-6.

Table 3. Livermore-I Dense Plasma Focus Parameters

$V = 27,000 \text{ V}$	$C = 3.55 \times 10^{-4} \text{ F}$
$L_o = 2.5 \times 10^{-8} \text{ H}$	$l_a = 0.382 \text{ m}$
$r_a = 0.0508 \text{ m}$	$r_c = 0.080 \text{ m}$
$* f = 0.175$	$* l_p = 0.0254 \text{ m}$
$* r_p = 0.0015 \text{ m}$	$\rho_i = 2.2 \times 10^{-4} \text{ kg/m}^3$

*Denotes assumed values.

In order to complete the development of the DPF model, the fusion fuels need to be defined. There are several desirable criteria to be considered in the choice of fusion fuels. The fusion fuels should have a high power density. Of all the fusion reactions being considered today, the $D-^3\text{He}$ reaction has the highest power density at 18.3 MeV per reaction. $D-T$ is second at 17.6 MeV, $^3\text{He}-^3\text{He}$ releases 12.9 MeV, and $p-^{11}\text{B}$ releases 8.7 MeV per reaction.

The fuel should have a high reaction rate parameter at low temperature to achieve good fusion burn before radiative losses overwhelm the system. The reaction rate parameter, $\langle\sigma v\rangle$, is a function of plasma temperature and determines how quickly these reactions proceed at a given temperature. Figure 6 shows the reaction rate parameters for some typical fusion fuels [41]. $D-T$ has the highest reaction rate parameter at low temperatures and the $D-^3\text{He}$ reaction rate parameter is slightly less. The other "advanced" fuels such as $p-^6\text{Li}$, $p-^{11}\text{B}$, and $^3\text{He}-^3\text{He}$ must be operated at very high temperatures [42,43] and may be impractical because synchrotron radiation losses increase in proportion to the electron temperature squared at the lowest order, thus making ignition difficult. The $D-D$ reaction has a reaction rate parameter which is slightly less than that for $D-T$, but this fuel has two major disadvantages. It has a much lower power density (about 4 MeV) and has 50% probability of producing a neutron with each reaction.

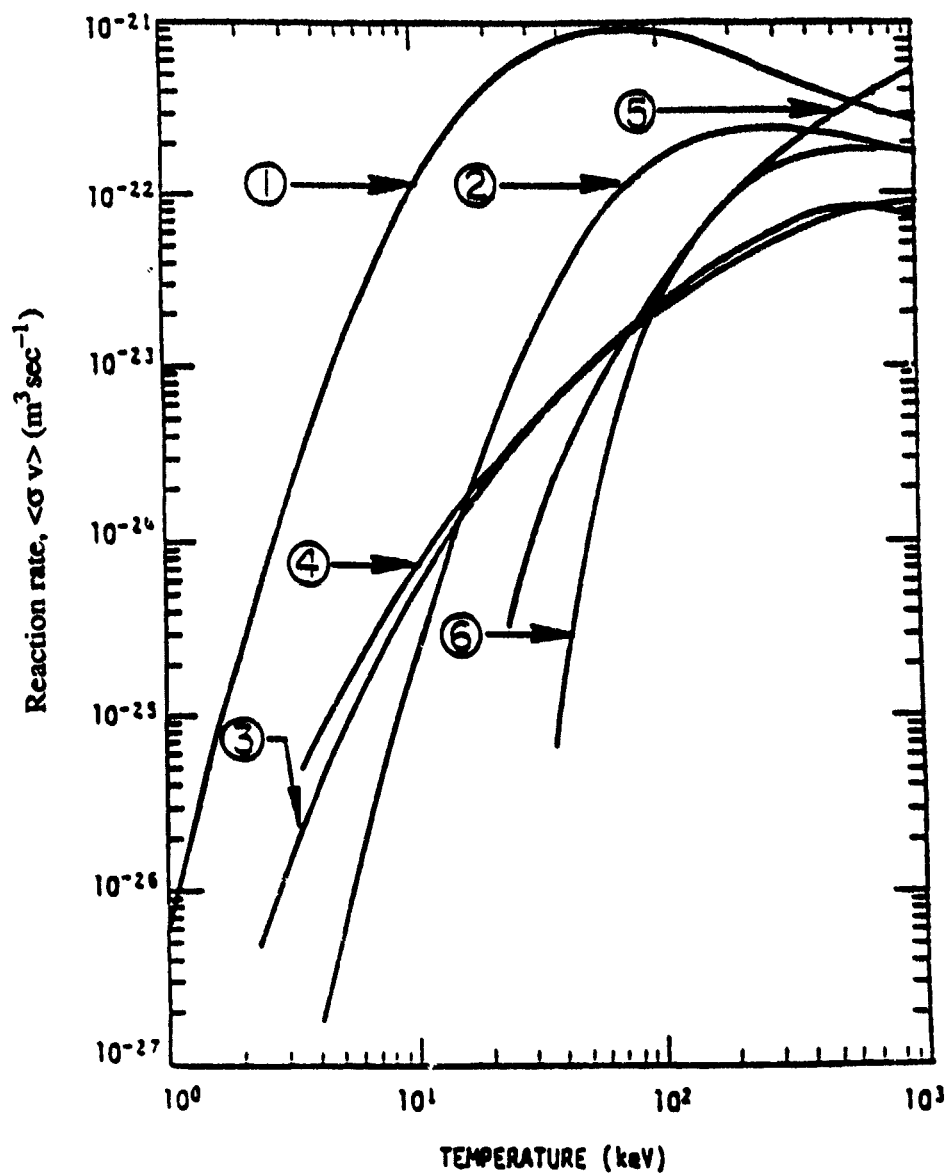


Figure 6. Reaction Rate Parameters for Various Fuels

(1) D-T, (2) D-³He, (3) D-D
(4) T-T, (5) T-³He, (6) p-¹¹B

Since neutrons cannot be directed to produce thrust by a magnetic field, it is desirable to minimize their production. An ideal reaction would release all of its energy in the form charged particles. Of the "easily" ignitable fuels, D-T releases about 80% of its energy as neutrons, while the $D-^3He$ reaction releases no neutrons. However, the secondary background D-D in $D-^3He$ reaction, which releases about 75% of its energy in neutron radiation, can contribute significant neutron production to the $D-^3He$ reaction. The other "advanced" fuels mentioned earlier are considered to be completely a neutronic.

After considering each fuel's characteristics in these three areas, $D-^3He$ was chosen as the fuel to be used in this DPF study. Its leaner neutron production (compared to D-T), high power density and high reaction rate parameter at relatively low temperatures were key factors in its selection.

II.1.2 DPF PROPULSION SYSTEM MODEL

The DPF fusion propulsion system (see Figure 7) consists of the feed and cooling system, the electrical power system and the thruster system. The feed and cooling system consists of three tanks for the hydrogen, helium-3, and deuterium, associated plumbing to control and direct the flow of these gasses, and the associated coolant passages. Also necessary in this system are a number of pumps to drive propellant and fuel flow, as well as to provide the pressure necessary for the coolant to enter the high pressure side of the turbine. The deuterium and helium-3 are used as the fuel to drive the thruster. The hydrogen is used for cooling, driving the turbine, and may then also be used as propellant to provide increased thrust.

The electrical system consists of a turbine, electric generator and the capacitor banks necessary to produce the large current pulses which are required by the thruster. The electricity produced by the turbo-generator is used to meet system requirements and to help recharge the capacitor banks for each shot.

The thruster system consists of the DPF itself as well as a mixing chamber and a magnetic nozzle if one chooses to operate the DPF at very high propellant temperatures. As will be seen later, the magnets necessary for our purpose are relatively small and constitute a small fraction of total system mass. The mixing chamber is only necessary if the DPF propulsion system is to be operated with hydrogen propellant. It is a hollow cylindrical cavity where the fusion reaction products will mix with cold hydrogen propellant. It is assumed that the resulting mixture leaves the chamber with a uniform temperature and produces thrust.

PLASMA FOCUS FUSION PROPULSION SYSTEM

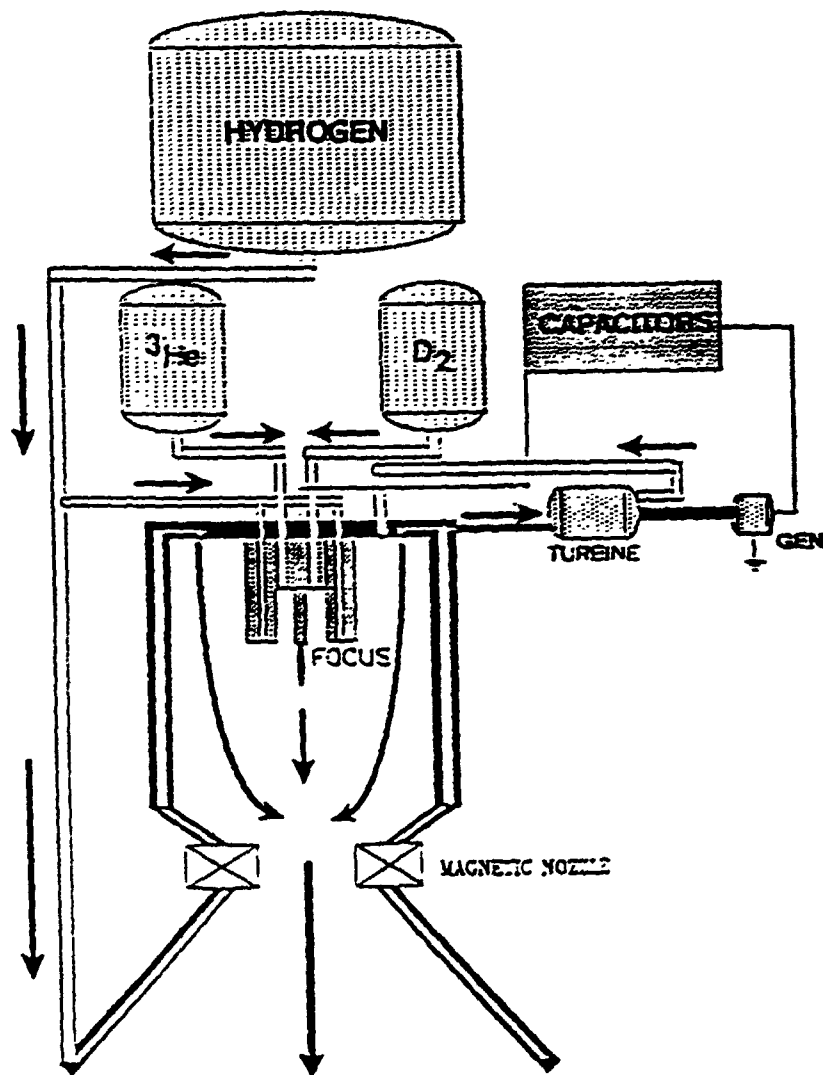


Figure 7. Plasma Focus Fusion Propulsion System

The exhaust power produced in any type of rocket engine is given by

$$P_{ex} = \frac{1}{2} \dot{m}_{propellant} U_{ex}^2 \quad (11)$$

where F is the thrust and U_{ex} is the propellant exhaust velocity. If one assumes that the thrust is parallel to the exhaust velocity and defines the specific impulse by

$$I_{sp} = \frac{U_{ex}}{g}, \quad (12)$$

and the thrust by

$$F = \dot{m}_{propellant} U_{ex}, \quad (13)$$

the exhaust power can then be written as

$$P_{ex} = \frac{1}{2} g F I_{sp}, \quad (14)$$

where g is the gravitational acceleration and specific impulse is a measure of how efficiently propellant is used [44]. Eqn. 14 shows the competing nature of thrust and specific impulse. Both are desirable, but for a fixed engine power an increase in one requires a decrease in the other. However, with the high exhaust powers attainable with fusion, it should be possible to attain reasonably high values of both parameters simultaneously.

Three possible modes of operation for the DPF propulsion system were investigated:

- 1) Pulsed operation of the DPF for long periods of time with no hydrogen propellant exhausted. The fusion products are produced and immediately expelled to produce thrust. The total time that the thruster is fired is comparable to the total trip time.
- 2) Pulsed operation of the DPF for long periods of time with the addition of moderate quantities of hydrogen propellant. The hydrogen is used to provide electric power and also provides additional thrust because of increased mass flow rate in the exhaust with some loss of I_{sp} .

- 3) Pulsed operation of the DPF for short periods of time during which large quantities of hydrogen are exhausted in a high thrust impulsive burn. This "impulsive" burn reduces gravitational losses, makes much higher thrust-to-weight ratios possible and would most likely be used during interplanetary travel.

Mode 1) Pulsed operation with no hydrogen propellant

This mode involves a closed coolant cycle and would therefore require large radiators (0.07 kg/kWe) [45] to dissipate the heat produced by resistive heating of the electrodes and radiative power losses in the thruster walls. It is still possible to generate electricity from the turbo-generator before the coolant enters the radiators. The calculations made for this mode are identical to those made using the FORTRAN code in appendix of this report, except that one must include the radiator mass and use a zero propellant mass flow rate. The system is similar to that shown in Figure 7, but with the addition of radiators in the coolant loop and removal of the mixing chamber.

When the fusion fuels react in the pinch, it is assumed that very little charged particle power is retained in the pinch. Thus, when the charged particles leave the pinch, their energies are known simply as a function of the fusion fuels used ($D-^3He$ produces 14.7 MeV protons and 3.6 MeV alpha particles). The velocities of these particles are very high (some over 10^7 m/s). These velocities lead to specific impulse values on the order of 10^6 s. However, because of the low mass flow rate exiting the pinch, thrust values are on the order of about 44.5 N (10 lbf), and the main contribution to this thrust comes from the expulsion of fill gases which are not trapped during the rundown and pinch phase of operation. For a manned Mars mission with a payload dominating mass of 10^5 kg [46], the system thrust-to-weight ratio (F/W) upper bound is about 5.0×10^{-5} . If the additional mass of radiators, shielding, capacitors, tanks, fuel, etc. are considered, F/W decreases further. This F/W value is many orders of magnitude less than conventional chemical rockets. In this mode, the DPF is comparable in performance to electric propulsion. Although these thrust levels have applications to certain types of missions (perhaps orbital transfer), manned interplanetary travel requires larger mission Δv 's and shorter trip times to reduce exposure to cosmic radiation and weightlessness. Therefore this mode was not considered beyond the conceptual state.

Mode 2) Pulsed operation with hydrogen propellant

One way to increase F/W values is by exhausting the heated coolant to increase the mass flow rate and corresponding thrust given in Eq. 13. In doing this one accepts the penalty of

decreased specific impulse as a necessary means to increase thrust. The increase in thrust will allow the DPF's use in a wide variety of missions, whereas operating without hydrogen propellant restricts the type of missions for which it can be used.

The Mode 2 system is illustrated schematically in Figure 7. As the capacitor banks are being discharged through the center anode, the fuel is injected and is caught up in the plasma sheath's rundown as illustrated in Figure 4. The plasma collapses and pinches at the end of the anode and produces large amounts of charged fusion products as well as Bremsstrahlung and synchrotron radiation and neutrons. It was assumed in this study that the Bremsstrahlung radiation, which is emitted in the UV spectrum, is completely lost. However, part of the synchrotron radiation was assumed to be absorbed by the plasma and part absorbed in the walls of the electrodes and mixing chamber. The portion absorbed in the walls and electrodes was assumed to be about 20% for the baseline case, but was left as a variable parameter to observe its effects on thruster performance. The heat generated by synchrotron radiation and ohmic heating is then cooled by the flow of cold liquid hydrogen propellant. Because of material limitations, the turbine entrance temperature was constrained to be no greater than 2,000 °K. This would require advances in material sciences since current materials restrict temperatures to less than about 1,100 °K [47]. This inlet temperature constraint then fixes the minimum mass flow rate of coolant which enters the mixing chamber. The gas is then expanded through a turbine used to run a generator which recharges the capacitor bank. Complete recharging of the capacitors is only possible at higher powers and larger coolant flow rates. The flow from the turbine is then used as propellant to absorb the energy of the charged particles produced in the pinch. An open cycle was chosen to avoid heavy radiators that would greatly increase total system mass. The propellant was assumed to absorb all of the fusion product energy after accounting for radiative losses and become completely dissociated and ionized in the mixing chamber. The resulting propellant plasma was assumed to come to a uniform temperature before it enters a meridional magnetic nozzle (axial field only). The magnetic nozzle (see Figure 8), which would require a maximum field of about 2 T [28], then further accelerates the particles out the exit to even higher velocities.

In doing the analysis, several simplifying assumptions were made. These assumptions concerned aspects of the pinch as well as advancements in other technologies applicable to the DPF. These assumptions are:

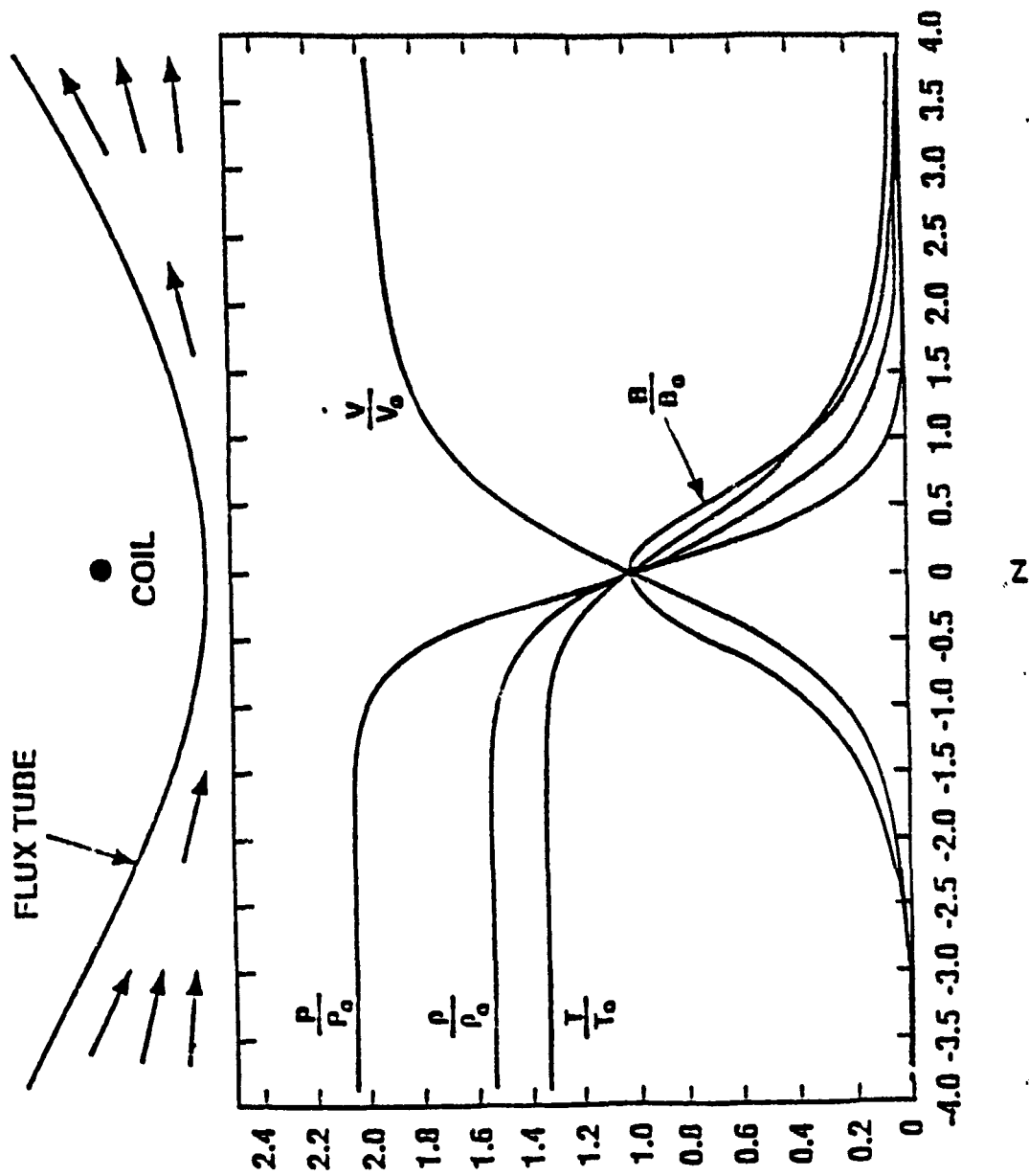


Figure 8. Axial Variation of Fluid Variables for a quasi-1D Meridional Magnetic Nozzle

- 1) Plasma pinch temperature scales as current squared.
- 2) Since no accurate measurements of actual pinch dimensions have been made, a rough estimate was used.
- 3) Ions come to thermal equilibrium inside the pinch allowing the use of Maxwellian reaction rate parameters.
- 4) Materials will be developed that can withstand temperatures much higher than currently possible. This would be necessary in the turbine and in the walls of the mixing chamber to minimize damages due to high heat fluxes.
- 5) Electrodes and mixing chamber walls can be sufficiently cooled to prevent damage. Film cooling may be possible, but at the cost of I_{sp} .
- 6) Propellant becomes completely dissociated and ionized in the mixing chamber at 5,000 °K.
- 7) Advances in capacitor bank technology will increase specific energies by a factor of 10 and allow for discharging rates of 100 Hz. Capacitors based on present technology offer a specific masses of about 0.2 kJ/kg [8].
- 8) Confinement times can be increased about a hundred times (to about 10^{-4} s) to allow for a good fusion burn (around 40%). Since reaction rates are determined by plasma temperature, longer confinement times allow for more fuel to be burned.
- 9) Any magnetic fields applied downstream do not adversely affect the pinch formation or confinement time.

With these assumptions, thruster performance was investigated while varying current, fraction of particles trapped in pinch, capacitor bank specific energy, total firing time, and fraction of synchrotron radiation absorbed in walls and electrodes.

Baseline case:

f	= Fraction of particles trapped in pinch	0.175
FRACT	= % synchrotron radiation absorbed in walls and electrodes	0.20
SPECEN	= Capacitor bank specific energy	20 kJ/kg
DAYS	= Total thruster firing time	30 days

For the cases of continuous pulsed operation (Modes 1 and 2), DAYS is defined as the length of time which the thruster is fired. The baseline case assumes that the thruster is fired for 30 days and that this is comparable to total trip time.

Figure 9 shows the pinch temperature dependence on current for several values of f , the fraction of particles trapped in the pinch. Using the assumed DPF dimensions and initial fill gas density, $f = 0.175$ gave pinch number densities which are close to experimentally determined values ($n \geq 10^{19} \text{ cm}^{-3}$) [14]. Although lower f gives lower pinch number density, Figure 9 shows lower f also gives higher plasma temperature. Operating at the very high temperatures necessary to ignite some advanced fuels, such as ^3He - ^3He and p - ^{11}B , may not be feasible since synchrotron radiation increases as T^2 .

Figure 10 shows the resulting propellant temperature at the entrance to the magnetic nozzle as a function of current for various values of f . As current is increased past a certain point, the extra fusion power produced cannot continue to raise the temperature of the increased coolant (and therefore propellant) flow which must be supplied due to greater heat flux to the walls and electrodes. Therefore, this function does not increase indefinitely, but has a definite maximum at about 15 MA for baseline values of f and FRACT. This corresponds to the maximum in specific impulse for the baseline case in Figure 11. As f increases, the number density in the pinch increases, so the resulting pinch temperature decreases: the reaction rate decreases because of the lowered temperature, and there is less fusion output to heat the propellant. A balance is established between plasma and magnetic pressures, so for higher values of f , and therefore particle density, a higher current is required to bring the plasma temperature up to its maximum. As the maximum current, I_{max} , increases, the propellant mass flow must correspondingly increase to cool electrodes of the focus device. Figure 12 shows that the current which maximizes specific impulse (about 15 MA for the baseline case in Figure 11), also produces a maximum F/W for the baseline case. As current is increased beyond this optimum, capacitor mass and required coolant mass increase resulting in a decrease in thrust-to-weight ratio. System F/W ratios are calculated by the program in the appendix taking into account all system masses. As seen in Figure 12, vehicle F/W peaks at about 15 MA and reaches almost 0.003 for the baseline case, while a typical value for a manned Mars mission using an impulsive burn is about 0.2 [46]. This would seem to be the optimum operating regime for the DPF in this mode operating at baseline conditions, as it maximizes both specific impulse and F/W.

Another problem is in the area of capacitor bank technology. Modern capacitors allow a specific energy of about 0.2 kJ/kg [8]. However, to supply the necessary currents to the thruster and magnet, these specific energies would require capacitor masses on the order of 40,000 kg (about 40% of the assumed payload for a manned Mars mission). Advancements in capacitor

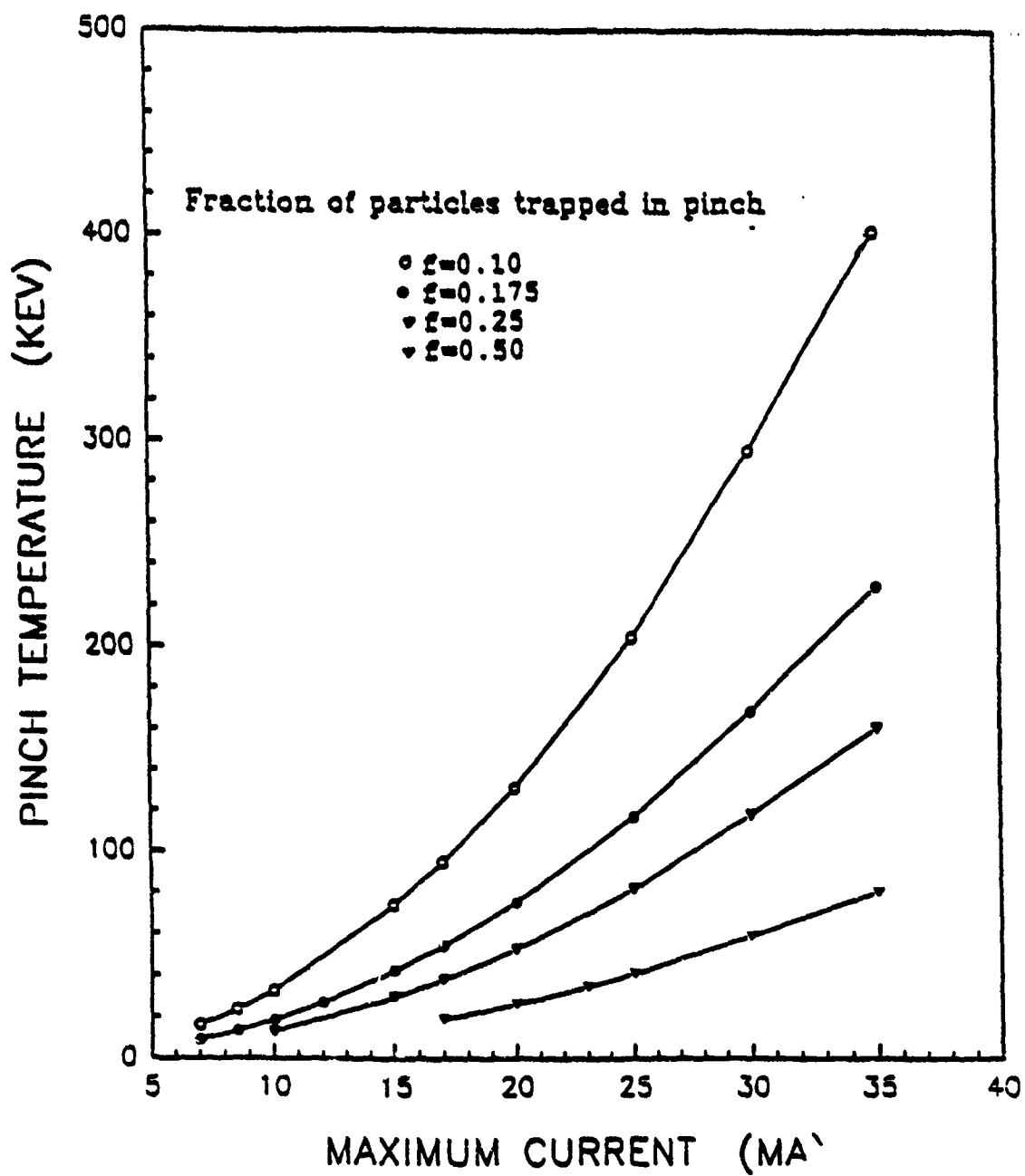


Figure 9. Plasma Pinch Temperature vs. Current

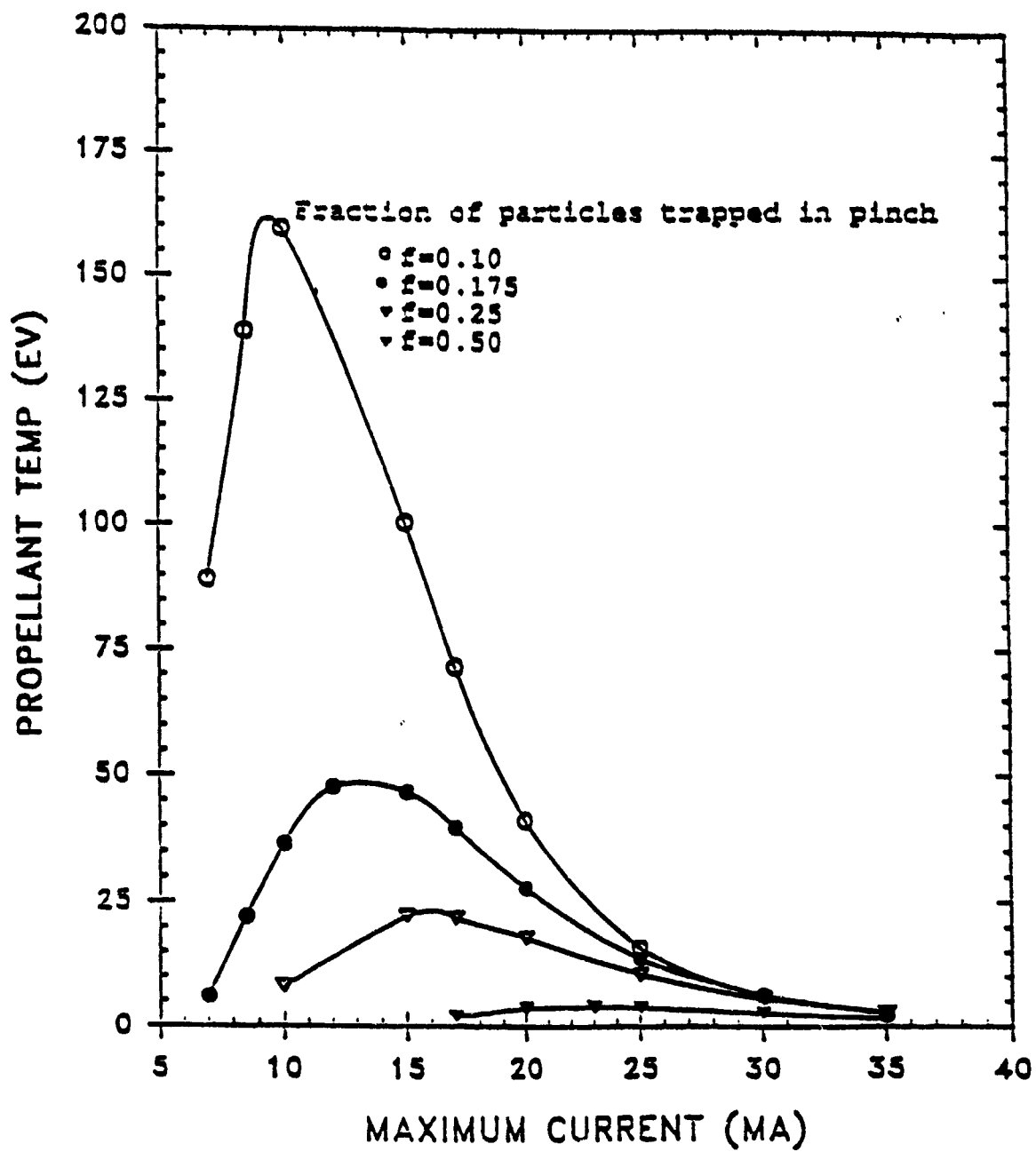


Figure 10. Propellant Temperature vs. Current

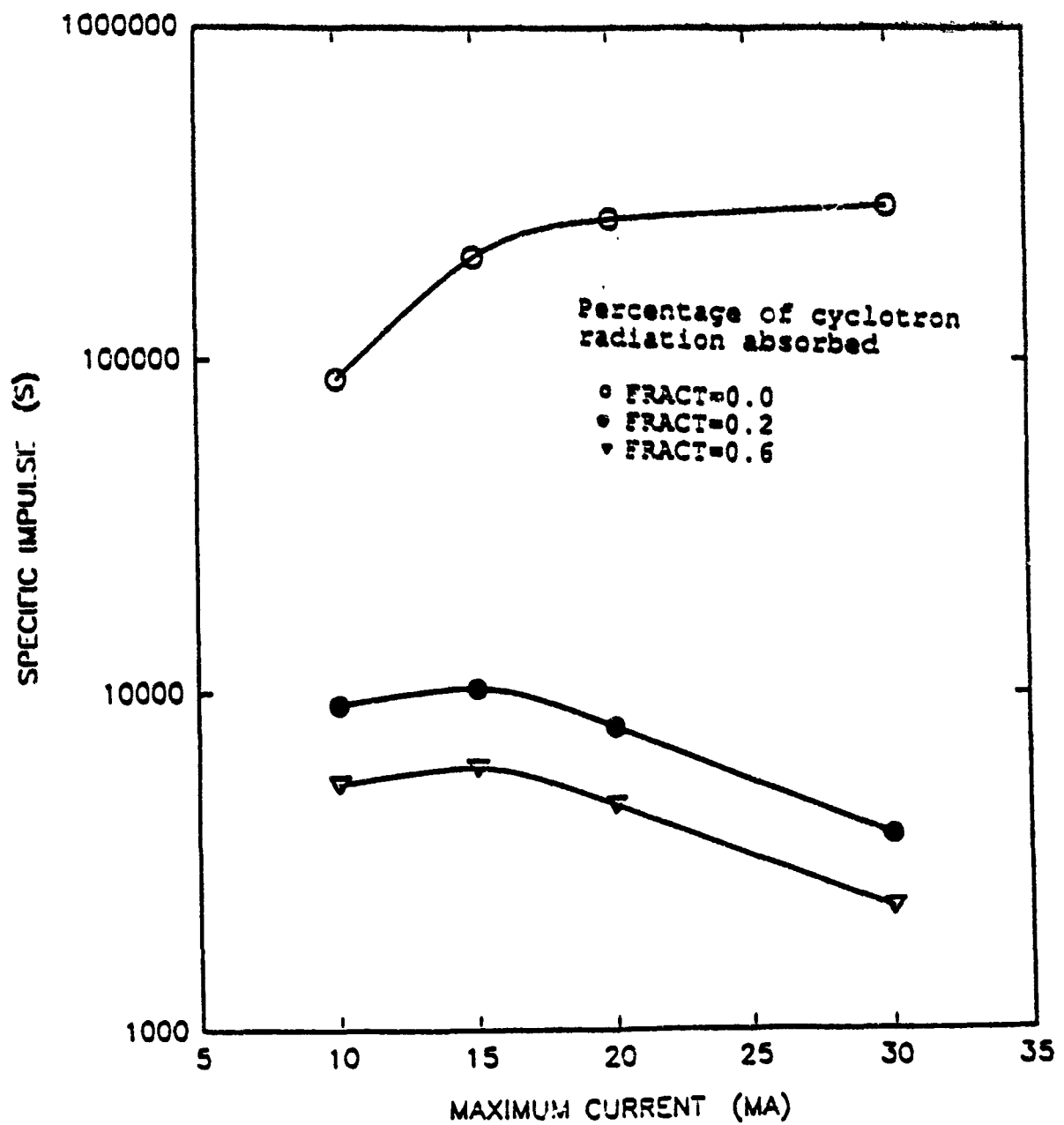


Figure 11. Specific Impulse vs. Current

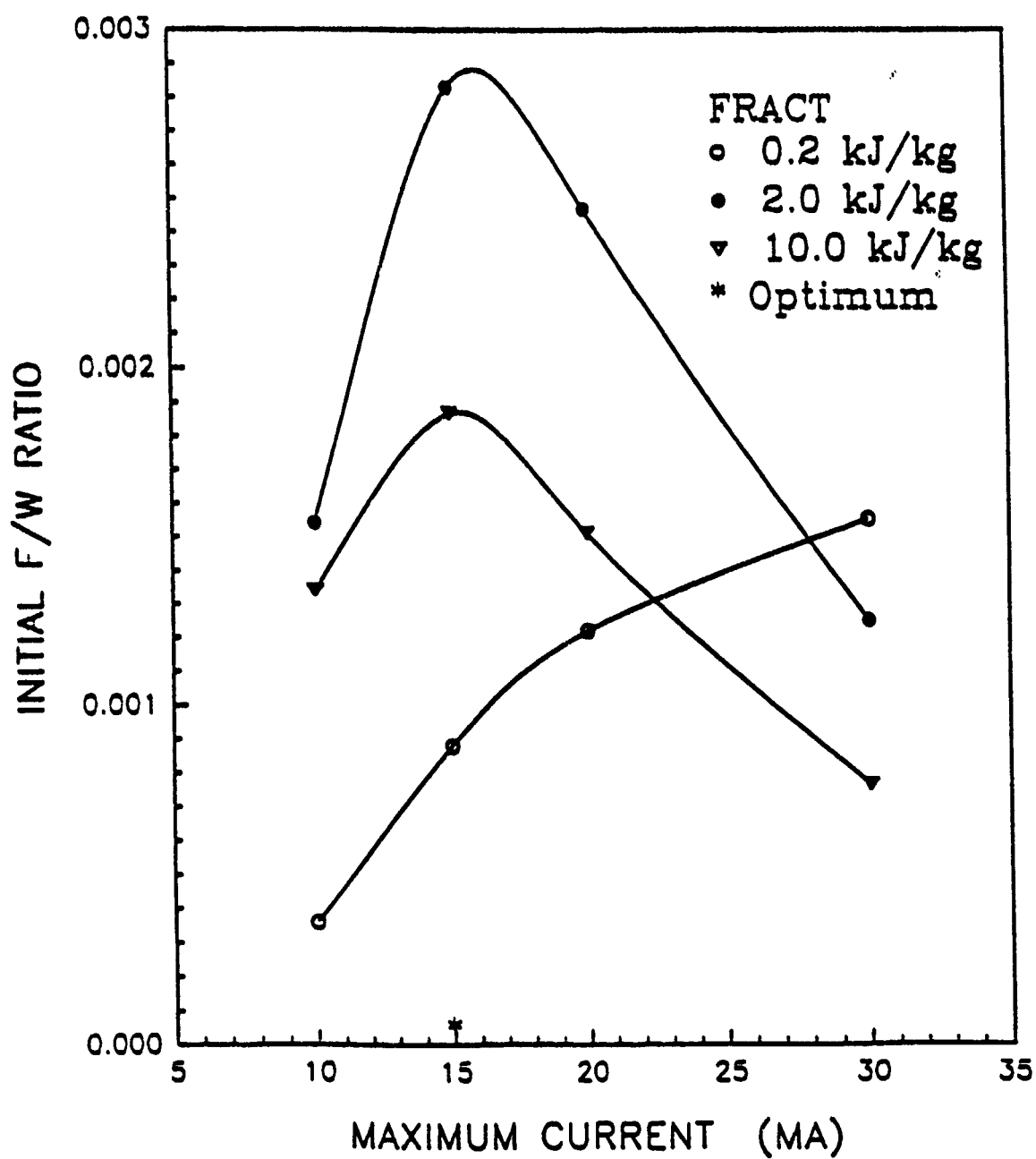


Figure 12. Thrust-to-Weight Ratio vs. Current

technology might allow specific energies of 2.0 kJ/kg and would make the total system mass much smaller and allow higher thrust-to-weight ratios (see Figure 13). Further increases over 2.0 kJ/kg change thrust-to-weight ratios only slightly because at high specific energies system mass is dominated by propellant and payload.

The final parameter was the total firing time. Figure 14 shows the expected decrease in F/W as firing time increases because of the increase in propellant mass which must be carried. Once again, the maximum value seems to occur at about 15 MA. Although thrust is increased, the problem with continuous operation is apparent. In this high I_{sp} , low F/W mode, mission times become extremely long and thrust-to-weight values drop even further, giving the DPF limited usefulness for interplanetary travel.

Mode 3) Impulsive firing with hydrogen propellant

The plasma focus propulsion system can also be operated by firing for a short period of time while exhausting great quantities of propellant. In this way, the propellant has been exhausted and is no longer considered to contribute to the total system mass. This decreased system mass allows larger acceleration for the same thrust resulting in larger F/W ratios. These higher F/W ratios decrease the required Δv for a given mission resulting in a decrease in trip time. By adding additional hydrogen flow to the coolant flow, thrust can be increased considerably but this reduces the propellant outlet temperature and therefore I_{sp} .

A key issue in this analysis is how the system masses are obtained. It is important to keep system masses low to improve F/W values and to minimize the cost of raising the vehicle from earth into low earth orbit (LEO). Payload mass is a constant and is fixed for a given mission. Propellant mass is fixed by the mission Δv and the exhaust velocity, and may be found from the rocket equation:

$$\frac{M_f}{M_i} = e^{\frac{-\Delta v}{U_e}} \quad (15)$$

where M_i is the initial mass (i.e., total system mass, payload and propellant) and M_f is the final mass after the burn (total system mass and payload only). The rocket equation can be simplified to

$$\Delta v_{\text{capable}} = g I_{sp} \ln \left(\frac{M_i}{M_f} \right) \quad (16)$$

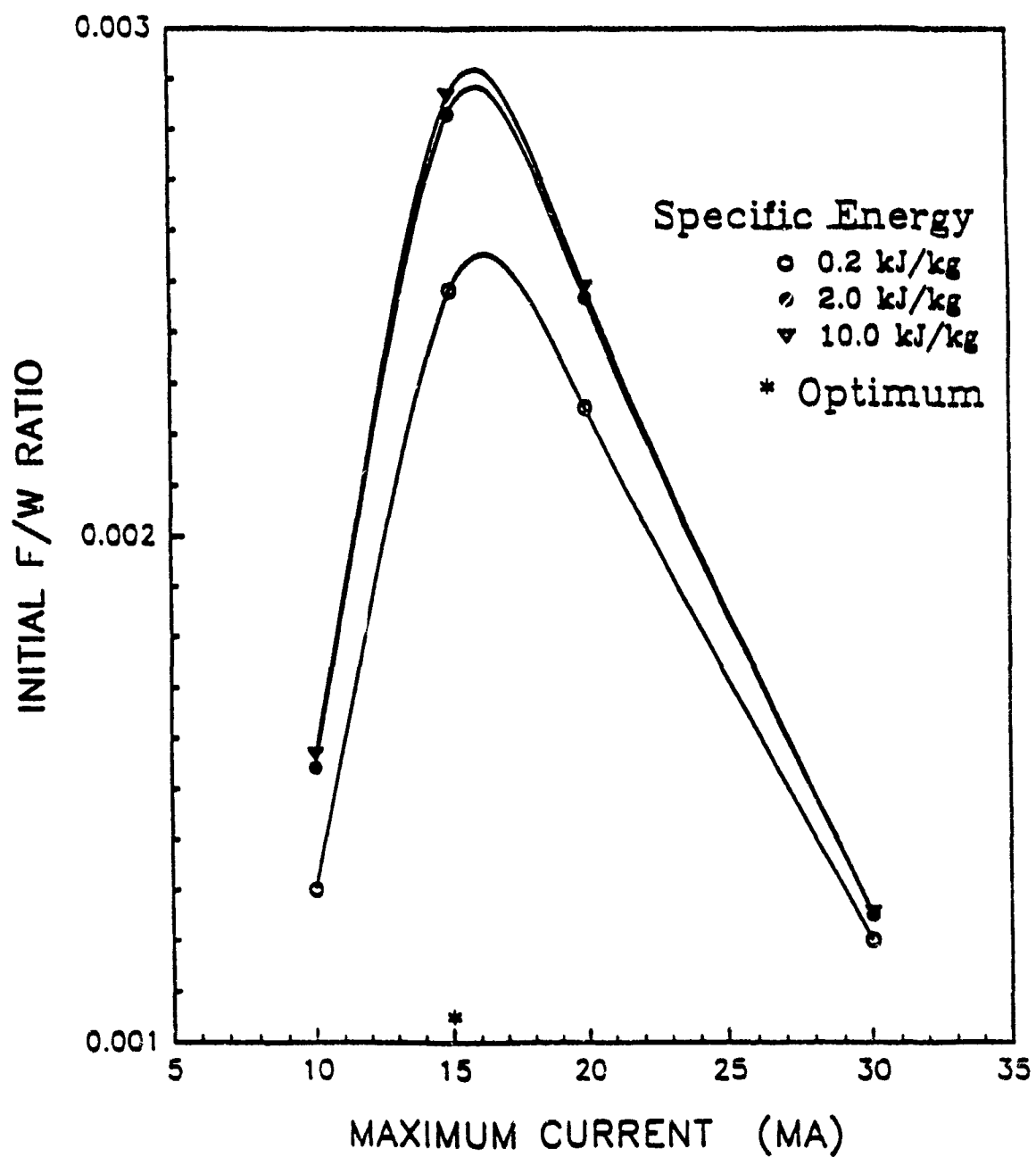


Figure 13. Thrust-to-Weight Ratio vs. Current

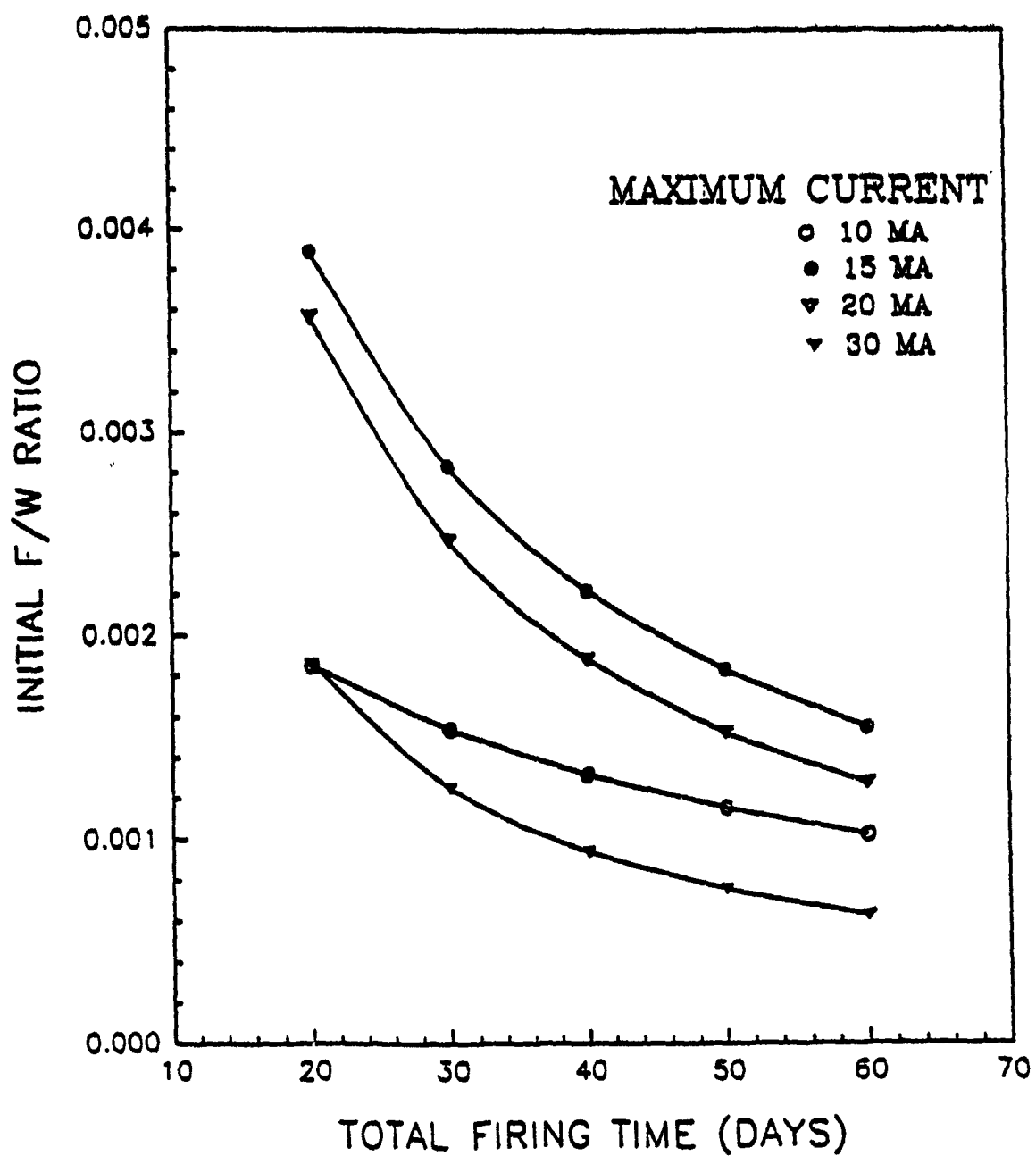


Figure 14. Thrust-to-Weight Ratio vs. Firing Time

Because of the possibility for high I_{sp} , the plasma focus is clearly capable of high Δv 's and quick trip times if adequate thrust-to-weight values can be attained. Figure 15 shows the total Δv capability of the DPF propulsion system as a function of payload mass fraction at $I_{sp} = 3,500$ sec and 111,250 N (25,000 lbf) of thrust. Another very important system mass is the capacitor mass. It is necessary to project the capacitor mass by scaling from some reference case. The "Livermore-I" device was chosen as the reference to remain consistent. It was initially assumed that the capacitor mass scaled as the current squared. The results presented thus far and to be presented here have been obtained with the I^2 scaling. However, by solving Eqs. 7-10, it can be shown that the capacitor mass scales as $I^{8/3}$. This seemingly small difference is in fact very important and the following analysis is repeated in Appendix A using $I^{8/3}$ scaling.

In this impulsive firing mode, it is important to find the optimum propellant mass flow rate in order to maximize F/W while maintaining acceptable specific impulse. Figures 16-20 show the dependence of F/W on propellant mass flow rate for various currents and mission velocity increments. Figure 16 would seem to show that F/W can be increased indefinitely by simply exhausting more propellant. However, this lowers the propellant outlet temperature which increases the total amount of propellant required in accordance with Eq. 15. This is not apparent in missions with small Δv 's since the originally required propellant mass is so small compared to other system masses. Figures 16 and 17 actually show cases where propellant becomes the dominant mass and an increase in propellant mass flow rate actually decreases system F/W. As a result of the I^2 scaling it is always advantageous to run the thruster at the highest current possible until the pinch temperature reaches the temperature corresponding to maximum in the $D-^3\text{He}$ reaction rate parameter curve. Optimum F/W ratios for the high Δv missions are still an order of magnitude below the desired value of 0.2 for a manned Mars mission. Figure 21 shows the variation of specific impulse for $\Delta v = 5$ km/s, but is in fact valid for any mission since the propellant exit velocity is only dependent on DPF system parameters.

Since F/W ratios are still below the desired value, it is obvious that extra thrust is needed while keeping system mass down. This may be possible by adding additional thrusters if the extra thrust produced more than compensates for the extra mass due to capacitors, shielding etc. The additional thrusters will not affect I_{sp} values and Figure 21 is still valid. Adding additional thrusters is also insurance against a failure in any one thruster. Figures 22 and 23 show the general trends of vehicle F/W as additional thrusters are added for 10 and 40 km/s mission Δv 's respectively. For low Δv missions, where required propellant mass is small, it is best to run several thrusters at high propellant mass flow rates. Figure 23 best to run several thrusters at relatively low propellant mass flow rates. Initial mass in low earth orbit (IMLEO) is probably

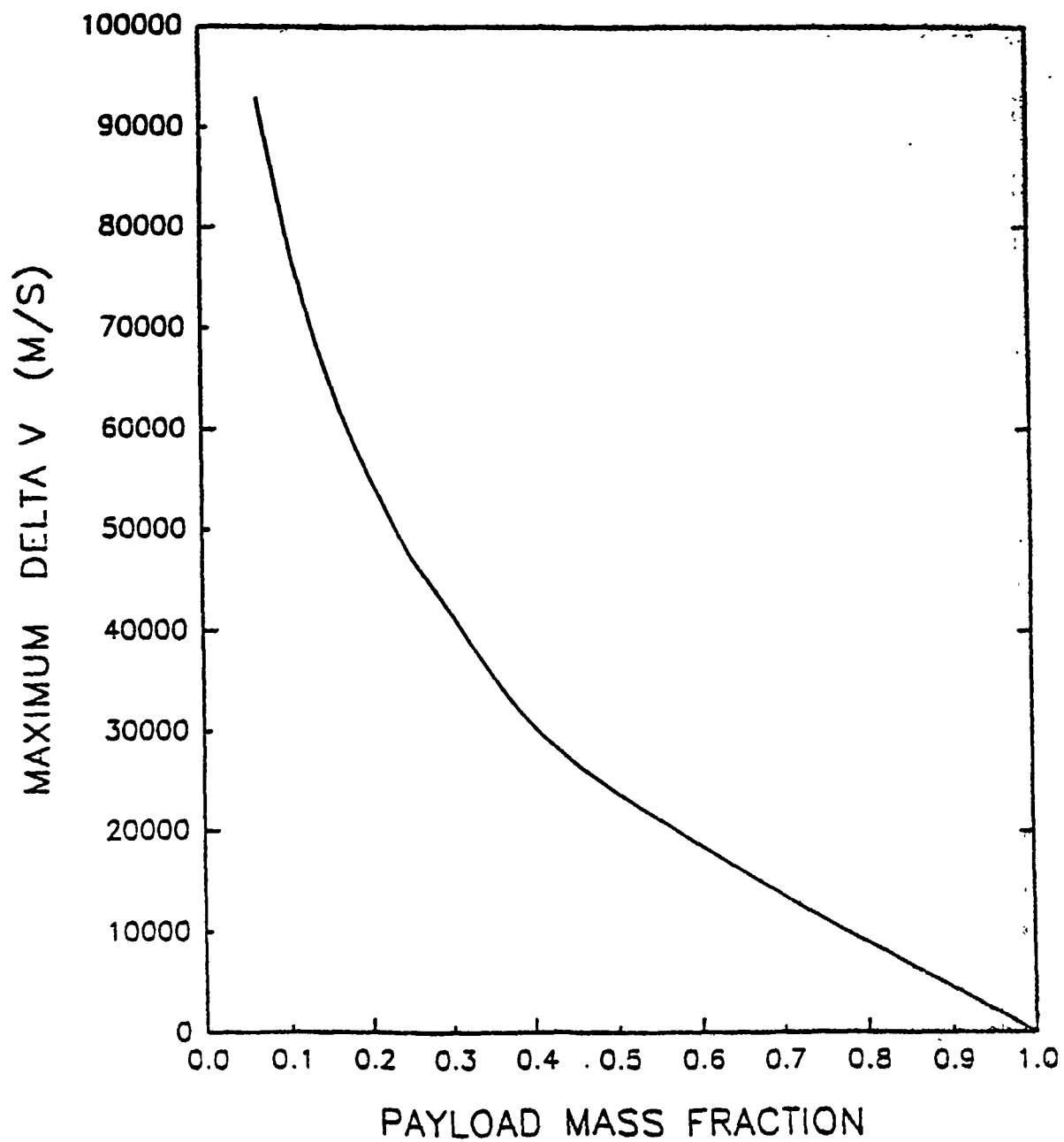


Figure 15. Δv Capability vs. Payload Mass Fraction

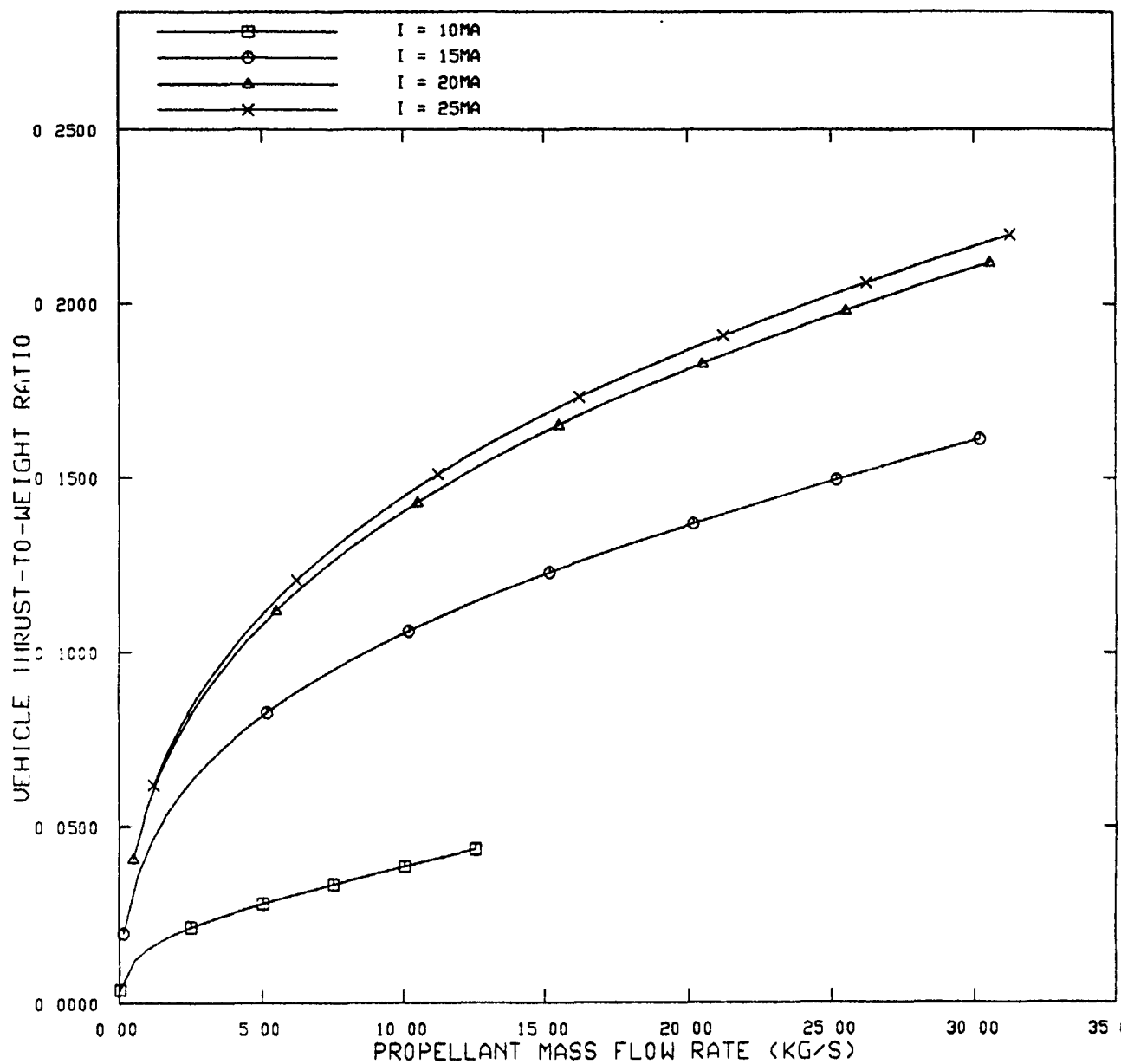


Figure 16. Vehicle F/W vs. Propellant Mass Flow Rate for $\Delta v=5$ km/s

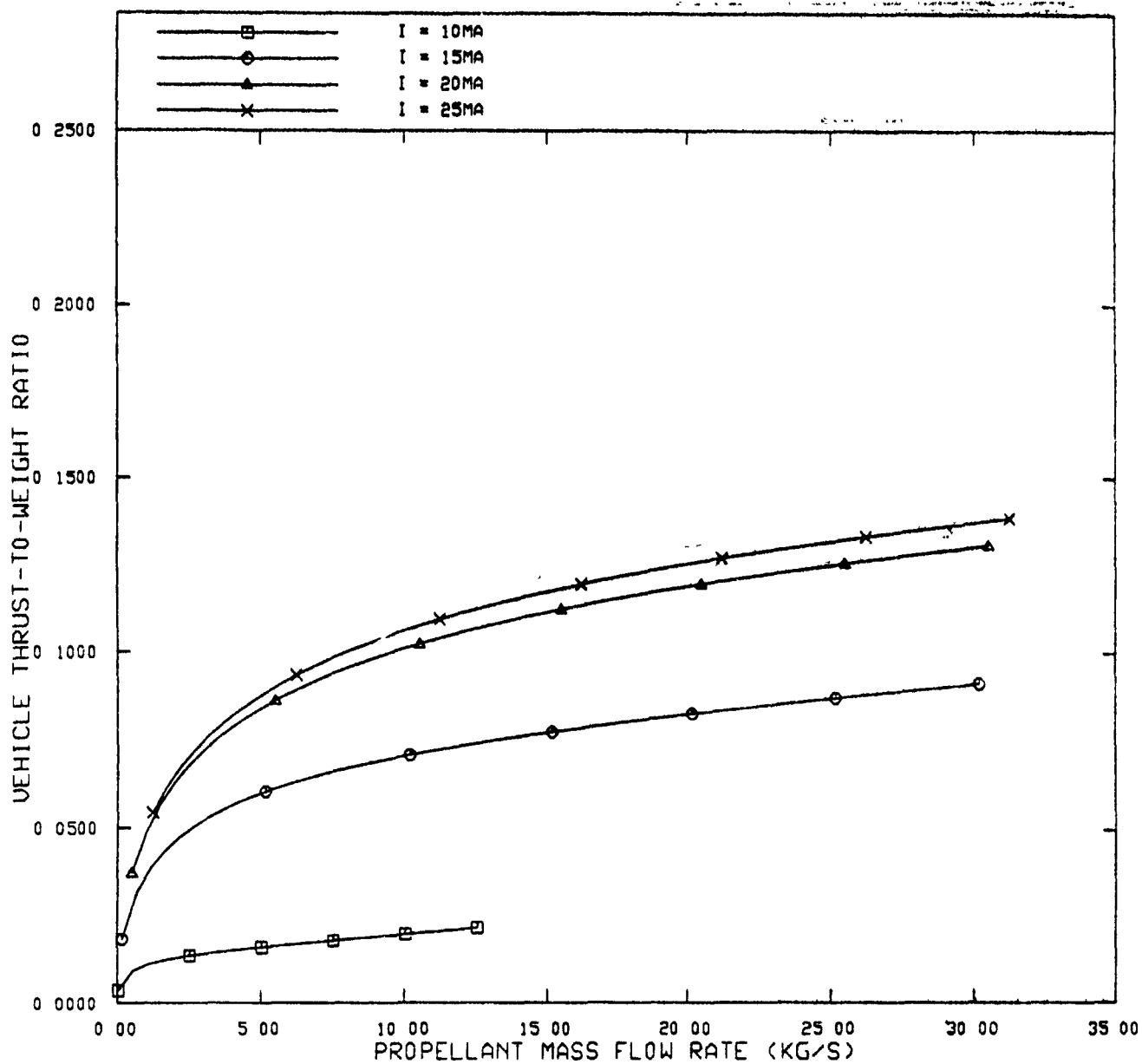


Figure 17. Vehicle F/W vs. Propellant Mass Flow Rate for $\Delta v=10$ km/s

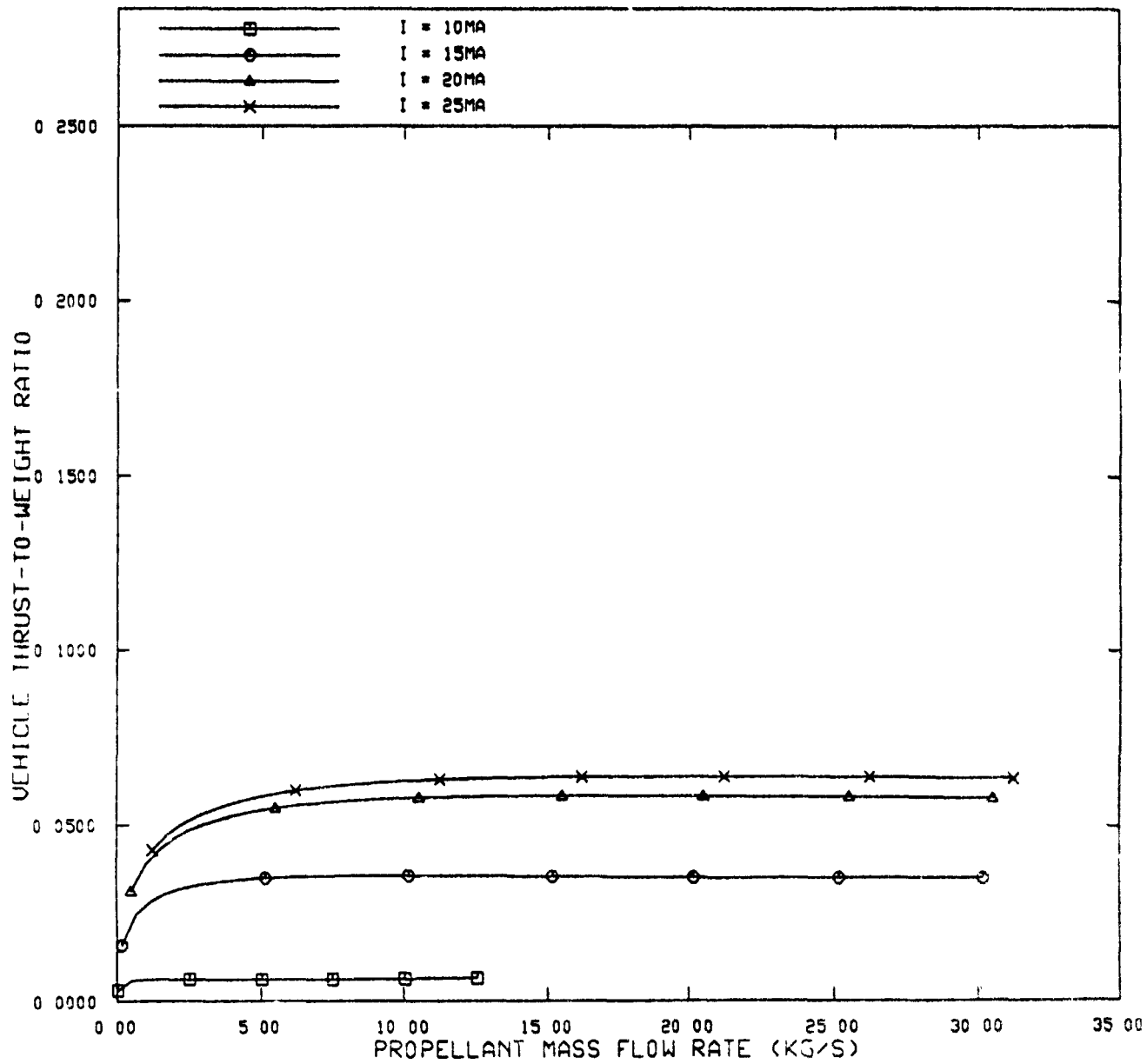


Figure 18. Vehicle F/W vs. Propellant Mass Flow Rate for $\Delta v=20$ km/s

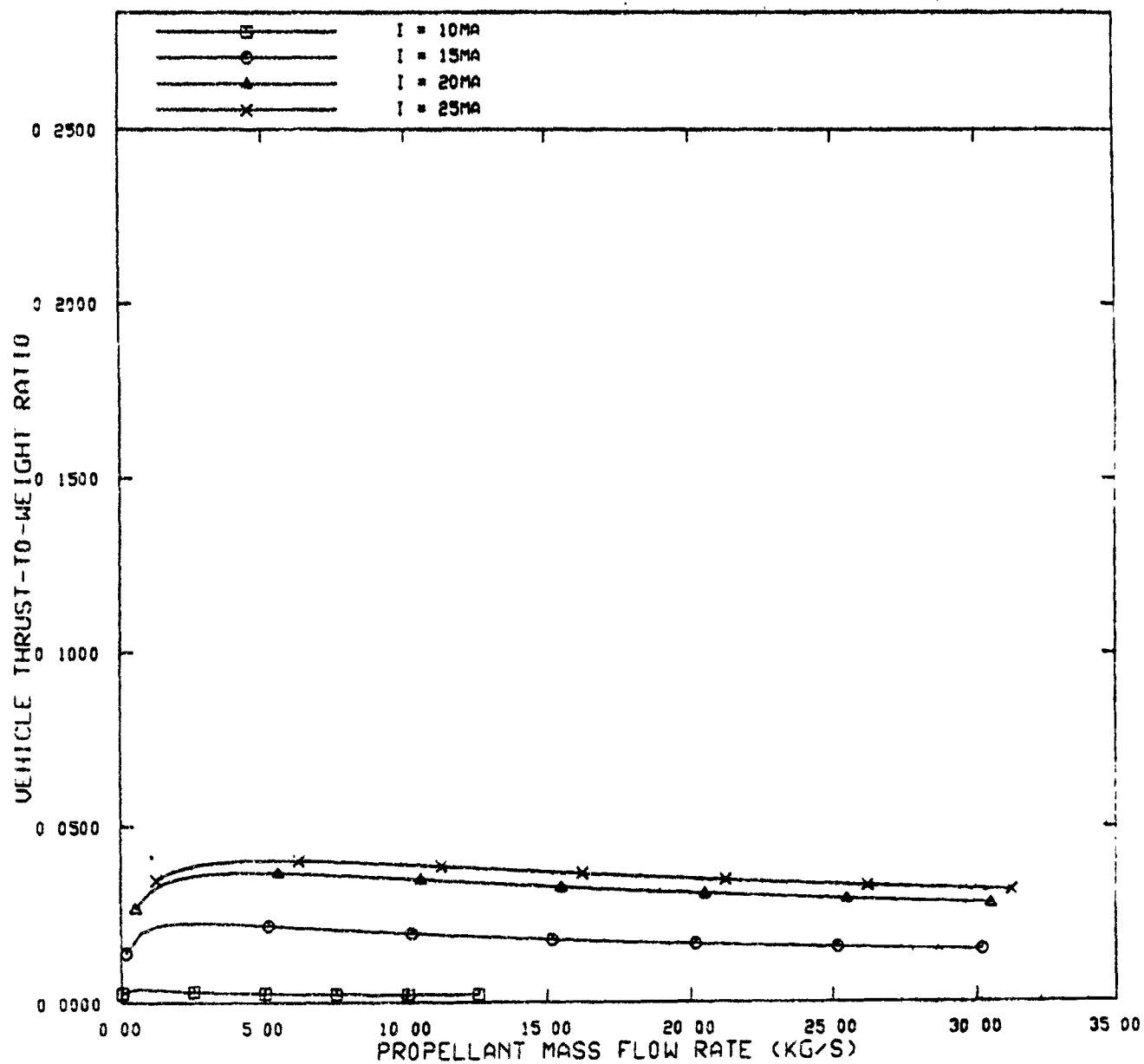


Figure 19. Vehicle F/W vs. Propellant Mass Flow Rate for $\Delta v=30 \text{ km/s}$

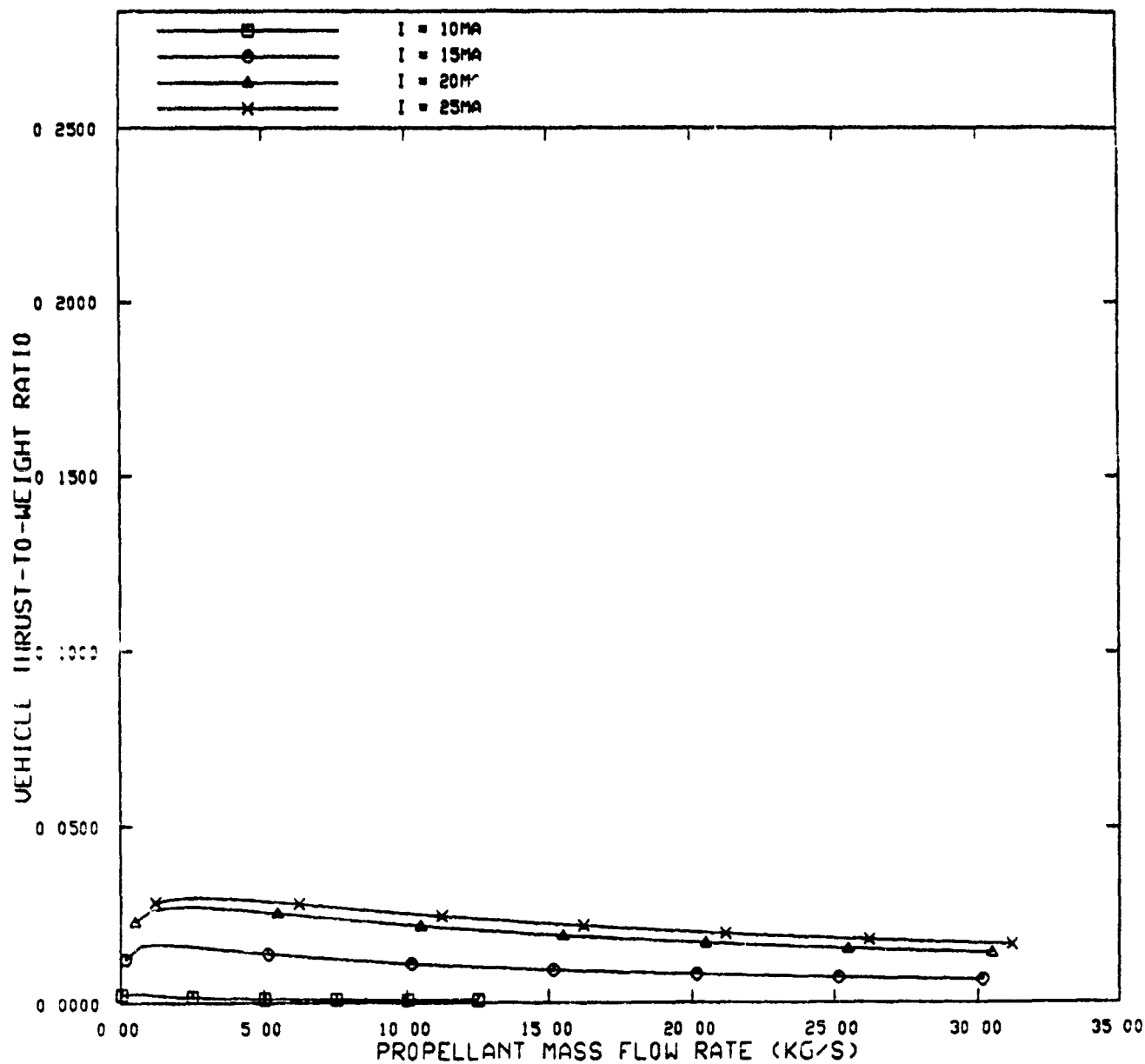


Figure 20. Vehicle F/W vs. Propellant Mass Flow Rate for $\Delta v=40$ km/s

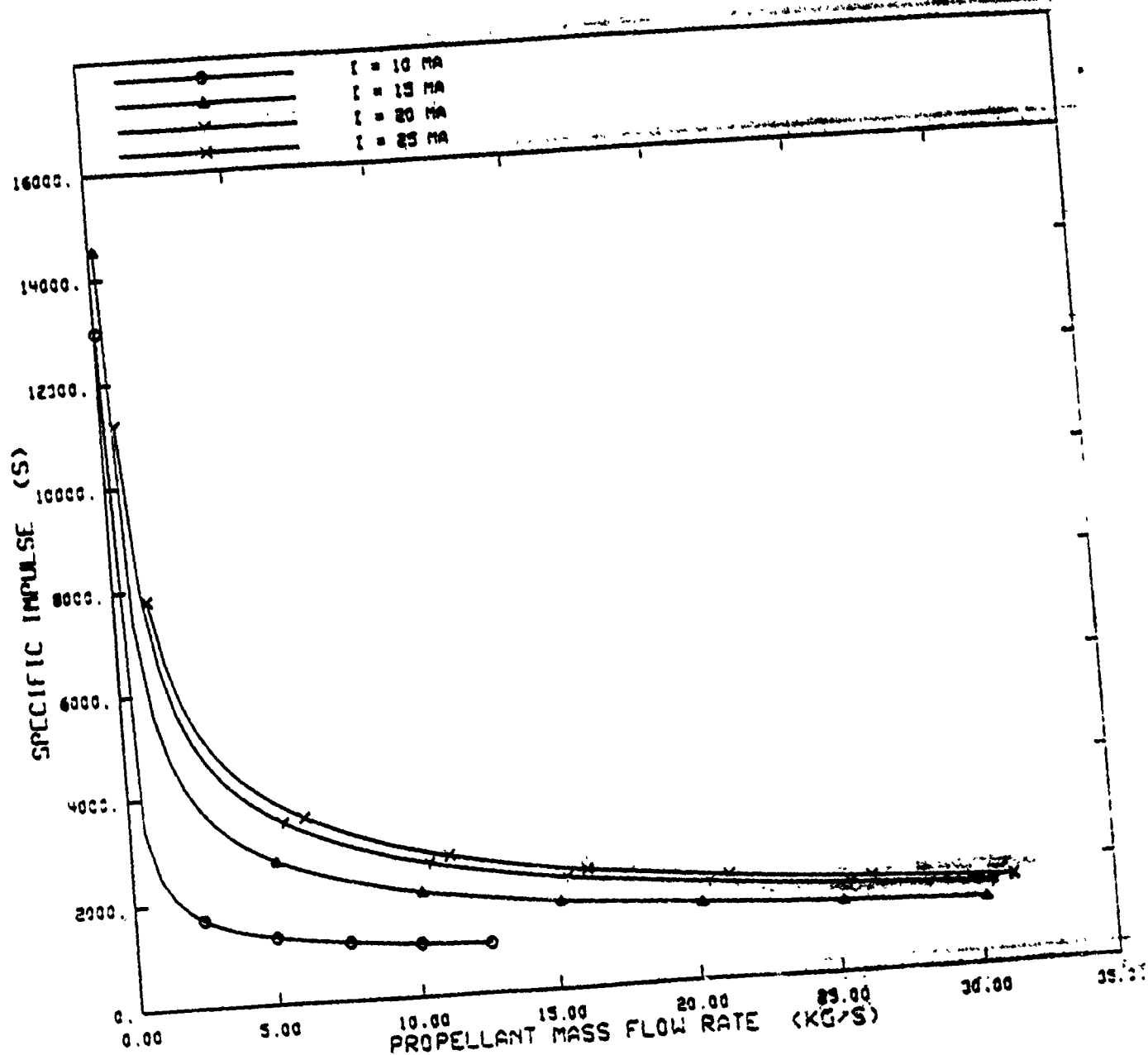


Figure 21. Specific Impulse vs. Propellant Mass Flow Rate (or any ΔV)

VEHICLE T/W VS PROPELLANT MASS FLOW AND NUMBER OF THRUSTERS

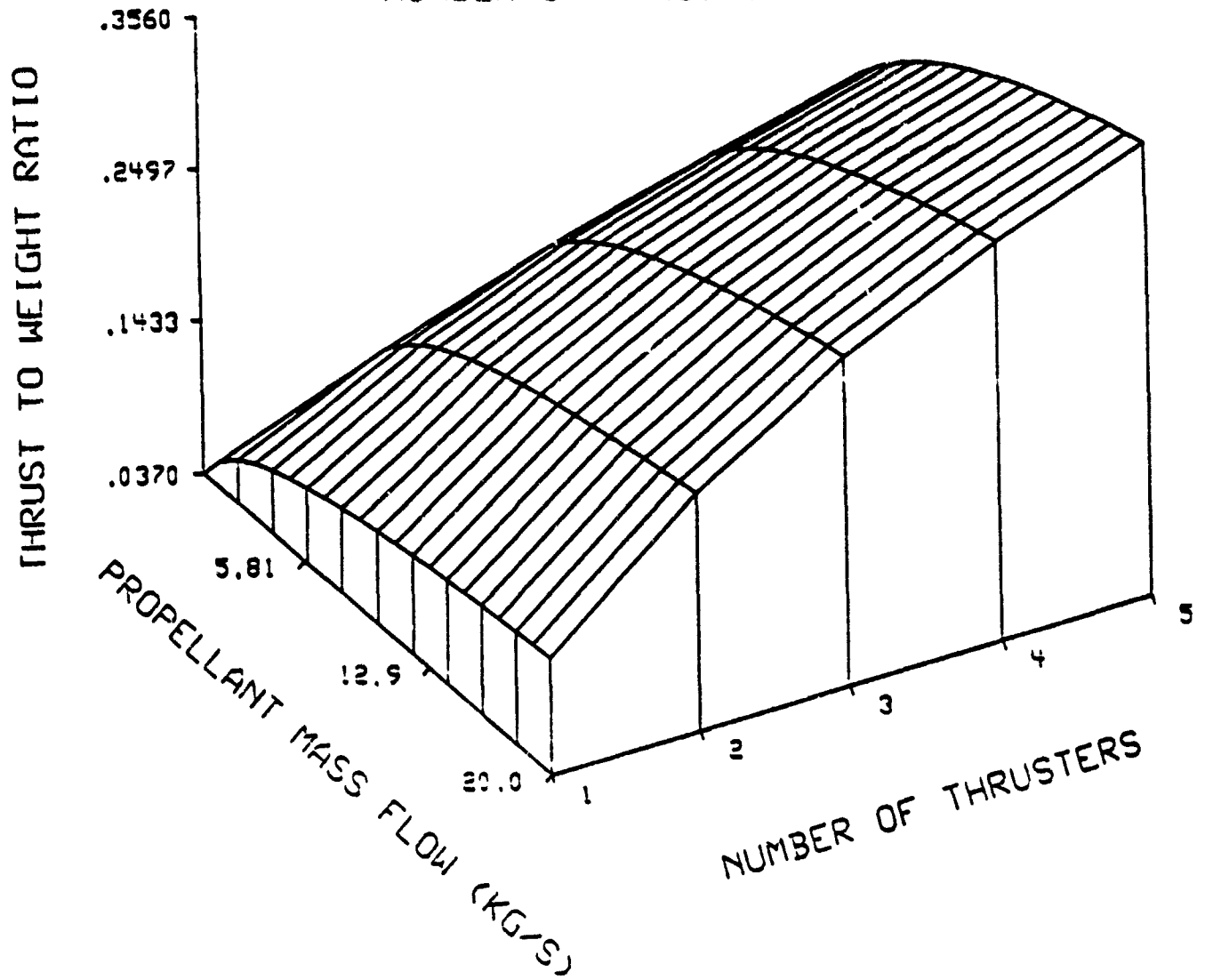


Figure 22. F/W Ratio vs. Propellant Mass Flow Rate and Number of Thrusters for $\Delta v=10$ km/s

VEHICLE T/W VS. PROPELLANT MASS FLOW AND NUMBER OF THRUSTERS

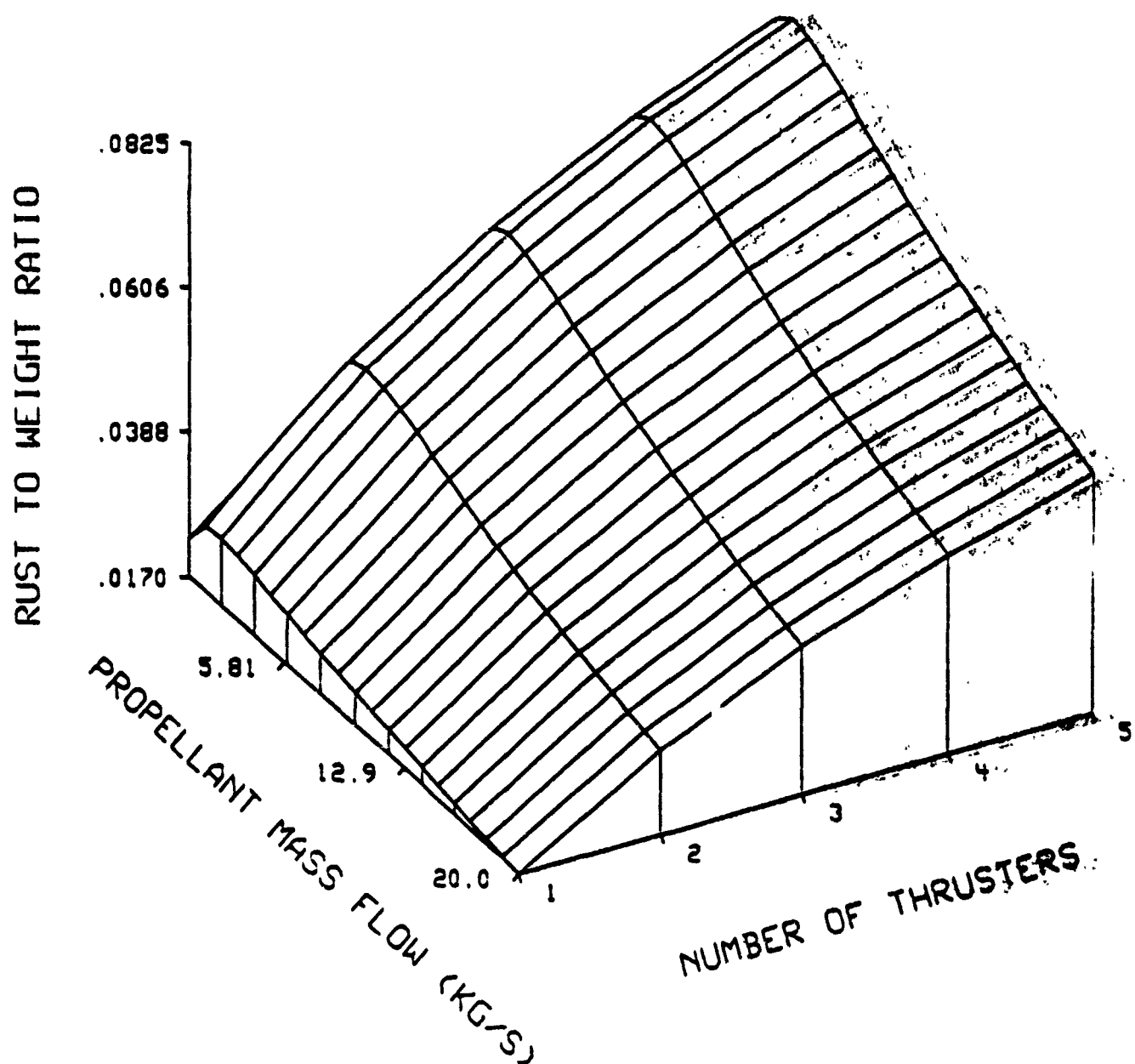


Figure 23. F/W Ratio vs. Propellant Mass Flow Rate and Number of Thrusters for $\Delta v = 40 \text{ km/s}$

the limiting factor for the number of thrusters since each thruster increases system mass and it is quite expensive to raise payload into LEO. Figure 24 shows quantitative results for 20 MA and 10, 20, 30 and 40 km/s Δv 's, respectively. Figure 25 shows that F/W ratios approaching 0.075 at an I_{sp} of about 4000 s are possible with 4 thrusters and a propellant mass flow rate of 4 kg/s. This value seems to be approaching those necessary for a manned Mars mission. In this mode, the DPF propulsion system can be competitive with chemical and nuclear fission rockets for use in distant space missions.

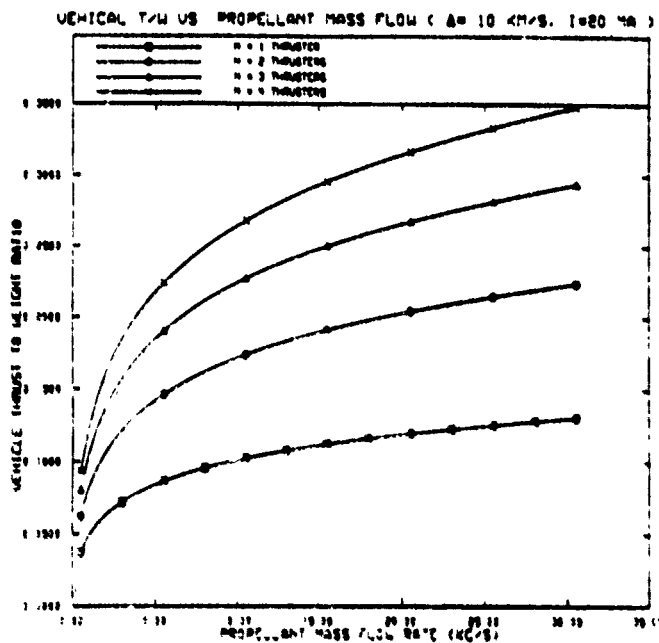
It is desirable to have F/W ratios as large as those offered by other means of propulsion, namely, chemical and nuclear fission rockets. At this time, these F/W values seem to be larger than the DPF propulsion system can produce. However, engineering breakthroughs and innovations may make these levels attainable. If capacitor specific energies can be increased to about 20 kJ/kg, system masses may be reduced until high F/W ratios are possible. Improvement in confinement time or repetition rate would also serve to increase F/W by increasing the exhaust power.

These parametric calculations are very sensitive to the assumed dimensions of the pinch. Since the fusion power depends on the plasma volume, any error in the estimation of pinch dimensions may greatly understate the amount of fusion power produced. This will in turn affect both thrust and I_{sp} . Caution should be taken when "using" these numbers in the realization that final results can depend greatly on assumed initial parameters. A computer code which calculates important propulsion parameters given the initial DPF parameters (e.g., Table 3) can be found in Appendix B.

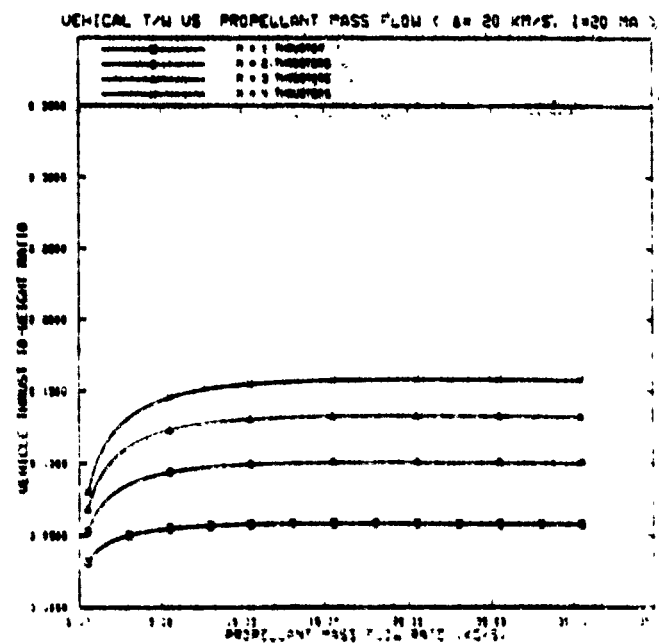
II.2. PARAMETRIC STUDIES OF DPF WITH SPIN-POLARIZED D-³He FUEL*

Recently, the effect of nuclear spin polarization of fusion fuels on fusion reactor operations has been investigated [48]. The plasma focus device analyzed Section II.1 is based on the "Livermore-I" dense plasma focus without spin-polarization. Table 4 lists all the assumed parameters used in the evaluation including the capacitor banks being capable of delivering a maximum current in excess of 10MA.

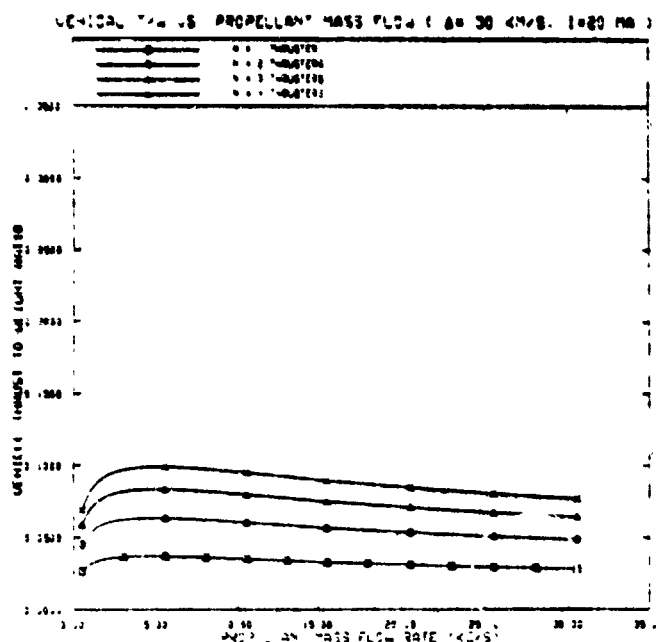
* The major portion of this section of the report has been documented as the M.S. project report by M. Wang as a partial requirement for the M.S. degree from Purdue University.



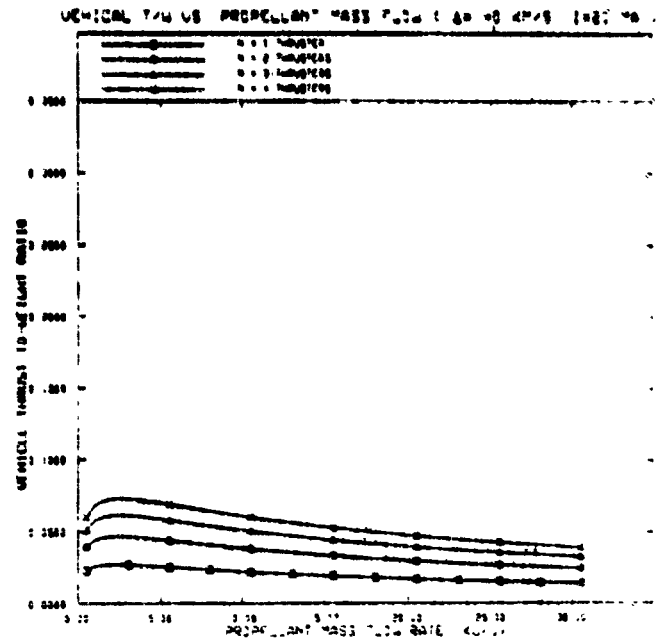
$\Delta v = 10$ km/s



$\Delta v = 20$ km/s



$\Delta v = 30$ km/s



$\Delta v = 40$ km/s

Figure 24. Vehicle F/W vs. Propellant Mass Flow Rate for $I=20$ MA and $\Delta v = 10 - 40$ km/s.

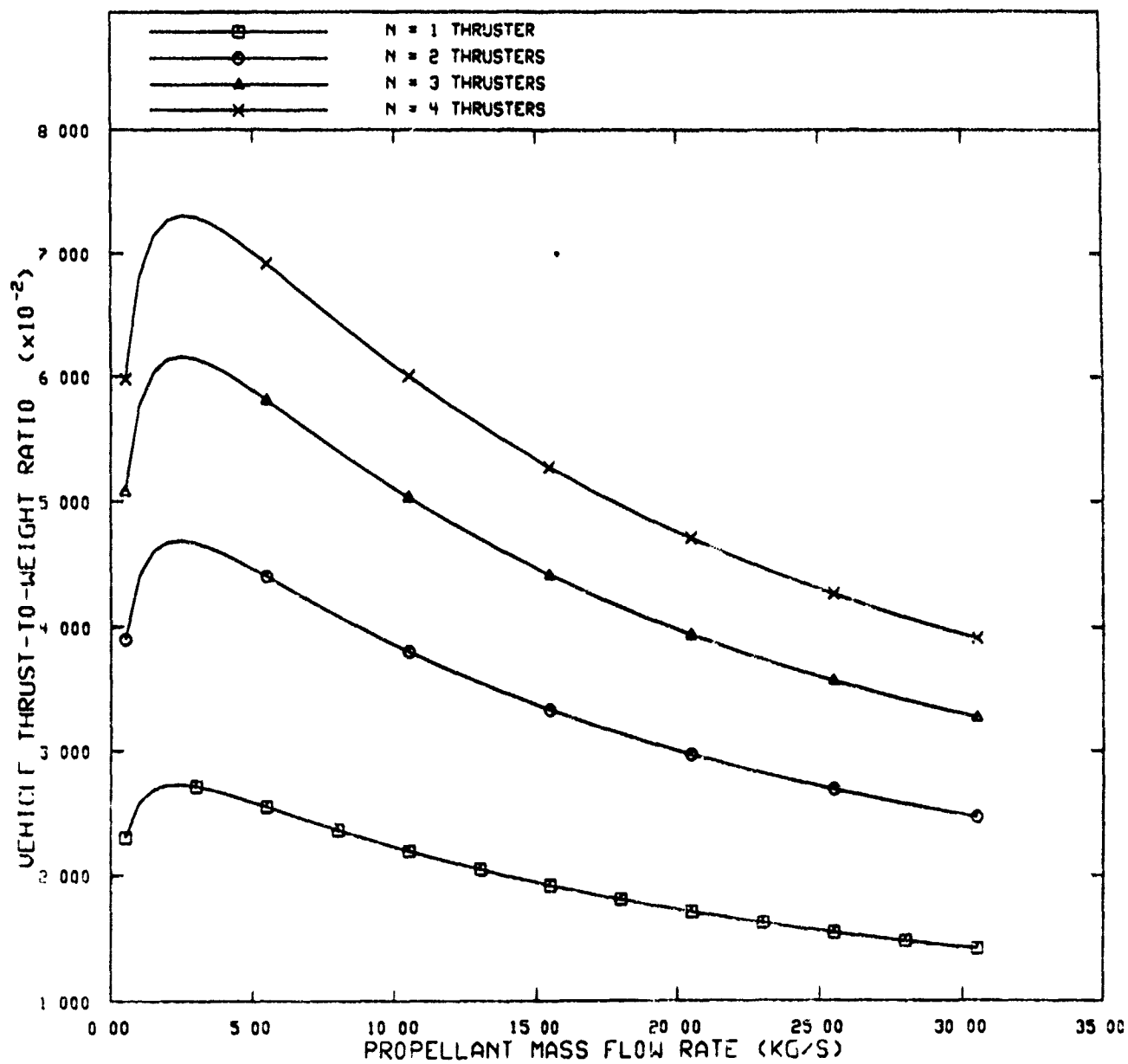


Figure 25. Vehicle F/W vs. Propellant Mass Flow Rate for $I=20$ MA and $\Delta v=40$ km/s

Table 4. Assumed Parameters of DFT Propulsion System

Plasma Focus Parameters

Capacitor Bank Charging Potential	V	(Volt)	27,000
Initial Conductance	L_0	(H)	2.50×10^{-8}
Initial Capacitance	C_0	(F)	1.25×10^{-4}
Initial Gas Fill Density	ρ_i	(kg/m ³)	2.30×10^{-4}
Snowplow Efficiency Factor	f_s		0.70
Pinch Efficiency Factor	f_p		0.25
Anode Radius	r_a	(m)	0.0008
Cathode Radius	r_c	(m)	0.00
Pinch Radius	r_p	(m)	0.0015
Anode Length	l_a	(m)	0.982
Pinch Length	l_p	(m)	0.0034
Maximum Discharge Current	I	(Amp)	15.00×10^6
Fraction of D in Initial Fill Gas	f_d		0.50
Fraction of ³ He in Initial Fill Gas	f_{he}		0.50
Plasma Focus Firing Rate	R_{rep}	(s ⁻¹)	700
Duration of Stable Pinch	t	(s)	1.00×10^{-4}
Fill Gas Discharge Time	t_{dis}	(s)	1.00×10^{-7}
Specific Energy		(kJ/kg)	2.00
Fraction of Cyclotron Radiation in Plasma	f_{cyc}		0.60
Fraction of Cyclotron Radiation in Wall	f_c		0.20

Systems Parameters

Power for Running Magnet	P_m	(MW)	0.01
Turbine Inlet Temperature	t_{in}	(°K)	2,000
Turbine Efficiency			20%
Turbine Exit Temperature	T_{out}	(°K)	700
Propellant Dissociated and Ionized Temperature	T_{di}	(°K)	5,000

Consistent with the earlier analysis in Section II.1, the impulsive operation mode is considered to be most suitable for interplanetary travel due to its higher F/W ratios. Thus this section attempts to make a comparison for impulsive operation of DPF propulsion system with the spin-polarized fuel. Since the system mass is very important for fusion propulsion with the capacitor mass being the major one among the system components, the scaling of the capacitor mass with its current becomes a key issue in the analysis. For the "Livermore-I" device, it was initially assumed that the capacitor mass scaled as the current squared. However, as indicated earlier in Section II.1 and also in Appendix A, it can be shown that the capacitor mass might possibly scale as $I^{8/3}$. In this section, both cases are discussed. Multiple thrusters are also considered since they not only provide insurance against a failure but also can raise the F/W values. The extra thrust produced by additional thrusters more than compensates for the extra mass due to capacitors, shielding, etc. As shown earlier in Figs. 22 and 23 for I^2 scaling, the F/W values with $I^{8/3}$ scaling (e.g., Figures 42 and 43) are more pessimistic than those with I^2 scaling, and in this case, multiple thrusters are much less effective than for I^2 case.

Figure 26 for the I^2 scaling case shows the variation of specific impulse for any Δv as well as any thruster number since the propellant exit velocity is only dependent on DPF system parameters and the additional thrusters will not affect I_{sp} values. From this figure, it is obvious that the spin polarization can increase the specific impulse. Figures 27 and 28 illustrate the dependence of F/W on propellant mass flow rate and F/W vs. I_{sp} , respectively, for low Δv ($\Delta v = 10$ km/s) from 1 to 4 thrusters. Figures 29 and 30 show the same parameters for high Δv ($\Delta v = 40$ km/s). All the figures prove again that the spin polarization makes the F/W values increase. Figure 27 seems to show that F/W can be increased indefinitely by simply exhausting more propellant; however, this lowers the propellant outlet temperature which in turn increases the total amount of propellant required for the mission. This is not apparent in missions with small Δv 's since the originally required propellant mass is so small compared to other system masses. Figure 29 actually shows the cases where propellant becomes the dominant mass and an increase in propellant mass flow actually decreases system F/W. But as one can see from Figures 27 and 29, the highest current no longer leads to the highest F/W as number of thruster increased. The optimum current now occurs at about 20MA. This is because for more thrusters the more propellant mass must be carried along with capacitor mass at higher current. And since the spin polarization can reduce the propellant mass, this makes the shift of the curves at 20MA and 25MA more obvious. The crossover between the 20 and 25MA case is due to the additional capacitor mass being compensated for by the additional propellant mass which must be carried along at the lower current. The x-axes of Figures 28 and 30 indicate propellant mass flow decreasing while specific impulse increases according to specific impulse changing

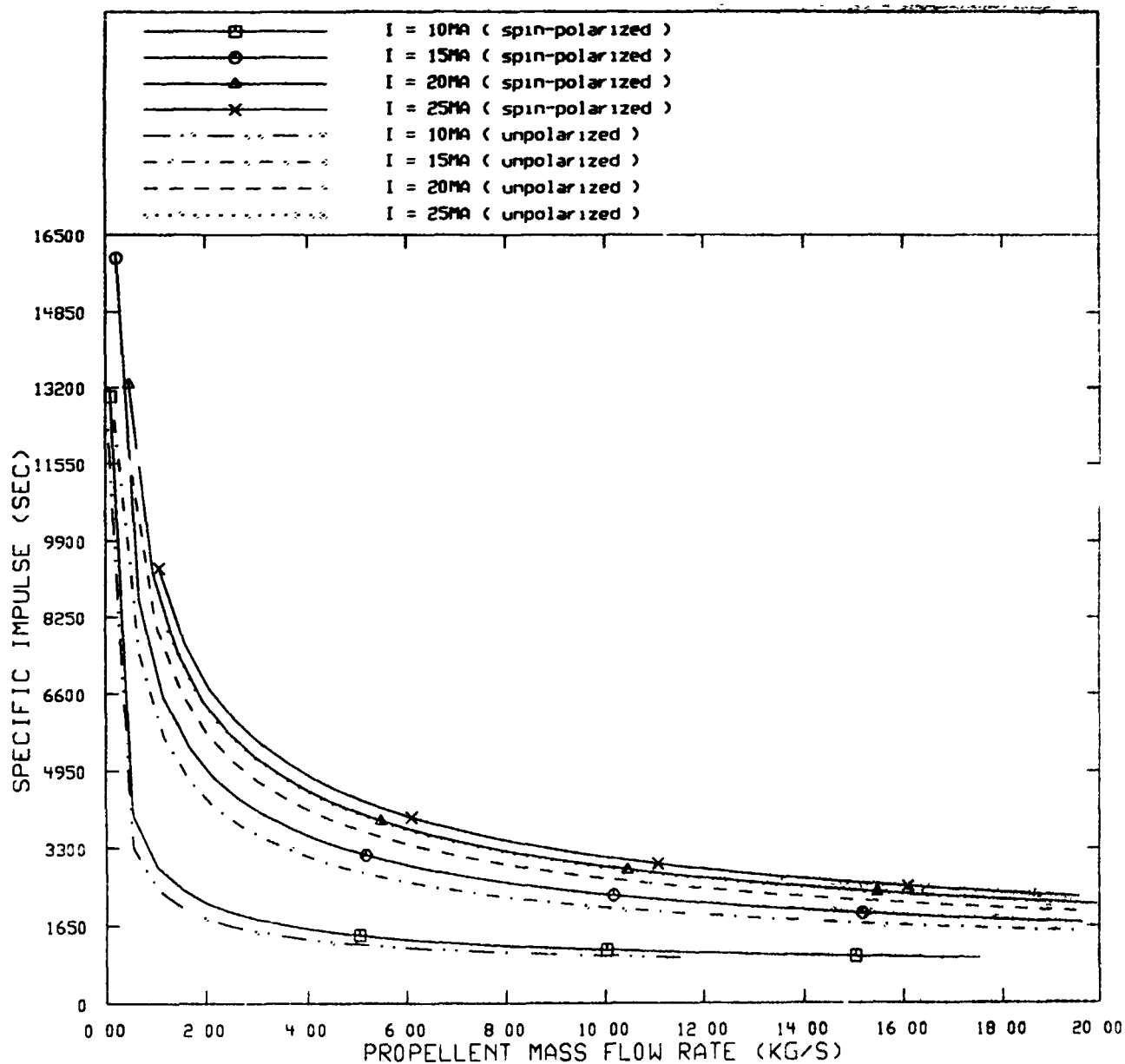
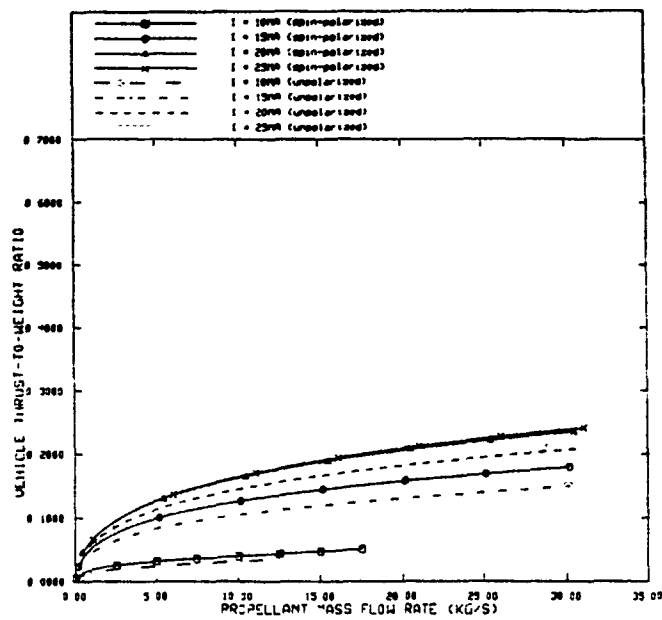
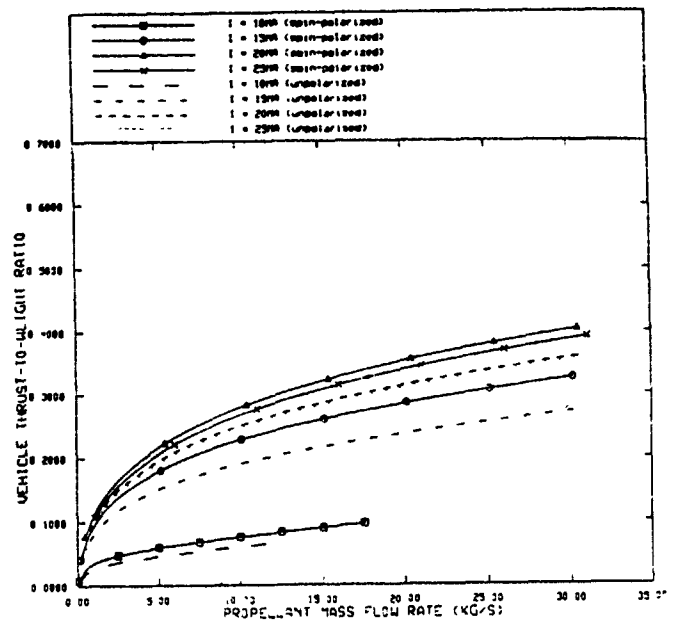


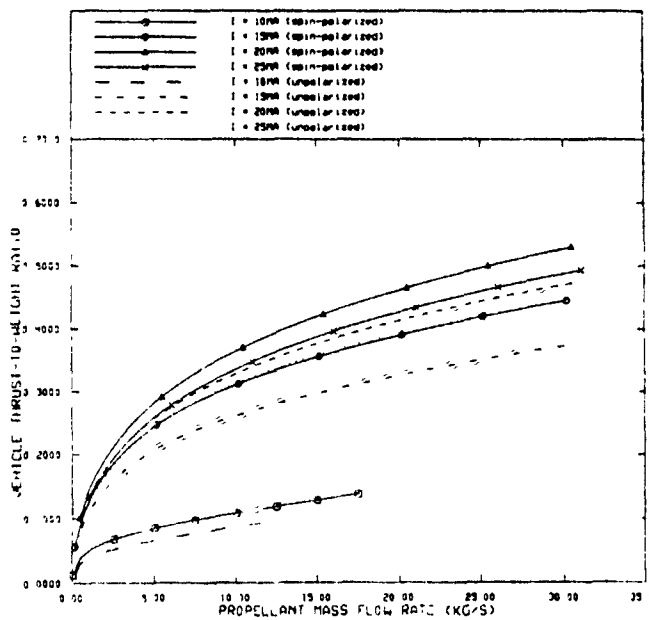
Figure 26. Specific Impulse vs. Propellant Mass Flow Rate



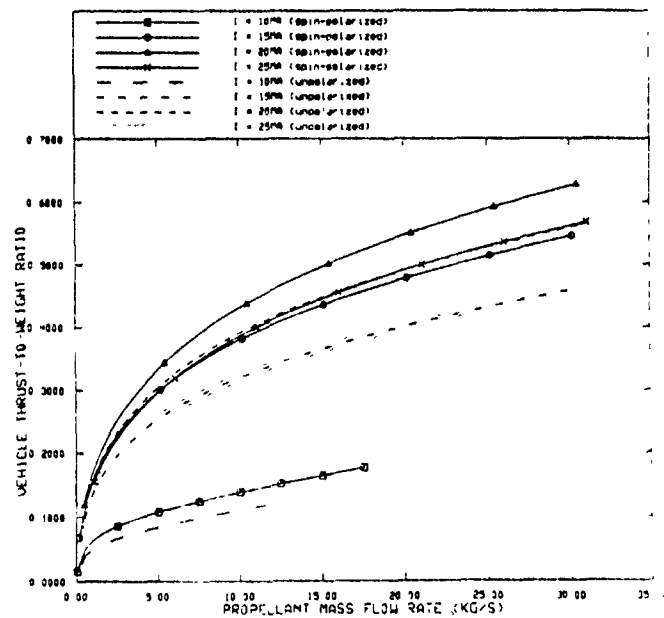
a) 1 thruster



b) 2 thrusters

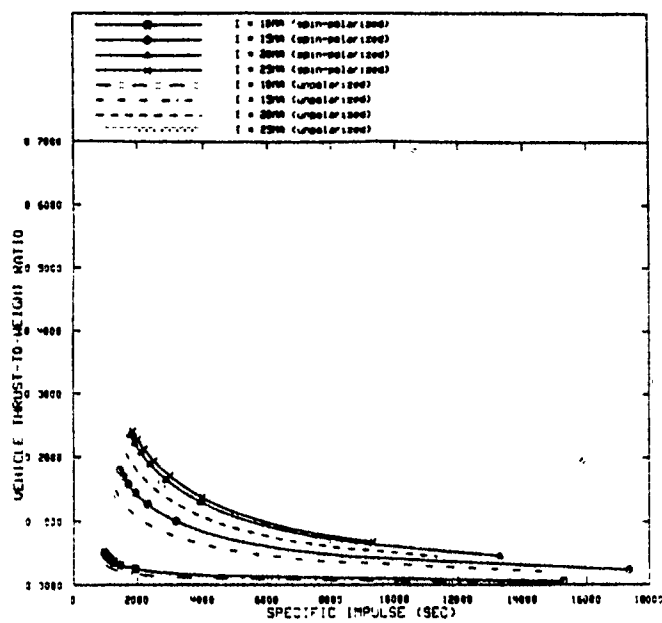


c) 3 thrusters

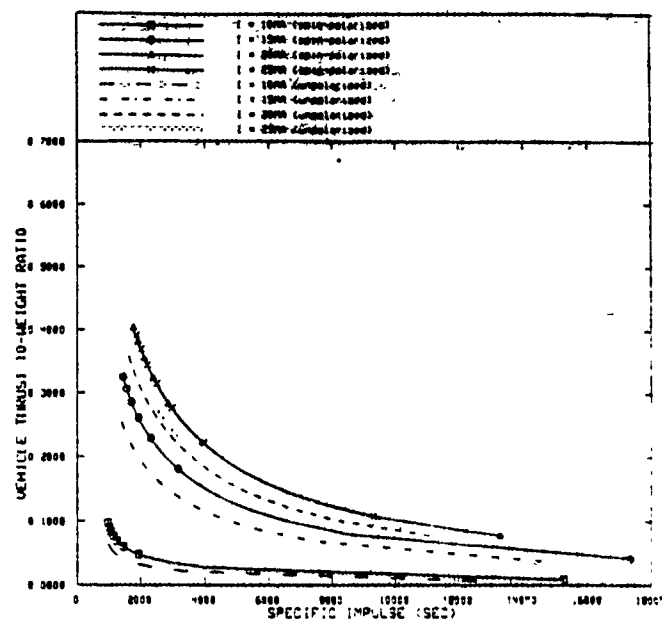


d) 4 thrusters

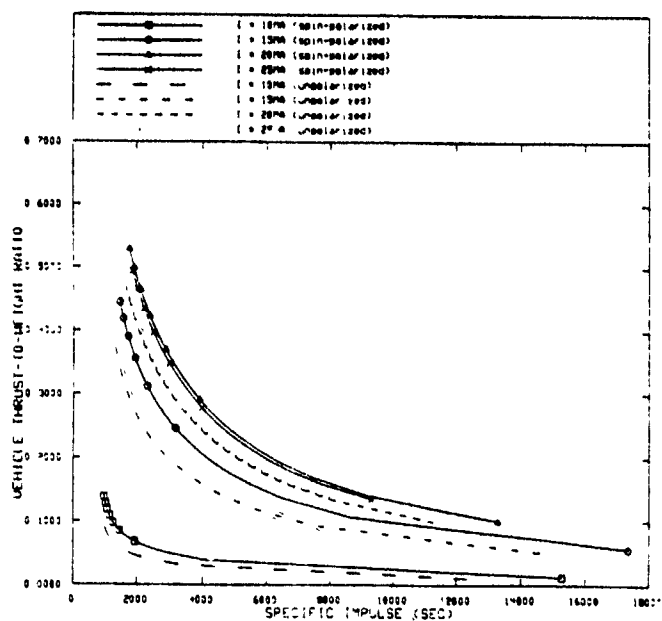
Figure 27. Vehicle F/W vs. Propellant Mass Flow Rate for $\Delta v=10\text{km/s}$ (I^2 Scaling)



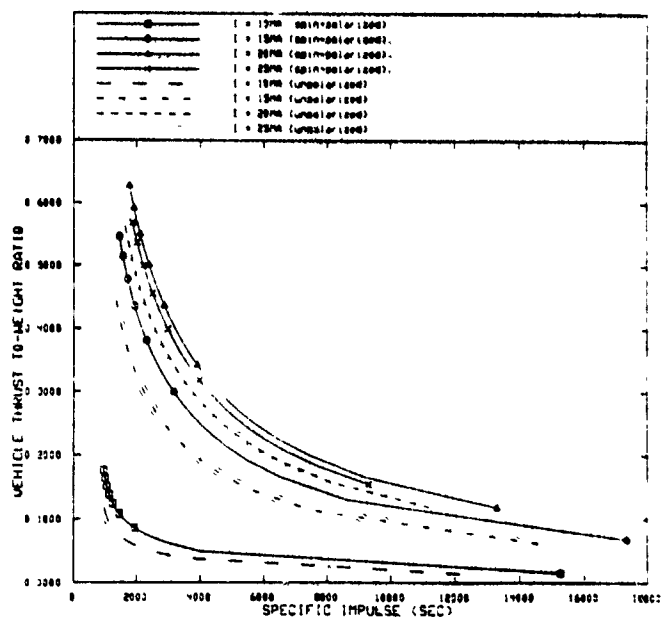
a) 1 thruster



b) 2 thrusters

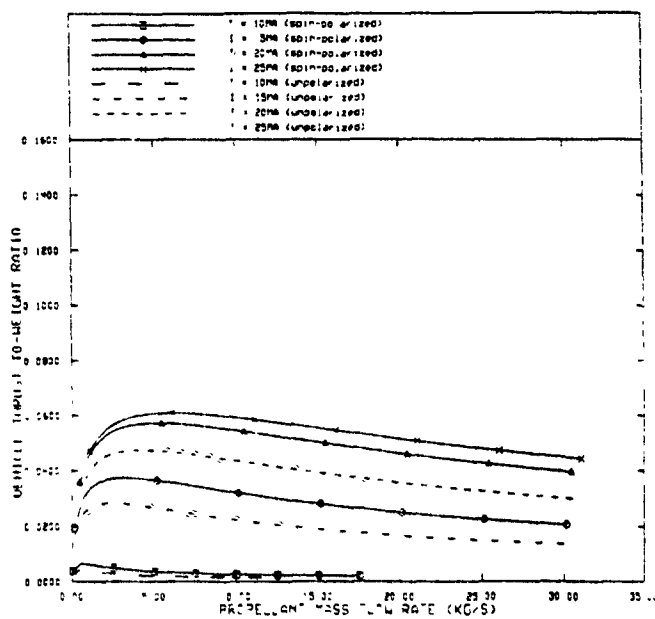


c) 3 thrusters

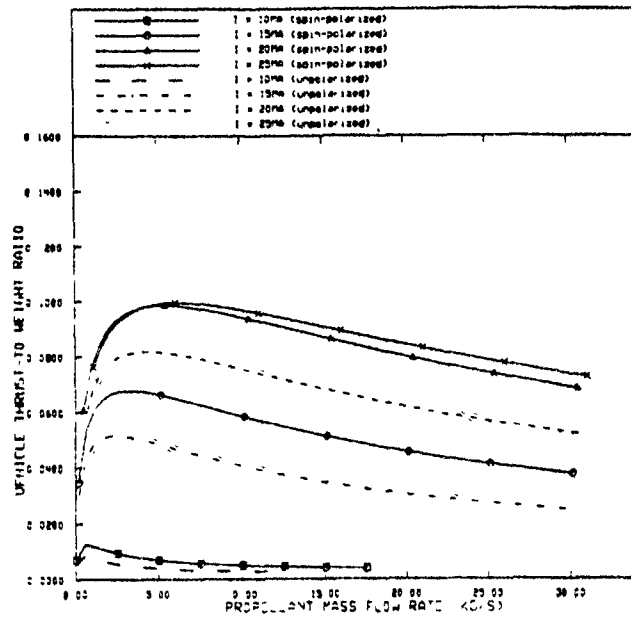


d) 4 thrusters

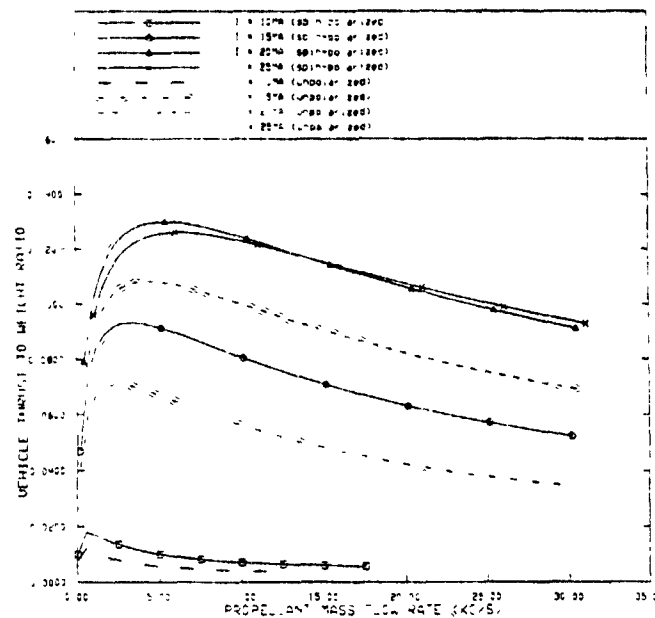
Figure 28. Vehicle F/W vs. Specific Impulse for $\Delta v=10\text{km/s}$ (I^2 Scaling)



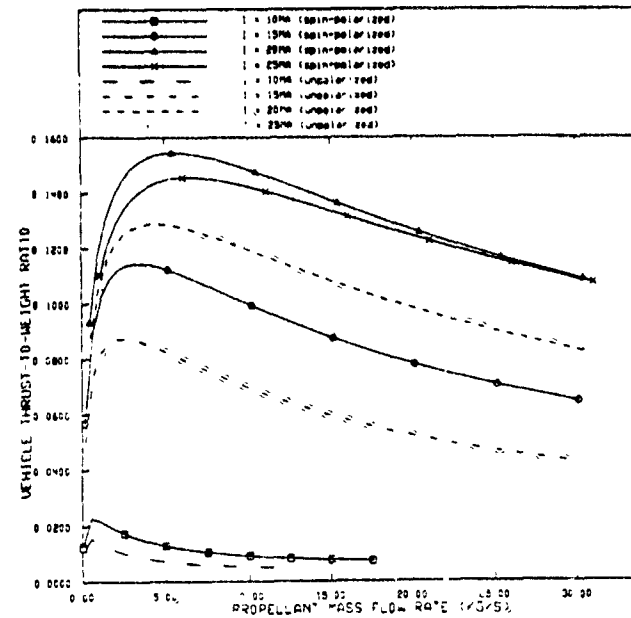
a) 1 thruster



b) 2 thrusters

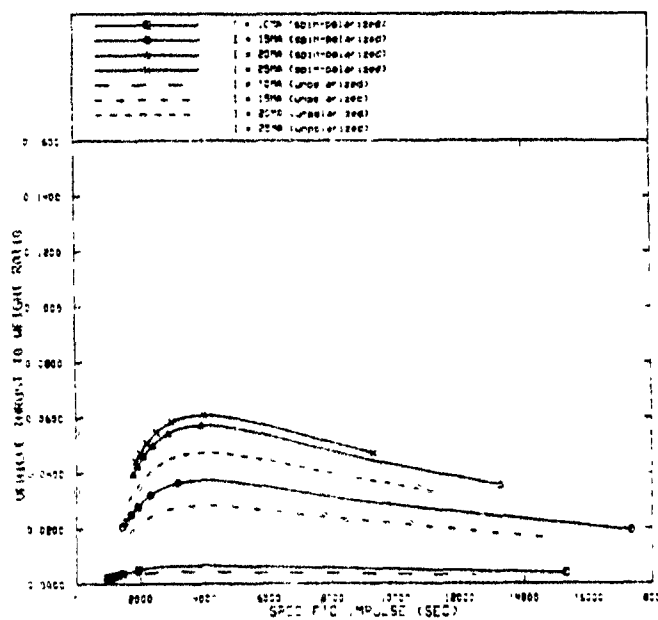


c) 3 thrusters

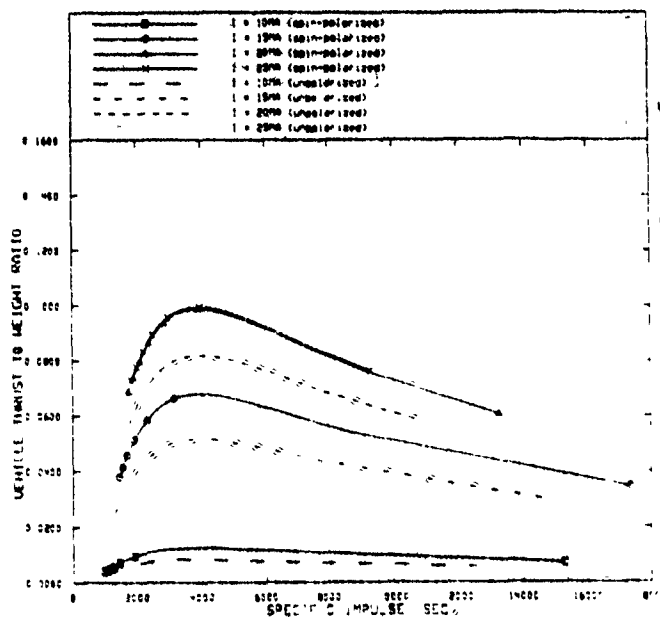


d) 4 thrusters

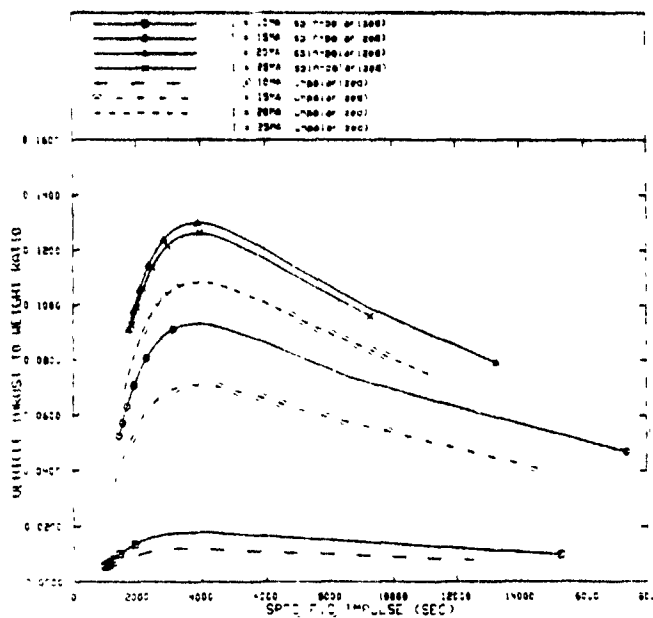
Figure 29. Vehicle F/W vs. Propellant Mass Flow Rate for $\Delta v=40\text{km/s}$ (I^2 Scaling)



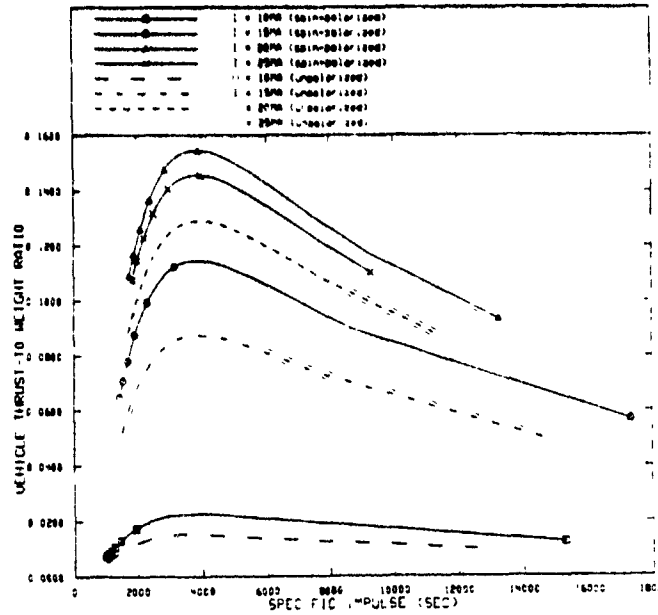
a) 1 thruster



b) 2 thrusters



c) 3 thrusters



d) 4 thrusters

Figure 30. Vehicle F/W vs. Specific Impulse for $\Delta v=40\text{km/s}$ (I^2 Scaling)

adversely with propellant mass flow as shown in Figure 26. The curves bend differently because the F/W increases with propellant at low Δv but has an optimum value at propellant mass flow about 5 kg/s (from Figure 29), i.e., specific impulse about 4000 s (from Figure 26) for spin-polarized case. Since the optimum current is 20MA and F/W values increase with number of thrusters, Figure 31 and 32 demonstrate the trend of F/W vs. propellant mass flow and F/W vs. I_{sp} for different Δv . Obviously, DPF propulsion can produce higher F/W for low Δv missions. This is consistent with the implication in Sect. II.1 that DPF propulsion systems are best suited for low Δv missions.

For the $I^{8/3}$ scaling case, almost the exact same information is presented except that the F/W values are lower and the optimum current becomes 15MA as shown in Figures 33 to 36. This is due solely to the increasing capacitor mass at higher currents which was not so evident before because of the I^2 scaling. Comparing Figure 24 to Figure 33, and Figure 35 to Figure 36, one notes thruster performance being adversely affected by the higher capacitor masses due to the new $I^{8/3}$ scaling relation. The increasing number of thrusters does little to increase F/W and the raising of the propellant mass flow rate drastically reduces F/W because of the large propellant masses involved. Again, spin polarization reduces propellant mass requirements at higher Δv which makes the 15MA curve rise up more rapidly.

From the analysis above, one recognizes that there is a corresponding optimum condition for each Δv and scaling relation. The conditions which can provide the maximum F/W, i.e., $\Delta v = 10$ km/s, $I = 20$ MA, and using 4 thrusters, are chosen to make the comparison between the base case and the spin-polarized case as listed in Tables 5-1 and 5-2 for low and high Δv 's, respectively. Various parameters in Tables 5-1 and 5-2 are described in the subsequent discussions.

The total fusion power produced by DPF is

$$P_F = \pi r_p^2 I_p [n_D n_{He} \langle \sigma v \rangle_{DH} W_{DH} + \frac{1}{2} n_D^2 (\langle \sigma v \rangle_{DDn} W_{DDn} + \langle \sigma v \rangle_{DDp} W_{DDp})] R_{rep} t \quad (17)$$

where R_{rep} is number of firings per unit time (s^{-1}), and t is pinch stable time(s), as described in Table 4. Due to low cross-sections at the operating temperatures of $D-^3He$, secondary reactions including D-T, T-T, and $^3He-^3He$ reactions are not included in Eq.(17).

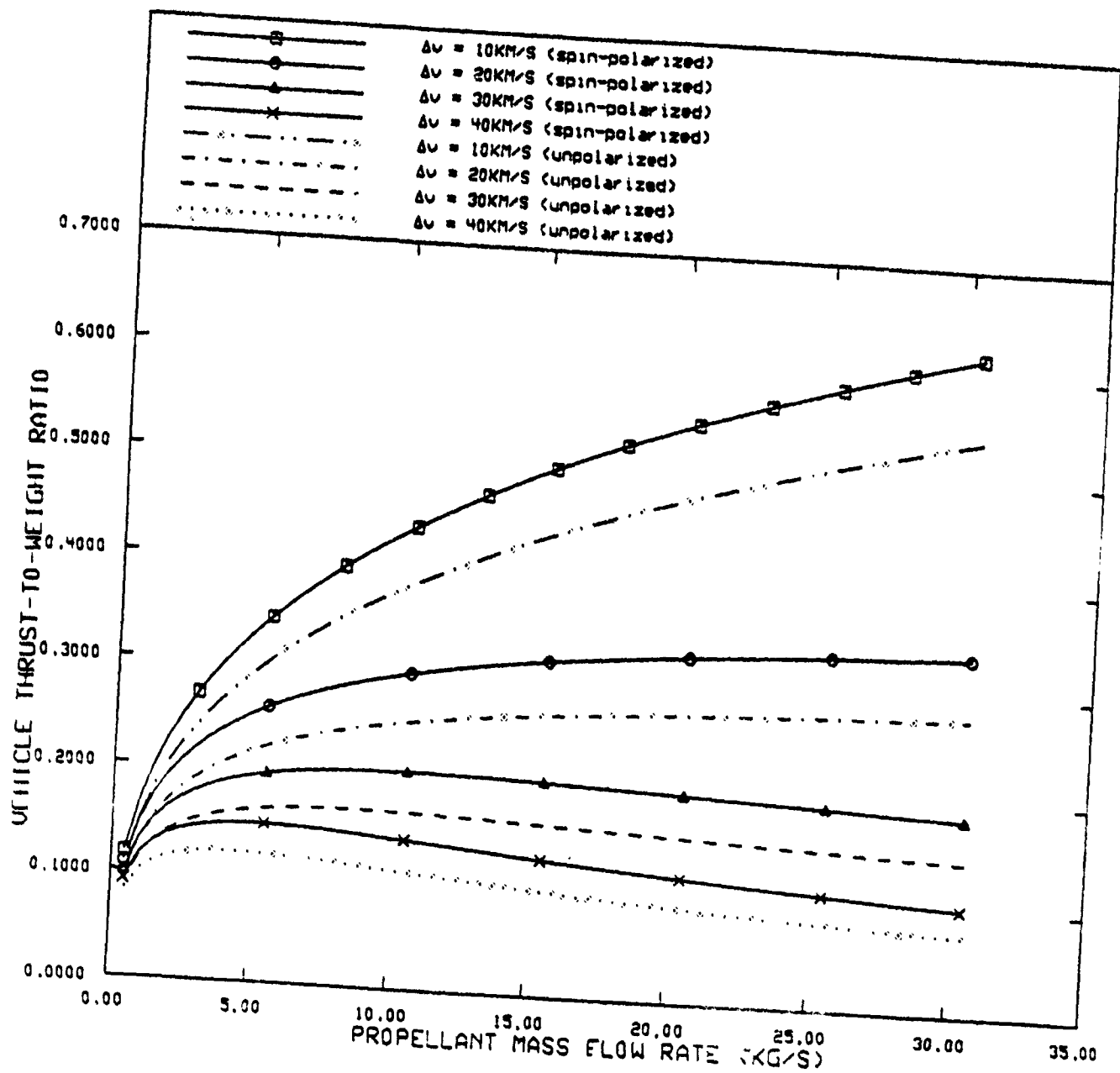


Figure 31. Vehicle F/W vs. Propellant Mass Flow Rate for $\Delta v = 10$ km/s ($I^{8/3}$ Scaling)
($I = 20$ MA, 4 Thrusters)

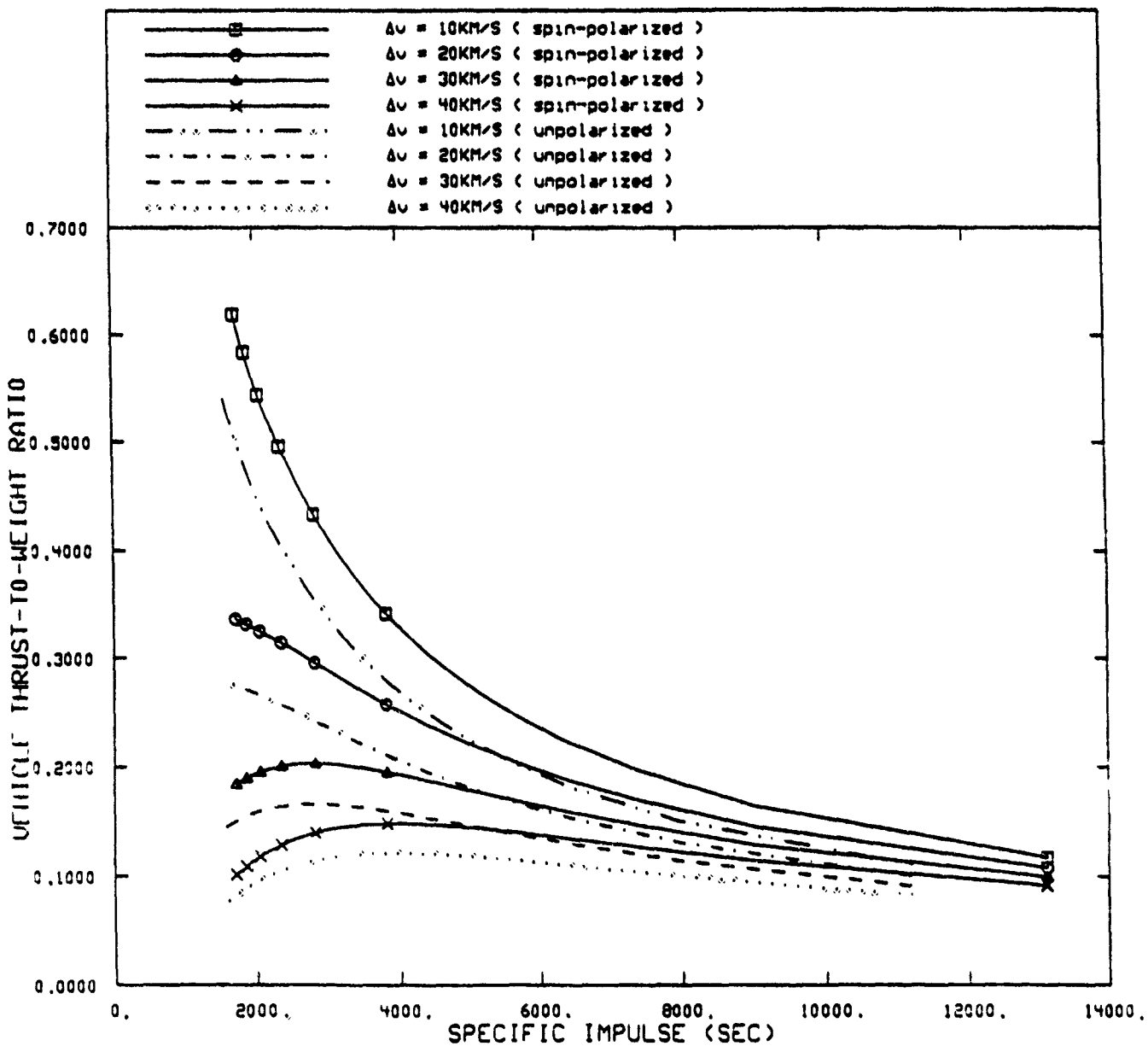
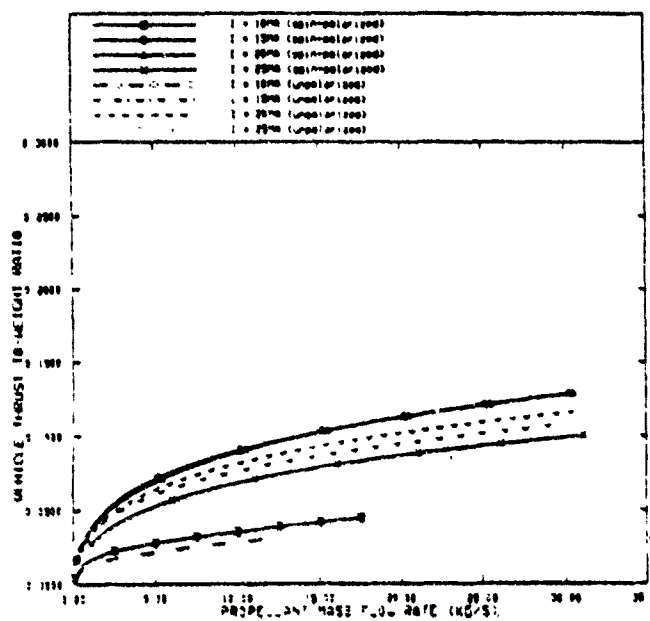
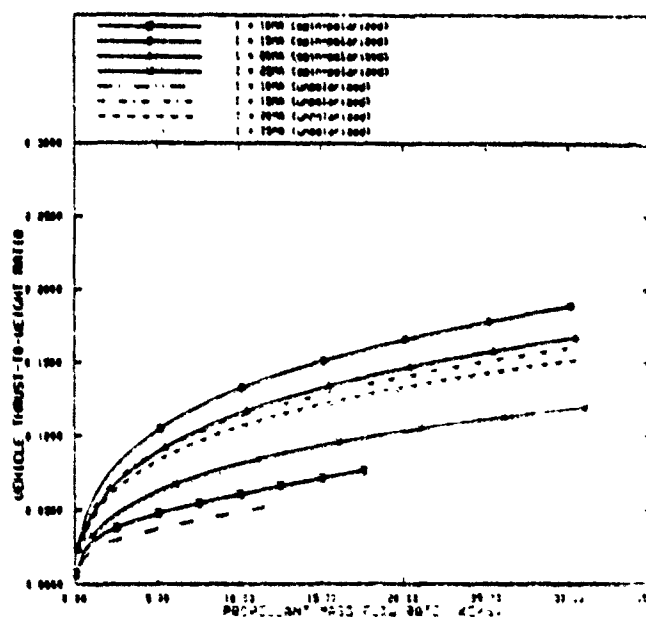


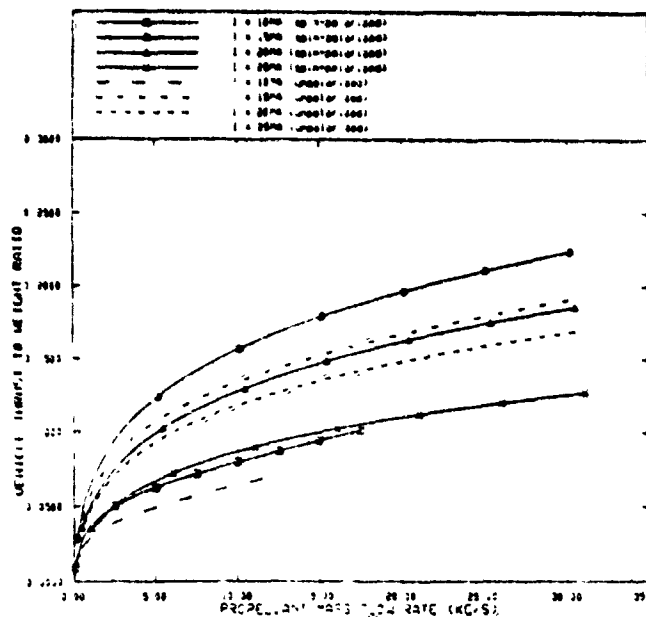
Figure 32. Vehicle F/W vs. Specific Impulse for Δv (I^2 Scaling)
($I=20\text{MA}$, 4 thrusters)



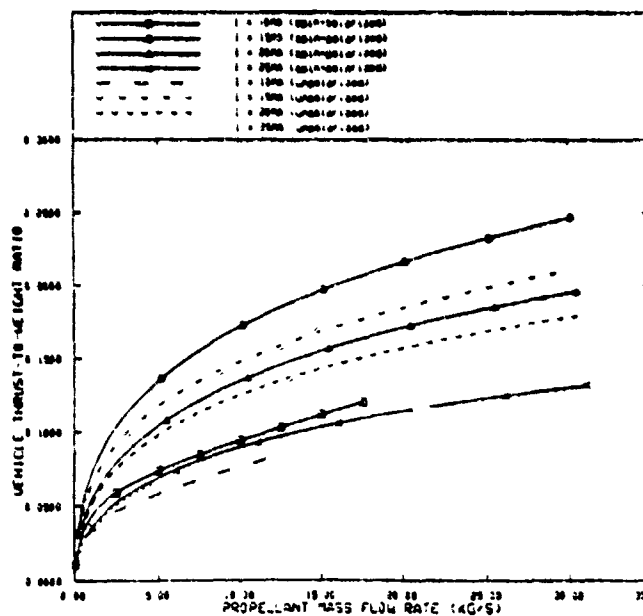
a) 1 thruster



b) 2 thrusters

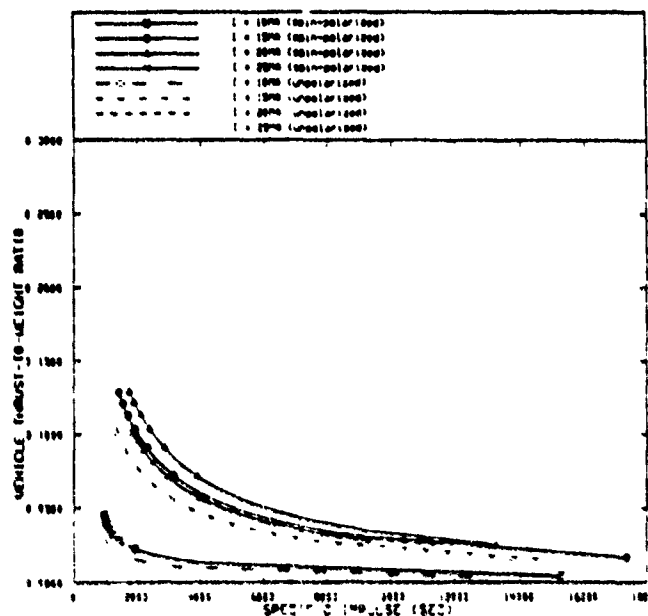


c) 3 thrusters

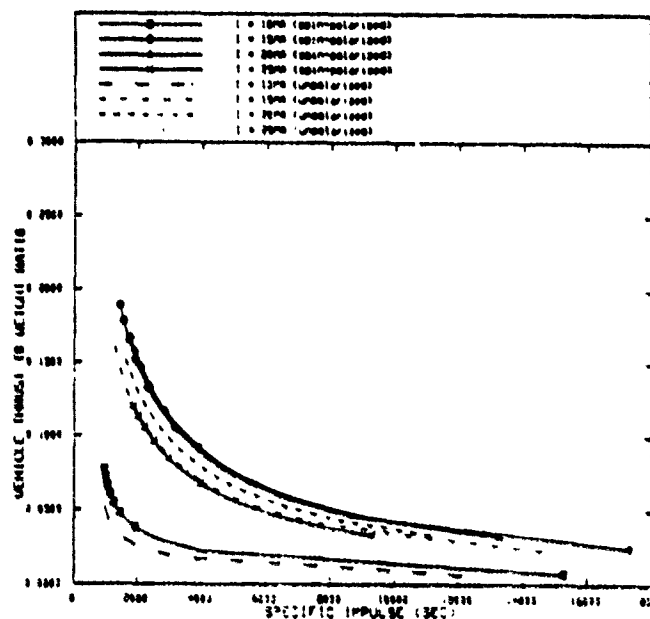


d) 4 thrusters

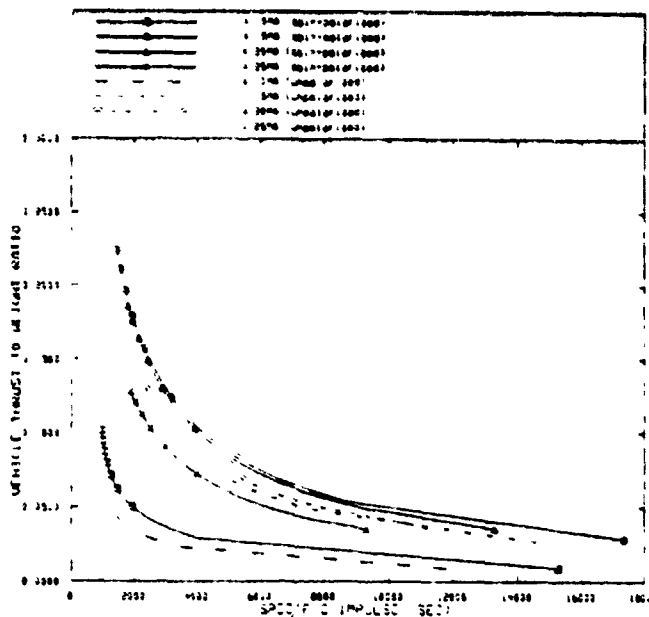
Figure 33. Vehicle F/W vs. Propellant Mass Flow Rate for $\Delta v=10\text{km/s}$ ($1^{8/3}$ Scaling)



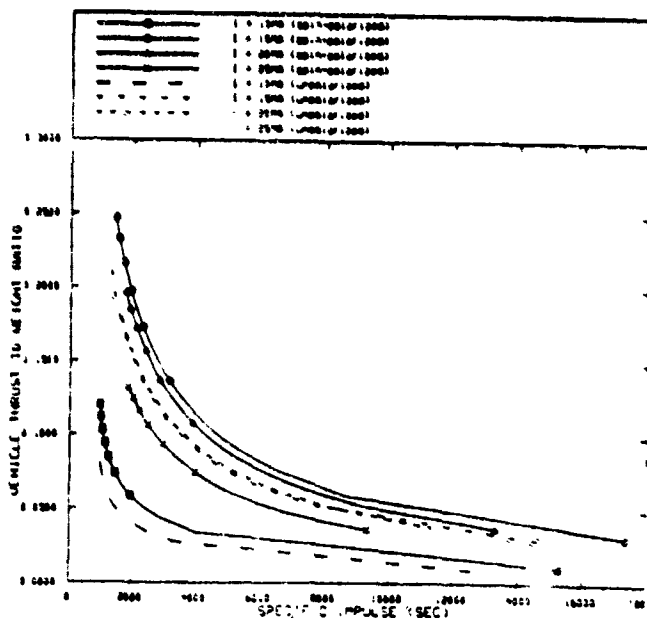
a) 1 thruster



b) 2 thrusters

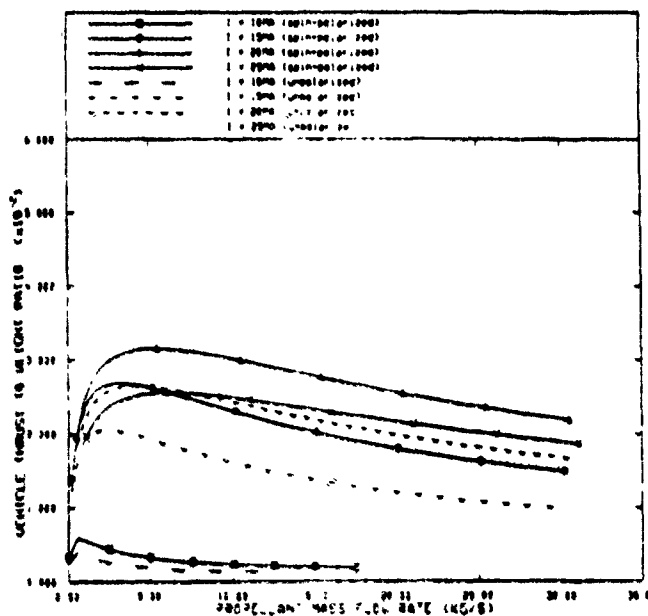


c) 3 thrusters

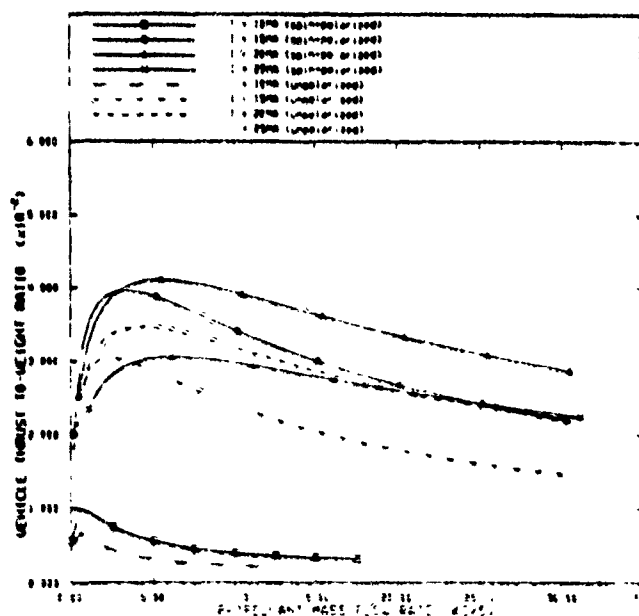


d) 4 thrusters

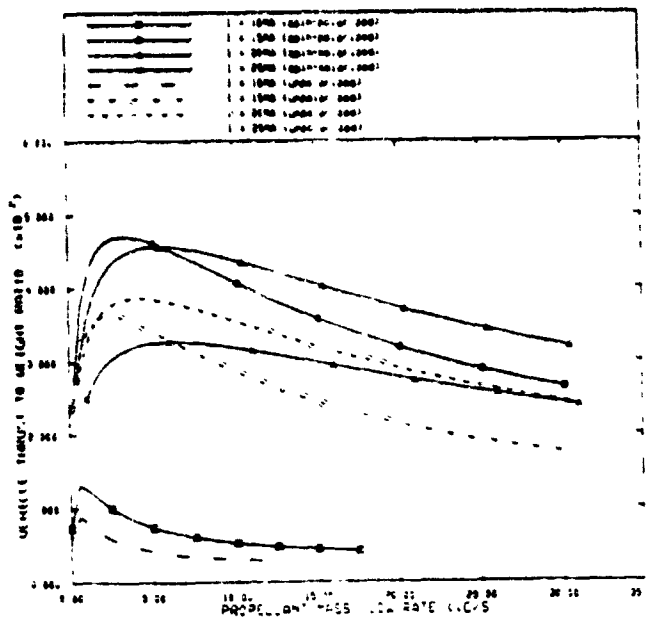
Figure 34. Vehicle F/W vs. Specific Impulse for $\Delta v=10\text{km/s}$ ($I^{8/3}$ Scaling)



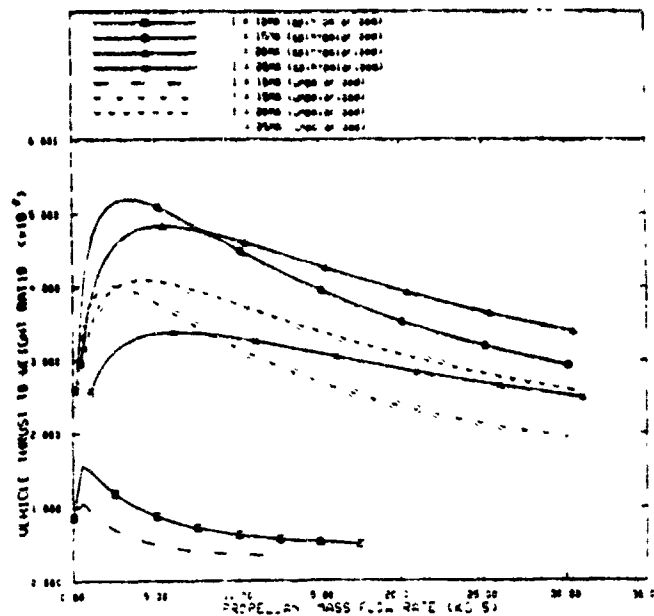
a) 1 thruster



b) 2 thrusters

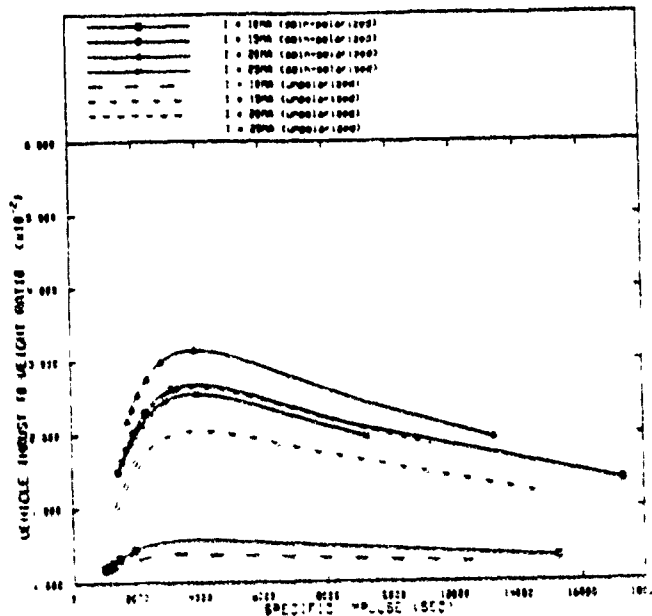


c) 3 thrusters

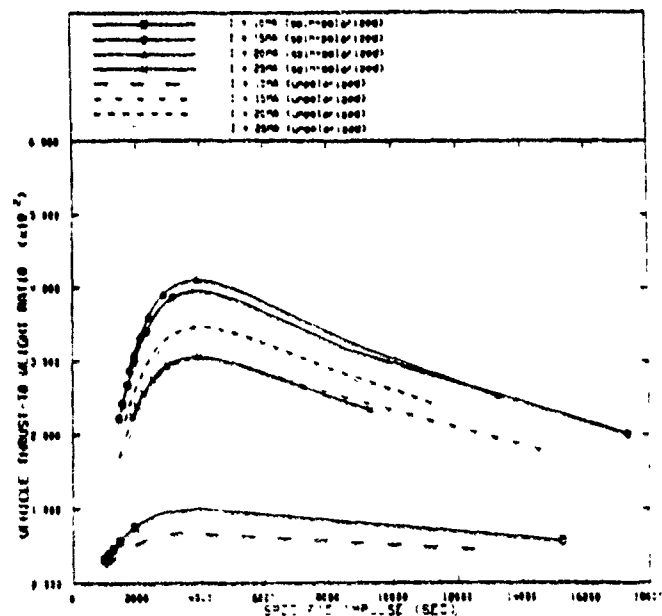


d) 4 thrusters

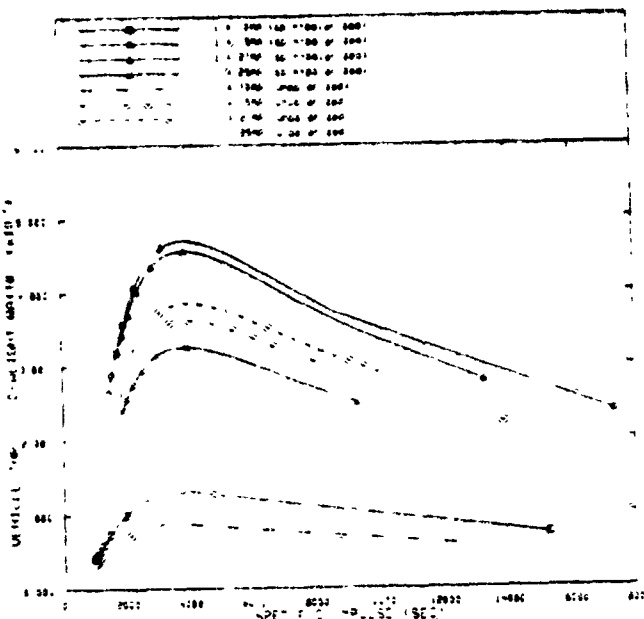
Figure 35. Vehicle F/W vs. Propellant Mass Flow rate for $\Delta v=40\text{km/s}$ ($I^{8/3}$ Scaling)



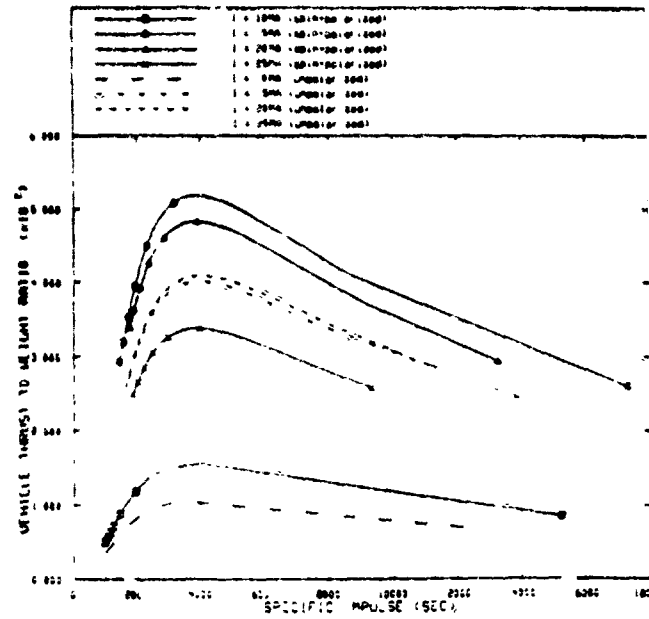
a) 1 thruster



b) 2 thrusters



c) 3 thrusters



d) 4 thrusters

Figure 36. Vehicle F/W vs. Specific Impulse for $\Delta v=40\text{km/s}$ ($I^{8/3}$ Scaling)

Table 5.1. Propulsion Parameters for Base Case and Spin-Polarized Case
 ($\Delta v = 10\text{km/s}$, $I = 20\text{ MA}$, $M_{ad}^* = 30\text{kg/s}$)

		Base case		Spin-Polarized	
D Burnup Fraction	f_D	0.63	0.70	0.63	0.70
^3He Burnup Fraction	f_{He}	0.48	0.58	0.48	0.58
D- ^3He Fusion Power	P_{DHe} (MW)	2959.41	3582.31	2959.41	3582.31
DD _n Fusion Power	P_{DDn} (MW)	11.09	9.05	11.09	9.05
DD _p Fusion Power	P_{DDp} (MW)	49.66	40.50	49.66	40.50
Total Fusion Power	P_F (MW)	3020.15	3631.86	3020.15	3631.86
Power to Focus	P_{in} (MW)	88.10	88.10	223.43	223.43
Bremsstrahlung Loss	P_B (MW)	16.28	13.09	16.28	13.09
Cyclotron Loss	P_C (MW)	84.23	74.42	84.23	74.42
Total Power Loss	P_L (MW)	100.51	87.51	100.51	87.51
Power Increase	ΔP (MW)	2831.54	3456.25	2696.20	3320.92
Total Mass Flow	M_T (kg/s)	31.02	30.96	31.02	30.96
Propellant Thrust	F_p (N)	4.85×10^5	5.25×10^5	4.85×10^5	5.25×10^5
Total Burn Time	t_b (s)	4852.44	4360.00	1.56×10^4	1.40×10^4
Payload Mass	M_L (kg)	1×10^5	1×10^5	1×10^5	1×10^5
Propellant Mass	M_p (kg)	1.48×10^5	1.33×10^5	4.76×10^5	4.27×10^5
Prop. Sys. Mass	M_{pays} (kg)	2.22×10^4	1.99×10^4	7.14×10^4	6.40×10^4
Fuel Mass	M_F (kg)	1.96	1.76	6.29	5.65
Fuel Sys. Mass	M_{Fsys} (kg)	0.20	6887.88	0.63	4.43×10^5
Capacitor Mass	M_C (kg)	6.89×10^4	6.89×10^4	4.43×10^5	4.43×10^5
Shield Mass	M_{sh} (kg)	1.27×10^4	1.30×10^4	1.37×10^4	1.40×10^4
Magnet Mass	M_B (kg)	270.20	270.20	270.20	270.20
Total Mass	M_T (kg)	3.52×10^5	3.42×10^5	1.10×10^6	1.09×10^6
Total Thrust	F (N)	1.94×10^6	2.10×10^6	1.94×10^6	2.10×10^6
Thrust-to-Weight	F/W	0.56	0.63	0.18	0.20
Specific Impulse	I_{sp} (s)	1622.50	1760.84	1622.50	1760.84
Increased Factor of Fusion Power		1.20		1.20	
Increased Factor of ΔP		1.22		1.23	
Increased Factor of F/W		1.13		1.11	
Increased Factor of I_{sp}		1.09		1.09	

*Additional hydrogen used for propellant besides coolant mass flow.

Table 5.2. Propulsion Parameters for Base Case and Spin-Polarized Case
 $(\Delta v = 40 \text{ km/s}, I = 20 \text{ MA}, M_{ad}^* = \text{kg/s})$

			Base case		Spin-Polarized	
D Burnup Fraction	f_D		0.63	0.70	0.63	0.70
^3He Burnup Fraction	f_{He}		0.48	0.58	0.48	0.58
D- ^3He Fusion Power	P_{DHe}	(MW)	2959.41	3582.31	2959.41	3582.31
DD _n Fusion Power	P_{DDn}	(MW)	11.09	9.05	11.09	9.05
DD _p Fusion Power	P_{DDp}	(MW)	49.66	40.50	49.66	40.50
Total Fusion Power	P_F	(MW)	3020.15	3631.86	3020.15	3631.86
Power to Focus	P_{in}	(MW)	88.10	88.10	223.43	223.43
Bremsstrahlung Loss	P_B	(MW)	16.28	13.09	16.28	13.09
Cyclotron Loss	P_C	(MW)	84.23	74.42	84.23	74.42
Total Power Loss	P_L	(MW)	100.51	87.51	100.51	87.51
Power Increase	ΔP	(MW)	2831.54	3456.25	2696.20	3320.92
Total Mass Flow	M_T	(kg/s)	5.02	4.96	5.02	4.96
Propellant Thrust	F_p	(N)	1.72×10^5	1.88×10^5	1.72×10^5	1.88×10^5
Total Burn Time	t_b	(s)	6.95×10^4	6.01×10^4	2.23×10^5	1.93×10^5
Payload Mass	M_L	(kg)	1×10^5	1×10^5	1×10^5	1×10^5
Propellant Mass	M_p	(kg)	3.14×10^5	2.68×10^5	1.01×10^6	8.60×10^5
Prop. Sys. Mass	M_{p-ys}	(kg)	4.71×10^4	4.02×10^4	1.51×10^5	1.29×10^4
Fuel Mass	M_F	(kg)	28.02	24.22	89.99	77.80
Fuel Sys. Mass	M_{Fsys}	(kg)	~ 90	6890.13	9.00	4.43×10^4
Capacitor Mass	M_C	(kg)	6.89×10^4	6.89×10^4	4.43×10^5	4.43×10^5
Shield Mass	M_{sh}	(kg)	1.51×10^4	1.53×10^4	1.62×10^4	1.64×10^4
Magnet Mass	M_B	(kg)	270.20	270.20	270.20	270.20
Total Mass	M_T	(kg)	5.45×10^5	4.99×10^5	1.72×10^6	1.59×10^6
Total Thrust	F	(N)	6.89×10^6	7.52×10^5	6.89×10^5	7.52×10^5
Thrust-to-Weight	F/W		0.13	0.15	4.09×10^{-2}	4.81×10^{-2}
Specific Impulse	I_{sp}	(s)	3888.86	4300.36	3888.86	4300.36
Increased Factor of Fusion Power			1.20		1.20	
Increased Factor of ΔP			1.22		1.23	
Increased Factor of F/W			1.15		1.18	
Increased Factor of I_{sp}			1.11		1.11	

*Additional hydrogen used for propellant besides coolant mass flow.

The initial number density $n_D = n_{He} = \frac{1}{2}n_i = 1.18 \times 10^{26} \text{ m}^{-3}$ and the reaction rate parameters of $\langle\sigma v\rangle_{D_{He}}$, $\langle\sigma v\rangle_{DD_n}$, and $\langle\sigma v\rangle_{DD_p}$ are used, consistent with the values used for the conventional D- ^3He case in Section II.1. For spin-polarized case, $\langle\sigma v\rangle_{D_{He}} = 1.5\langle\sigma v\rangle_{D_{He}}$, $\langle\sigma v\rangle_{DD_n} = \langle\sigma v\rangle_{DD_n}$, and $\langle\sigma v\rangle_{DD_p} = \langle\sigma v\rangle_{DD_p}$ were used. During the pinch stable time, the number densities of D and ^3He were actually functions of time which decreased with time. Since the D- ^3He reaction rate was increased by spin polarization and the deuterium particles decreased at faster rate, the fusion power produced by DDn and DDp reactions were slightly decreased. Deuterium burn up fraction was 0.63 as compared to that of ^3He with 0.48 as listed in Table 5.

As one can see from Tables 5.1 and 5.2, the total fusion power was increased by a factor about 1.2. Also one can find that bremsstrahlung and synchrotron losses are slightly suppressed by spin polarization because of the faster decrease of D and ^3He number densities. The increased fusion power and the decreased total power loss lead to the fact that more power can be absorbed by propellant to produce the thrust for spin-polarized case. This is why the total thrust, the sum of propellant thrust and the thrust produced by expelled fuel increased. One thing should be noted is that the power required to operate plasma focus is

$$P_{in} = IVR_{rep}t_{dis} , \quad (18)$$

where t_{dis} is time for fill gas to be discharged with other parameters in Eq.(18) given in Table 4. For the I^2 scaling case, $V \propto I$, then $P_{in} \propto I^2$. But for the $I^{8/3}$ scaling case, $V \propto I^{4/3}$, then $P_{in} \propto I^{7/3}$. Thus this current relationship is very sensitive to the different scaling laws.

Part of the synchrotron radiation will be absorbed in walls and electrodes. Since the synchrotron was lowered by spin polarization, the amount of power that should be removed from the walls and electrodes is correspondingly decreased. Therefore the coolant mass flow which is needed to keep inlet temperature to turbine below $2,000^\circ\text{K}$ is lowered; hence, the total mass flow which is the sum of additional propellant and coolant mass flows is reduced for the spin-polarized case.

Since the specific impulse is increased due to increased fusion power, the exhaust velocity, v_{ex} , is also increased. Thus the propellant system masses are decreased via

$$M_p = (e^{\Delta v/v_{ex}} - 1) (M_L + M_C + M_B) , \quad (19)$$

assuming

$$M_{psys} = 0.15M_p . \quad (20)$$

Reduced propellant mass also reduces the propellant burn time, and thus the fuel and fuel system masses are reduced since $M_F \propto t_b$ and $M_{Fsys} = 0.1M_F$.

As shown in Tables 5.1 and 5.2, capacitor mass for $I^{8/3}$ scaling case is much bigger than that for I^2 scaling since at $I^{8/3}$ scaling

$$\frac{M_C}{M_{C0}} = \left[\frac{V}{V_0} \right]^2 = \left[\frac{I}{I_0} \right]^{8/3} , \quad (21)$$

and this large mass makes the F/W ratios in $I^{8/3}$ scaling much smaller than those of I^2 scaling.

The thrust-to-weight ratios in Tables 5.1 and 5.2 increase due to the raised thrust as well as lowered mass, and the specific impulse also increased due to increased fusion power by the spin polarization for both I^2 and $I^{8/3}$ scaling cases.

III. CONCLUSIONS AND RECOMMENDATIONS

If plasma temperature scaling holds, the dense plasma focus could be a relatively easy way of obtaining hot, high density plasmas. Further study of the dynamics of the pinching process and of the eventual disruption of the pinch due to MHD instabilities is necessary. Trapping a strong axial magnetic field inside the pinch may stabilize it by reducing the rate at which the instabilities grow. Accurate measurements of pinch dimensions is critical in the computation of important propulsion parameters.

The most important issue to be resolved is how various parameters scale. Scaling of plasma temperature with capacitor current must be investigated at currents larger than 1 MA, where I^2 scaling may break down. Also of extreme importance is the scaling of capacitor mass with current. Both I^2 and $I^{8/3}$ scalings were considered in this study.

For impulsive thrusting for non-spin polarized case, the increase in capacitor mass is sufficiently large to reduce F/W values beyond currents of 20 MA for impulsive thrusting. The scaling also determines the effectiveness of using multiple thrusters on a mission. At I^2 scaling, multiple thrusters serve to greatly increase F/W values as well as serve as insurance against the failure of a thruster. However, at $I^{8/3}$ scaling, multiple thrusters are much less effective in increasing F/W because of the large increase in capacitor mass. For $\Delta v = 40$ km/s, F/W ratios of almost 0.08 are possible at around 4000 sec of I_{sp} with 4 thrusters at 20 MA. This seems to be the optimum operating regime for the DPF propulsion system in the impulsive firing mode.

The F/W ratios for the continuous firing modes of operation of the DPF propulsion system for non-spin polarized case fall about 2 orders of magnitude short of that which is required for manned space travel. Although none of the three modes of operation of the DPF propulsion system are suitable for long missions in space, each may have a mission for which it is very well suited. They are probably best suited for low Δv missions such as orbital transfer or perhaps a lunar shuttle, which do not require large F/W values.

The greatest benefit from spin polarizing D- 3 He analysis is an increase in the D- 3 He output power by 20% up to possibly 50%. The power increase by spin polarization indeed increases the thrust-to-weight ratio and specific impulse. With the possible suppression of D-D reactions, this 50% power increase could actually be envisioned as the total power increase. This indicates that a 50% power increase with little or no reactor modifications. Examining the benefit to fusion propulsion one finds the actual total power increase is less than 50% because of the decrease of ion number densities during the pinch lifetime, which leads the reaction rate to decrease with time. The spin-polarized case presented here can probably be improved by optimization of the

plasma and the propulsion parameters; e.g., this work treated the DD reaction as unchanged by spin polarization. Though the F/W values and specific impulse indeed increased by adopting spin polarization, for high Δv missions, however, F/W ratios of the DPF propulsion system is still too low (cf. 0.2). At present, DPF propulsion is best suited for low Δv missions as described above.

REFERENCES

1. W.H.T. Loh, Jet Rocket, Nuclear, Ion and Electric Propulsion: Theory and Design, Springer-Verlag, N.Y. (1968).
2. i) R.W. Bussard and R.D. Delauer, Nuclear Rocket Propulsion, McGraw-Hill, N.Y. (1958).
ii) R.H. Fox, "Nuclear Propulsion," Astronaut Aerospace Eng., 1, (1963).
iii) S.N.B. Murthy, "Advanced Nuclear Devices in Space-A Survey," 23rd Int. Astronautical Federation, Int. Astronautical Congress, Vienna, Austria, Oct. 8-15 (1972).
iv) H.W. Loeb, "Nuclear Energy in Space," Earth-Oriented Applications of Space Technology, 2, (1982)1.
v) S.K. Borowski, "Nuclear Propulsion: A Vital Technology for Exploration of Mars and the Planets Beyond," NASA-TM-101354, Case for Mars 3, July 18-22, (1987) Boulder, Co.
3. i) E. Stuhlinger, Ion Propulsion for Space Flight, McGraw-Hill, N.Y. (1964).
ii) H.R. Kauffman, "One Dimensional Analysis of Ion Rockets," NASA Tech. Note, D-261, March (1960).
iii) R. Deutsch, "Ion Acceleration in the Plasma Focus," Report IPF-82-6, Institute für Plasmaforschung, Stuttgart, W. Germany (1982).
iv) Micheal J. Patterson and Vincent K. Rawlin, "Performance of 10-kW class xenon ion thrusters," NASA Technical Memorandum No. 101292, (1988), 30p.
v) J. R. Beattie, J. N. Matossian, and R. R. Robson, "Status of Xenon Ion Propulsion Technology," J. of Propulsion and Power, 6, (1990) 145-150.
vi) J. N. Matossian, and J. R. Beattie, "Model for Computing Volume-averaged Plasma Properties in Electron Bombardment Ion Thrusters," J. of Propulsion and Power, 5, (1989) 188-196.
vii) D. G. Fearn, A. R. Martin, and A. Bond, "U.K. Ion Propulsion Programme: Past Status and New Results," Acta Astronautica, 15, (1987) 353-365.
viii) Ramon E. Lopez, "Argon Ion Propulsion of the Magnetosphere," NASA Conference Publication No. 2359, (1985) 675-692.

4. i) M. M. Mekar and D. P. Boyarski, "Solar Powered Electric Propulsion Orbit Transfer Vehicle Design and Operation Effectiveness," AIAA, NY, (1986) No. 0381, 11p.
- ii) E. J. Roschke, "Solar Dynamic Systems for Spacecraft Power Applications," AIAA, NY, (1986) No. 0382, 10p.
- iii) W. T. Callaghan, P. K. Henry, and P. A. McGuire, "Cherry Hill Revisited: Economic Payoff for Technical Achievements in Flat-plate Photovoltaics 1975-1985," 18th IEEE Photovoltaic Specialists Conf., IEEE (Cat. No. 85CH2208-7), Piscataway, NJ USA (1985) 214-220.
- iv) E. J. Conway and R. J. Young, "Solar-Pumped Laser Research," 5th IEEE/OSA Conf. on Lasers, MD, USA, (CLEO 1985) May 21-24, IEEE Publication, p. 264.
5. i) R.G. Jahn, Physics of Electric Propulsion, McGraw-Hill, N.Y. (1968).
- ii) W.R. Mickelsen and H.R. Kaufman, "Status of Electrostatic Thrusters for Space Propulsion," NASA Tech. Note, D-2172, May (1964).
6. Space Propulsion Workshop Preliminary Notes (cf. Steve Howe), Denver, CO, (April 1991).
7. i) F. Mead, Jr., "Future Possibilities for Non Conventional Propulsion Developments at the Air Force rocket Propulsion Laboratory," 1986 JANNAF Propulsion Meeting, Vol. 1, p. 419, Aug. (1986) Baltimore, MD.
- ii) W. Bostick, "Plasma Motors," Advanc. Astronaut. Sci., 2 (1957) 2-1, Plenum Press; J.R. Roth, "A Preliminary Study of Thermonuclear Rocket Propulsion," J. British Interplanetary Soc., 18 (1962) 59.
- iii) C. Powell, O.J. Hahn, and J.R. McNally, "Energy Balance in Fusion Rockets," Astronautica Acta, 18 (1973) 59.
- iv) J.D. Balcomb, and K. Boyer, "Systems Studies of Fusion Powered Pulsed Propulsion Systems," 7th Amer. Inst. of Aeronautics and Astronautics Conf., Salt Lake City, UT. June 14-18 (1971).
- v) J.J. Reinmann, "Fusion Rocket Concepts," 6th Symp. on Advanced Propulsion Concepts, Niagara Falls, N.Y., May 4-6 (1971); and NASA-TM-X-67826 (1971).

- vi) J.R. Roth, W. Rayle, and J. Reinmann, "Fusion Power for Space Propulsion," New Scientist, 54 (1972) 125; and NASA-TM-X-2106 (1970).
- vii) D. Dooling, Jr., "Controlled Thermonuclear Fusion for Space Propulsion," Spaceflight 14 (1972) 26.
- viii) W.E. Moeckel, "Comparison of Advanced Propulsion Concepts for Deep Space Exploration," J. Spacecraft, 12 (1972) 863.
- ix) F. Winterberg, "Rocket Propulsion by Staged Thermonuclear Microexplosions," J.Br. Interplanet Soc., 30, (1977) 333.
- x) F. Winterberg, "Chemically Ignited Thermonuclear Reactions: A Near-Term Means for a High Specific Impulse-High Thrust Propulsion System," 33rd Int. Astronautical Federation, Int. Astronautical Congress, Paris, France, Sept. 27-Oct. 2 (1982).
- xi) Y. Arakawa, I. Kimura, and M. Onishi, "Prospects for Inertial-Confinement Fusion Rocket Propulsion," 14th Int. Symp. on Space Technology and Science, Tokyo, Japan, May 27-June 1 (1984), p. 129.
- xii) P.W. Garrison, "Advanced Propulsion Activities in the U.S.A.," 37th Int. Astronautical Congress on Space, Innsbruck, Austria, Oct. 4-11 (1986), Acta Astronautica, 16 (1987).
- xiii) T. Kammash and D. Galbraith, "A Fusion-Driven Rocket Propulsion Scheme for Space Exploration," Trans. Am. Nucl. Soc., 54 (1987) 118.
- xiv) J.R. Roth, "Space Applications of Fusion Energy," Fusion Tech, 15 (1989) 1375.
- xv) N.R. Schulze, and J.R. Roth, "The NASA-Lewis Program on Fusion Energy for Space Power and Propulsion, 1958-1978," Fusion Tech., 19 (1991) 11-28.
- xvi) Robert W. Bussard, "Fusion as Electric Propulsion," J. Propulsion, 6 (Sept.-Oct. 1990) 567-574.
- xvii) H.D. Froning and F.B. Mead, "Propulsion for Rapid Transits Between Earth and Mars," Mars Case IV International, Boulder, CO, June 4-8.
- xviii) San-Mou Jeng and Dennis Keeter, "Theoretical Evaluation of Laser-Sustained Plasma Thruster Performance," J. Propulsion, 5 (Sept.-Oct. 1989) 577-581.

- xix) T. Kammash and D.L. Galbraith, "A Fusion reactor for Space Applications," Fusion Tech., 12 (1987) 11-21.
- xx) L.K. Rudolph and D.Q. King, "100-kWe Magnetoplasmdynamic Thruster System Design," J. Spacecraft, Nov.-Dec. 1984, 563-572.
- xxi) S. Gartenhaus and L.M. Tannenwald, "Propulsion from Pinch Collapse," in Plasma Acceleration (Ed., Sidney W. Kash), Stanford Univ. Press, Stanford, CA. (1960).
- xxii) R.L. Forward, "21st Century Space Propulsion Study," AL-TR-89-040, Astronautics Laboratory, Edwards AFB, CA, Aug. (1990).
- xxiii) D.L. Cravens, "Electric Propulsion Study," AL-TR-89-040, Astronautics Laboratory, Edwards AFB, CA, Aug. (1990).
- xxiv) John McKee, "Plasma Focus Fusion Conceptual Propulsion Systems in a Mission Context," McDonnell Douglas Space Systems Co., Huntington Beach, CA., Feb. (1991).
- xxv) P.W. Garrison and J.F. Stocky, "Future Spacecraft Propulsion," J. Propulsion, 4 (1988) 520-525.
- xxvi) R.F. Bourque, K.R. Shultz, and Project Staff, "Fusion Application and Market Evaluation (FAME) Study," GA-A 18658, UCRL 21073, General Atomics, San Diego, CA., Feb. (1988).
- xxvii) P.M. Koloc, "Plasmak Star Power for Energy Intensive Space Applications," Fusion Tech. Vol. 15, NO. 2, Part 2B, pp. 1136-1141 (1990).
- xxviii) R.B. Pittman, "The Plasmak Solution: The Answer for Space Power & Propulsion," 1989, 24th Intersociety Energy Conversion Engineering Conference, Vol. 1, pp. 501.
- xxix) J.F. Santarius, "Magnetic Fusion Energy and Space Development," 1989 24th Intersociety Energy Conversion Engineering Conference, Vol. 5, p. 2525.
- 8. V. E. Haloulakos and R. F. Bourque, "Fusion Propulsion Study," AL-TR-89-005, Astronautics Laboratory (AFSC), Edwards AFB, CA July (1989).
- 9. N. R. Schulze, "Fusion Energy for space Missions in the 21st Century," NASA Technical Memoranda 4297 and 4298, (1991).

10. A.C. Ducati, et al., "Experimental Results in High Specific Impulse Thermo-Ionic Acceleration," AIAAJ, 2 (1964) 1452.
11. B. Brunelli and G.G. Leotta (Editors), "The Plasma Focus," Uncoventional Approaches to Fusion, Plenum Press, N.Y. (1982).
12. J. Mather, in Methods of Experimental Physics, Academic Press, N.Y. (1971).
13. N. Filippov, in Plasma Physics and Controlled Nuclear Fusion, Proc. 7th European Conf. (Prague, 1977), p. 63.
14. R.H. Lovberg, and H.R. Griem, Methods of Experimental Physics, Academic Press, N.Y., 1971, p. 187.
15. H. Herold and H.J. Keppeler (Editors), Proc of the Third Int. Workshop on Plasma Focus Research, IPF-83-6, Institute für Plasmaforschung der Universität Stuttgart, Sept. 12-13, (1983), Stuttgart, W. Germany.
16. S. Denus (Editor), Proc. of the Fourth Int. Workshop on Plasma Focus and Z-Pinch Research, Sept. 9-11 (1985), Warsaw, Poland.
17. V. Nardi, H. Sahlin, and W.H. Bostick (Editors), Second International Conf. on Energy Storage Compression and Switching, Venice, Italy, Dec. 5-8, 1978 [Published by Plenum Press as Energy Storage, Compression and Switching, Vol. 2, (1983)].
18. R. Gullickson, J. Luce, and H. Sahlin, "Operation of a Plasma-Focus Device with D_2 and 3He ," J. Appl. Phys. 48 (1977) 3718-3722.
19. i) J. Brzosko, J. Rager, B. Robouch, H. Bahr, H. Klapdor, E. Anderson, and D. Herges, "Measurements of the D (d,n) and He^3 (d,p) Reaction Yields for the 1-MJ Plasma Focus Device Operating with a D_2 - 3He Gas Mixture," Nuclear Tech./Fusion, 4 (1983) 263-276.
 ii) Jan S. Brzosko, H. Contrads, Jean Pierre Rager, B.V. Robouch, and Karl Steinmetz, "Investigations of High-Energy Deuterons in a Dense Plasma Focus Device by Means of Neutrons emitted in the $^7Li + D$ Process," Nuclear Tech./Fusion, 5 (1984) 209-223.
20. R. Gullickson and H. Sahlin, "Measurement of High-Energy Deuterons in the Plasma-Focus Device," J. Appl. Phys., 49 (1978) 1099-1105.
21. A. Mozer, M. Sadowski, H. Herold, and H. Schmidt, "Experimental Studies of Fast Deuterons, Impurity and Admixture-Ions Emitted from a Plasma Focus," J. Appl. Phys.,

53 (1982) 2959.

22. R.L. [redacted] and R.G. Jahn, "Measured Performance of a Multimegawatt MI [redacted] 20 (1983) 299-304.
23. D.J. Merz, A.J. [redacted] and R.G. Jahn, "MPD Thruster Performance: Propellant Distribution and S [redacted] 'J. Propulsion, 2 (1986) 317-322.
24. Hiroshi Mura, [redacted] and Isao Kudo, "Thrust Measurement of an Ion Engine System," J. Space [redacted] 96-100.
25. H. Herold, A. Jerzykiewicz, M. Sadowski, and H. Schmidt, "Comparative Analysis of Large Plasma Focus Experiments Performed at IPF, Stuttgart and at IPJ, Swierk (Poland)," Nuclear Fusion, 29 (1989) 1255-1269.
26. Yoshihiro Arakawa, and Chinami Hamatani, "Reduction of Plasma Loss to Discharge Chamber Walls in a Ring Cusp Ion Thruster," J. Propulsion, 3 (Jan.-Feb. 1987) 90-91.
27. Jeffrey M. Hiatt, and Paul J. Wilbur, "Ring Cusp Discharge Chamber Performance Optimization," J. Propulsion, 2 (Sept.-Oct. 1986) 390-397.
28. R.A. Gerwin, G.J. Marklin, A.G. Sgro, and A.H. Glasser, "Characterization of Plasma Flow Through Magnetic Nozzles," AI-TR-89-052, Astronautics Laboratory (AFSC), Edwards AFB, CA., Feb. (1990).
29. S. Borowski, NASA Space Propulsion Projects, ICENES Conf., Monterey, CA. (June 1991).
30. Private Communication with Jan Brzosko (May, 1991).
31. M.A. Leontovich, "Two-Dimensional MHD Model for the Dense Plasma Focus of a Z Pinch," in Revs. Plasma Phys., Vol. 8, Consultants Bureau, N.Y. (1960)
32. P. Eltgroth, "Comparison of Plasma Focus Calculations," Phys. Fluids, 25 (1982) 2408-2414.
33. D.E. Potter, "Numerical Studies of the Plasma Focus," Phys. Fluids, 14 (1971) 1911-1924.
34. V.F. D'yachenko and V.S. Imshennik, "MHD Theory of the Pinch Effect in a Dense High-Temperature Plasma (Dense Plasma Focus)," Revs. Plasma Phys., Consultant Bureau, N.Y., pp. 447-495.

35. M. Auweter-Kurtz, H.L. Kurtz, H.O. Schrade, and P.C. Sleziona, "Numerical Modelling of the Flow Discharge in MPD Thrusters," J. Propulsion, 5 (1989) 49-55.
36. Masafumi Tanaka and Itsuro Kimura, "Current Distribution and Plasma Acceleration in MPD Arcjet with Applied Magnetic Fields," J. Propulsion, 4 (1988) 428-436.
37. Michael Minovitch, "Generalized Theory of Rocket Propulsion for Future Space Travel," J. Propulsion, 3 (1987) 320-328.
38. Pradosh Ray, "Characterization of Advanced Electric Propulsion Systems," J. Spacecraft, 20 (1983) 305-309.
39. G. Sargent Janes, "Scaling Relations for Plasma Devices," in Plasma Acceleration (Ed., Sidney W. Kash), Stanford Univ. Press, Stanford, CA. (1960).
40. T.J. Dolan, Fusion Research, Volume II, Pergamon Press, N.Y., 1982, p. 313.
41. T.J. Dolan, Fusion Research, Volume I, Pergamon Press, N.Y. 1982, pp. 54-56.
42. L.T. Cox, "Thermonuclear Reaction Bibliography with Cross Section Data for Four Advanced Reactions," AFAL-TR-89-006 (March 1989).
43. L.T. Cox, "The Barn Book," AL-TR-90-053 (1990); Fusion Technology, 18, (1990) 325-339.
44. G.P. Sutton, Rocket Propulsion Elements, McGraw Hill, 3rd Edition.
45. R. Cerbone, (Brookhaven National Laboratory), personal conversations, July 1990.
46. Dave Perkins (AL), personal conversations, July 1990.
47. K. Farmer, "SSME System Modelling Code," NASA Marshall Technical Report, 1987.
48. i) C.K. Choi, "Nuclear Spin Polarization of Advanced Fusion Fuels," AL-TR-89-036, Astronautics Laboratory (AFSC), Sept. 1989.
- ii) R.M. Kulsrud, H.P. Furth, E.J. Valeo, M. Goldhaber, "Fusion Reactor Plasma with Polarized Nuclei," Physical Review Letter, Vol. 49, 1982, p. 1248.
- iii) R.M. Kulsrud, H.P. Furth, E.J. Valeo, R.V. Budny, D.L. Jassby, B.J. Micklich, D.E. Post, M. Goldhaber, and W. Happer, "Fusion Reactor Plasma with Polarized Nuclei," Plasma Physics and Controlled Nuclear Fusion Research 1982, Vol. 2, IAEA, 1983, p. 163.

- iv) R.M. Kulsrud, E.J. Valeo, and S.C. Cowley, "Physics of Spin-Polarized Plasma," Nuclear Fusion, Vol. 26, 1986, p. 1443.

APPENDIX A

$I^{8/3}$ CURRENT SCALING RELATION

It is important to get good estimates of system masses in order to make accurate calculations of system F/W ratios. One very important mass to be calculated is the capacitor mass. It is necessary to extrapolate the required electrical parameters from some reference case. The reference case is chosen as the "Livermore-I" device and is denoted here by the subscript "o". Assuming a constant capacitance and capacitor specific energy, the capacitor charging potential can be found as a function of current by consistently solving Eqs. 7-10 with Eq. 2 in Section II.i. It can be shown that the charging potential scales as $I^{4/3}$

$$\frac{V}{V_o} = \left[\frac{I}{I_o} \right]^{4/3}.$$

Since capacitor mass is proportional to capacitor energy which is proportional to the square of the charging potential, capacitor mass scales as $I^{8/3}$

$$\frac{M_c}{M_{c,o}} = \left[\frac{V}{V_o} \right]^2 = \left[\frac{I}{I_o} \right]^{8/3}.$$

Figures 37-41 show F/W ratios for various Δv 's for the new scaling law. Immediately apparent in these Figures is that the highest current no longer leads to the highest F/W. This is due solely to the increasing capacitor mass at higher currents which was not evident before because of the I^2 scaling. The optimum current now occurs at about 20 MA. Figures 39 and 40 show a crossover between the 15 and 25 MA cases. It is here where the additional capacitor mass is compensated for by the additional propellant mass which must be carried along at the lower current. Figures 39-41 show that F/W decreases as additional propellant flow is added due to the fact that propellant is now the dominant system mass. It should be recognized that at some very high propellant mass flow rate (or at a higher Δv) the highest current will eventually yield the highest F/W ratios as the difference in capacitor mass is small compared to propellant mass.

Again, it is possible to use multiple thrusters to enhance performance. Figures 42 and 43 show thruster performance at 20 MA and 10 and 40 km/s, respectively. Thruster performance is obviously adversely affected by the higher capacitor masses due to the new scaling law (compare to Fig. 22), and the additional thrusters have only a minor effect on vehicle F/W for

low Δv while significantly increasing IMLEO. Similarly, in Figure 43, the effect of the increasing number of thrusters on F/W is not as significant as for the I^2 scaling (e.g., Figure 23). Raising the propellant mass flow rate drastically reduces F/W because of the large propellant masses involved. Figures 44 and 45 give some quantitative results and shows that for $\Delta v = 40$ km/s the DPF propulsion system is still about in order of magnitude below desirable F/W ratios for a manned Mars mission.

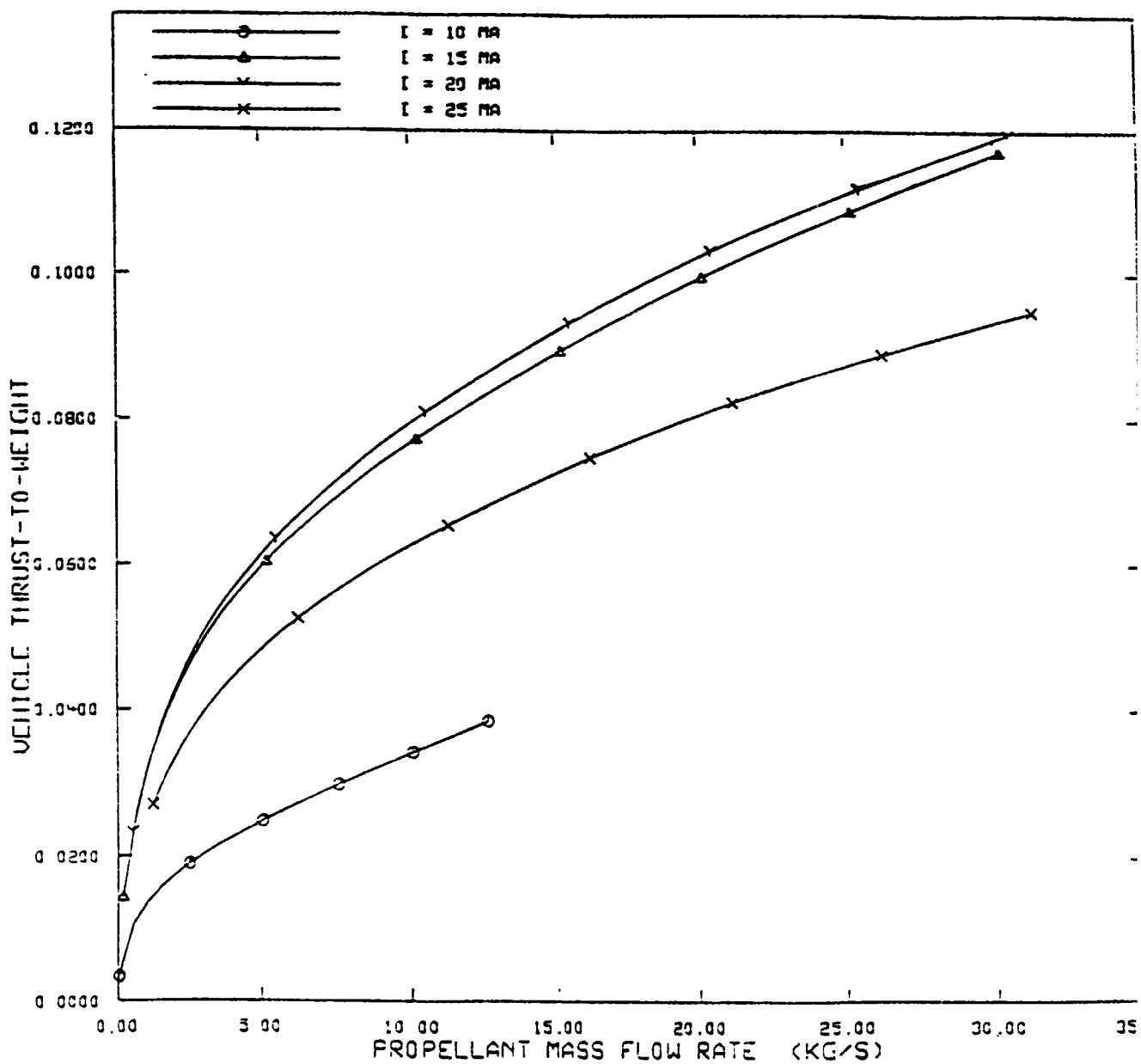


Figure 37. Vehicle F/W vs. Propellant Mass Flow Rate for $\Delta v = 5 \text{ km/s}$ ($I^{8/3}$ scaling)

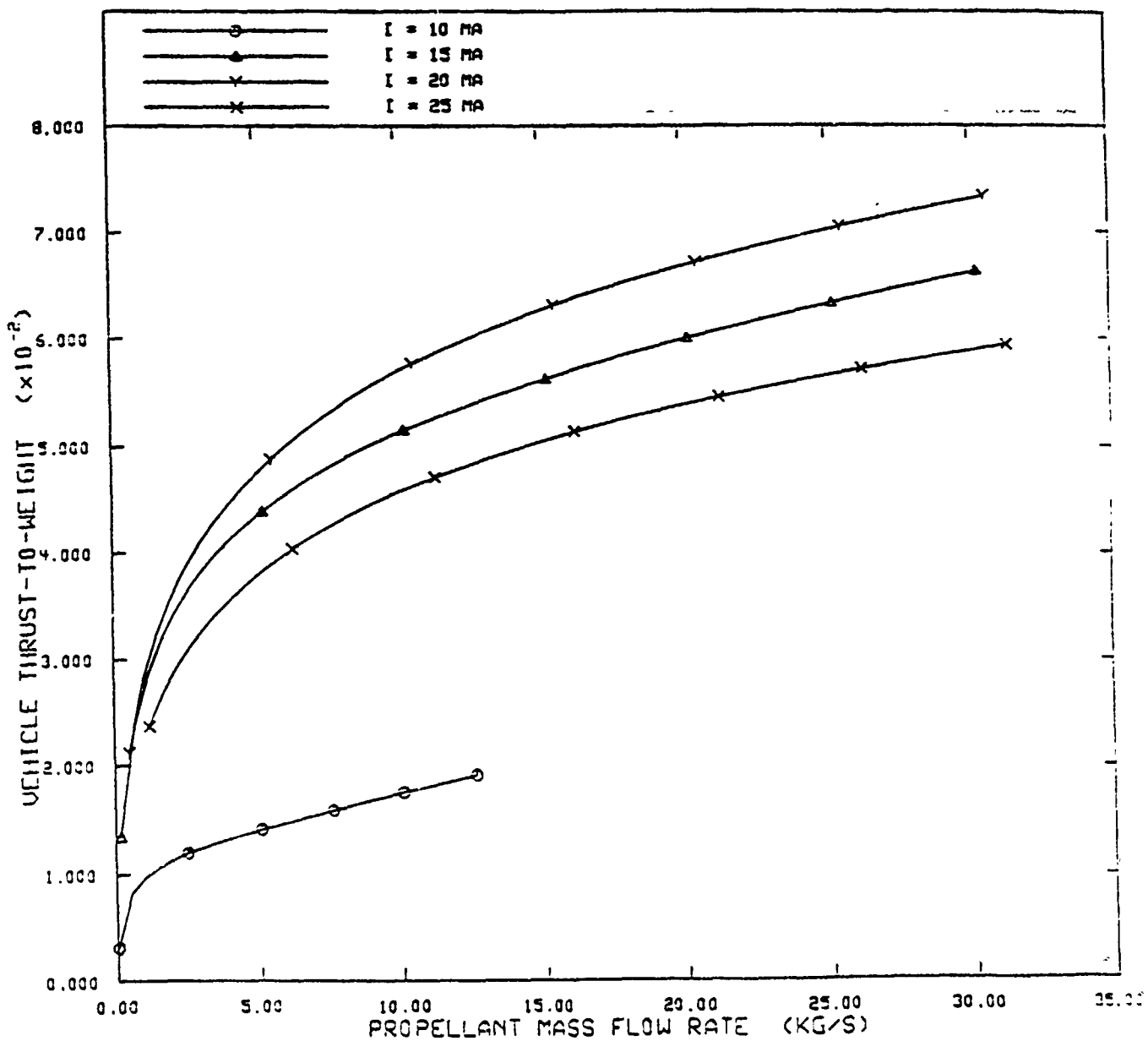


Figure 38. Vehicle F/W vs. Propellant Mass Flow Rate for $\Delta v = 10 \text{ km/s}$ ($I^{8/3}$ scaling)

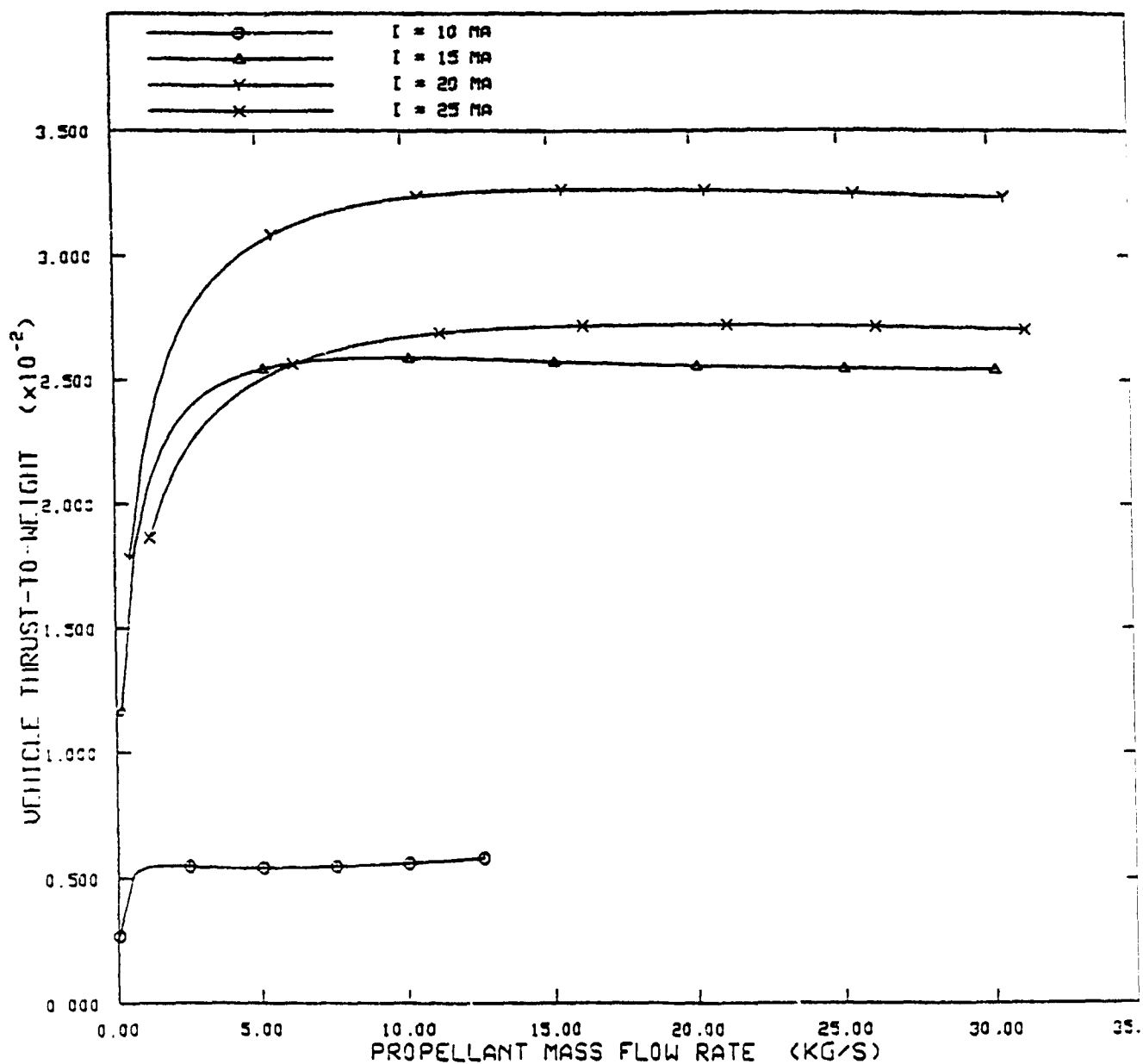


Figure 39. Vehicle F/W vs. Propellant Mass Flow Rate for $\Delta v = 20 \text{ km/s}$ ($I^{8/3}$ scaling)

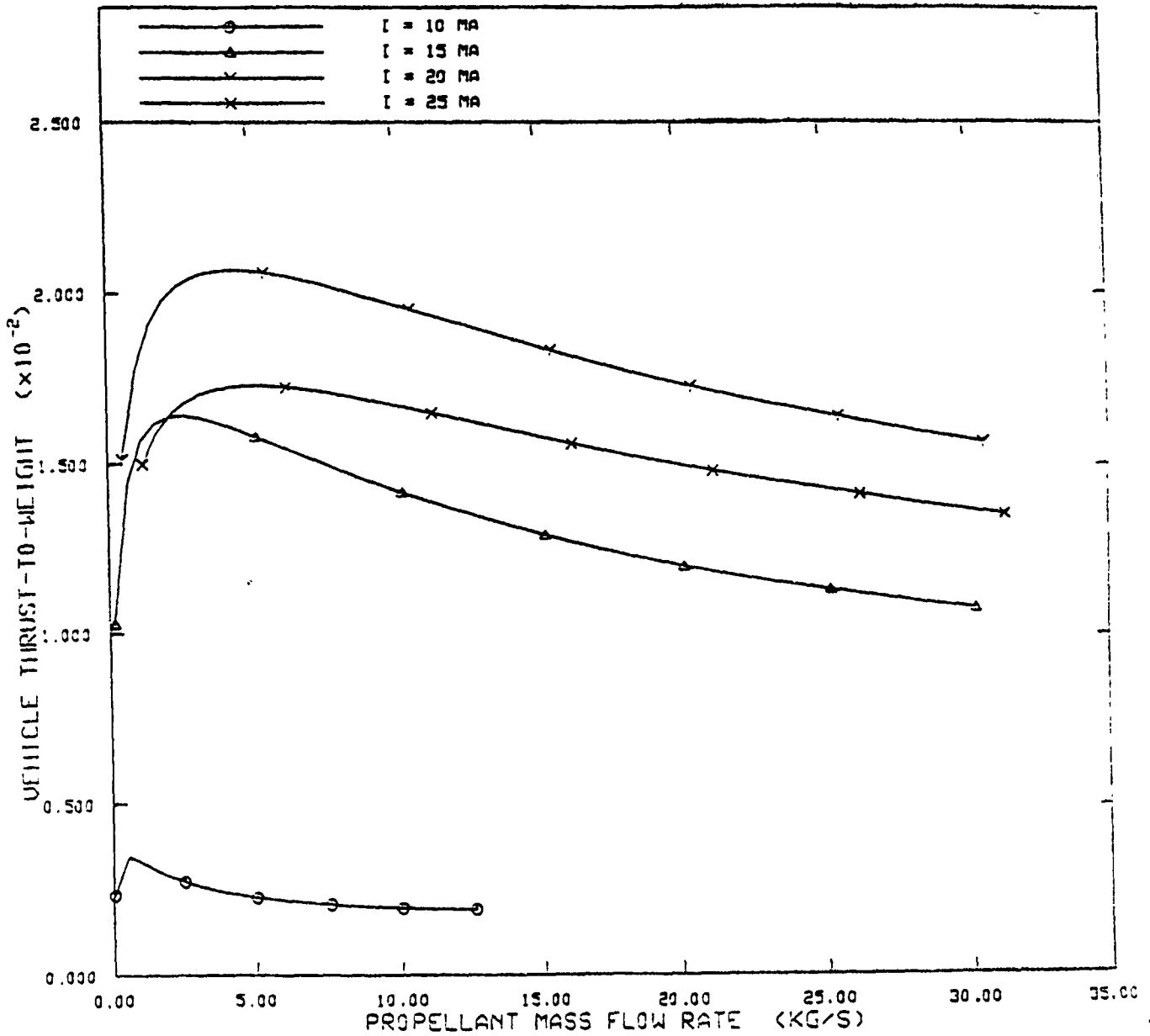


Figure 40. Vehicle F/W vs. Propellant Mass Flow Rate for $\Delta v = 30 \text{ km/s}$ ($I^{8/3}$ scaling)

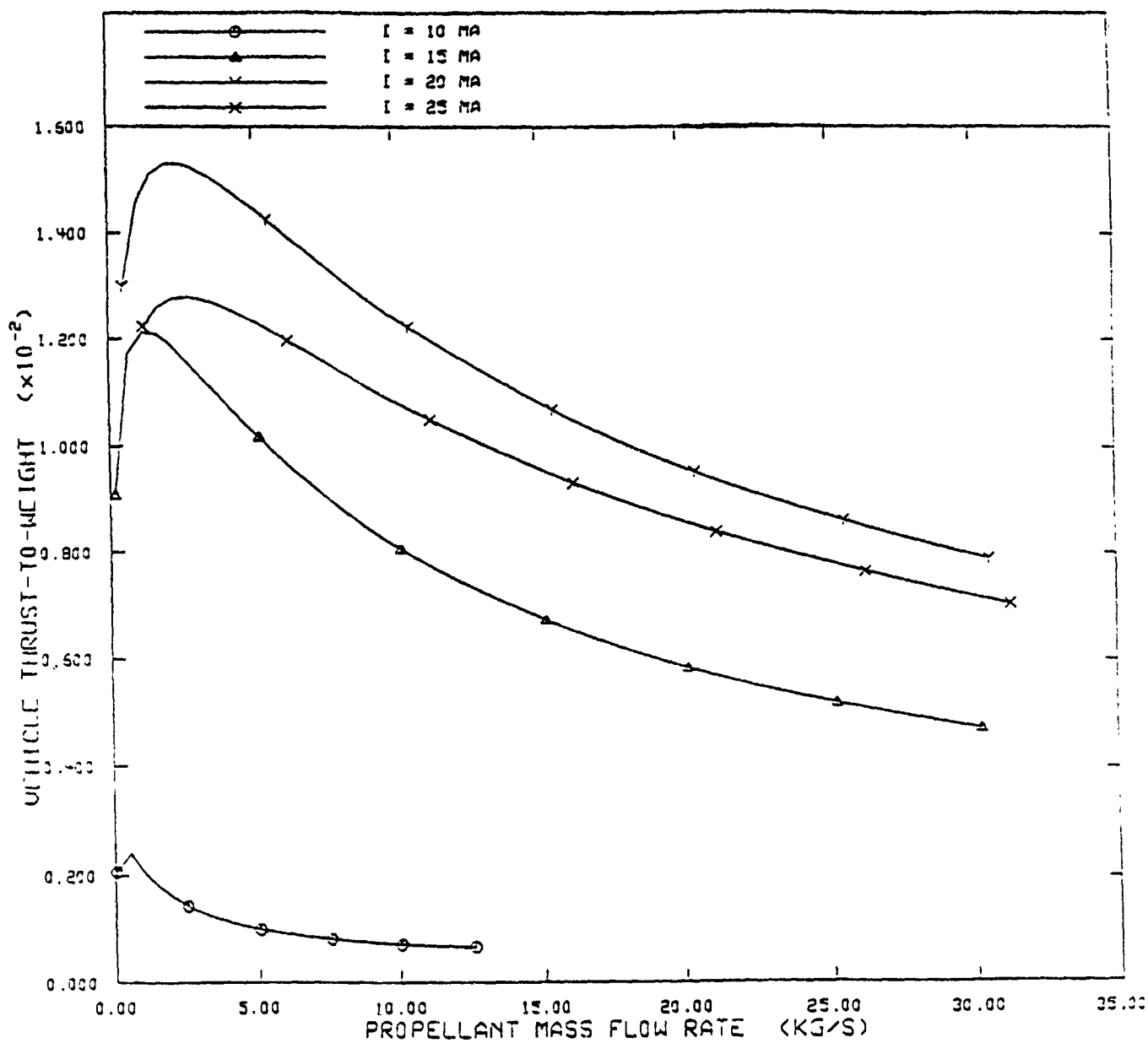


Figure 41. Vehicle F/W vs. Propellant Mass Flow Rate for $\Delta v = 40\text{km/s}$ ($I^{8/3}$ Scaling)

VEHICLE T/W VS PROPELLANT MASS FLOW AND NUMBER OF THRUSTERS

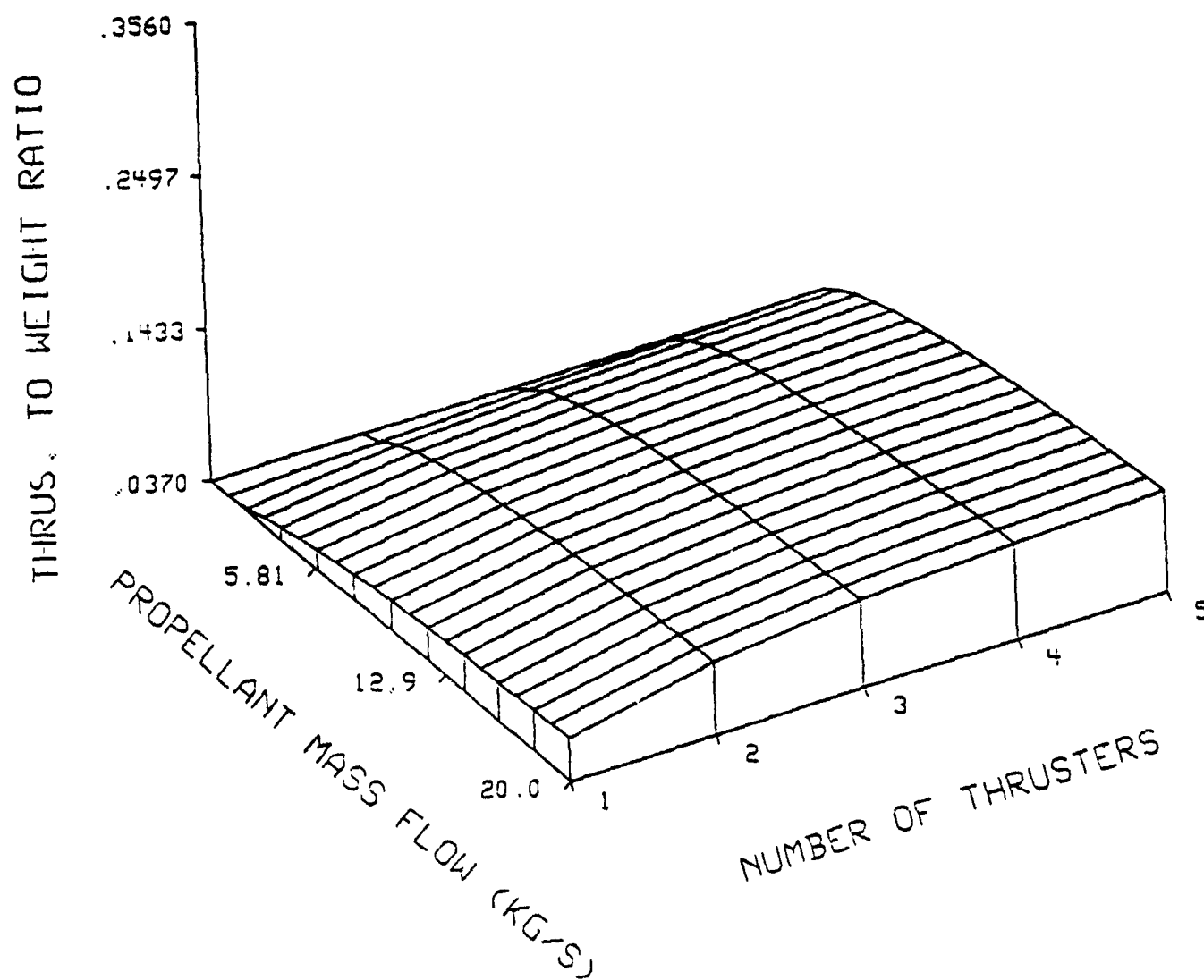


Figure 42. F/W Ratio vs. Propellant Mass Flow Rate and Number of Thrusters
for $\Delta v = 10\text{km/s}$ ($I^{8/3}$ Scaling)

VEHICLE T/W VS PROPELLANT MASS FLOW AND NUMBER OF THRUSTERS

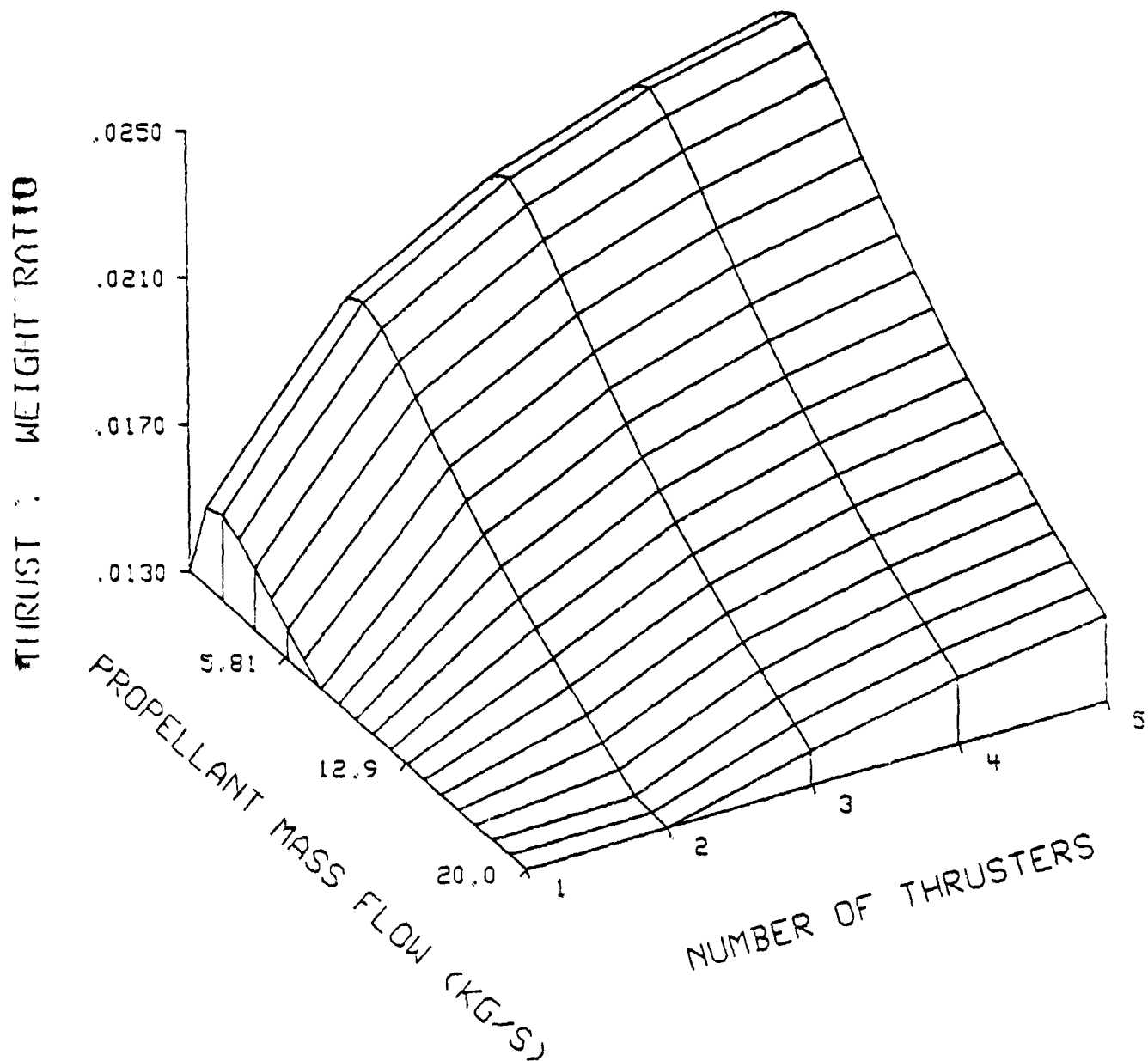


Figure 43. F/W Ratio vs. Propellant Mass Flow Rate and Number of Thrusters
for $\Delta v = 40\text{km/s}$ ($I^{8/3}$ Scaling)

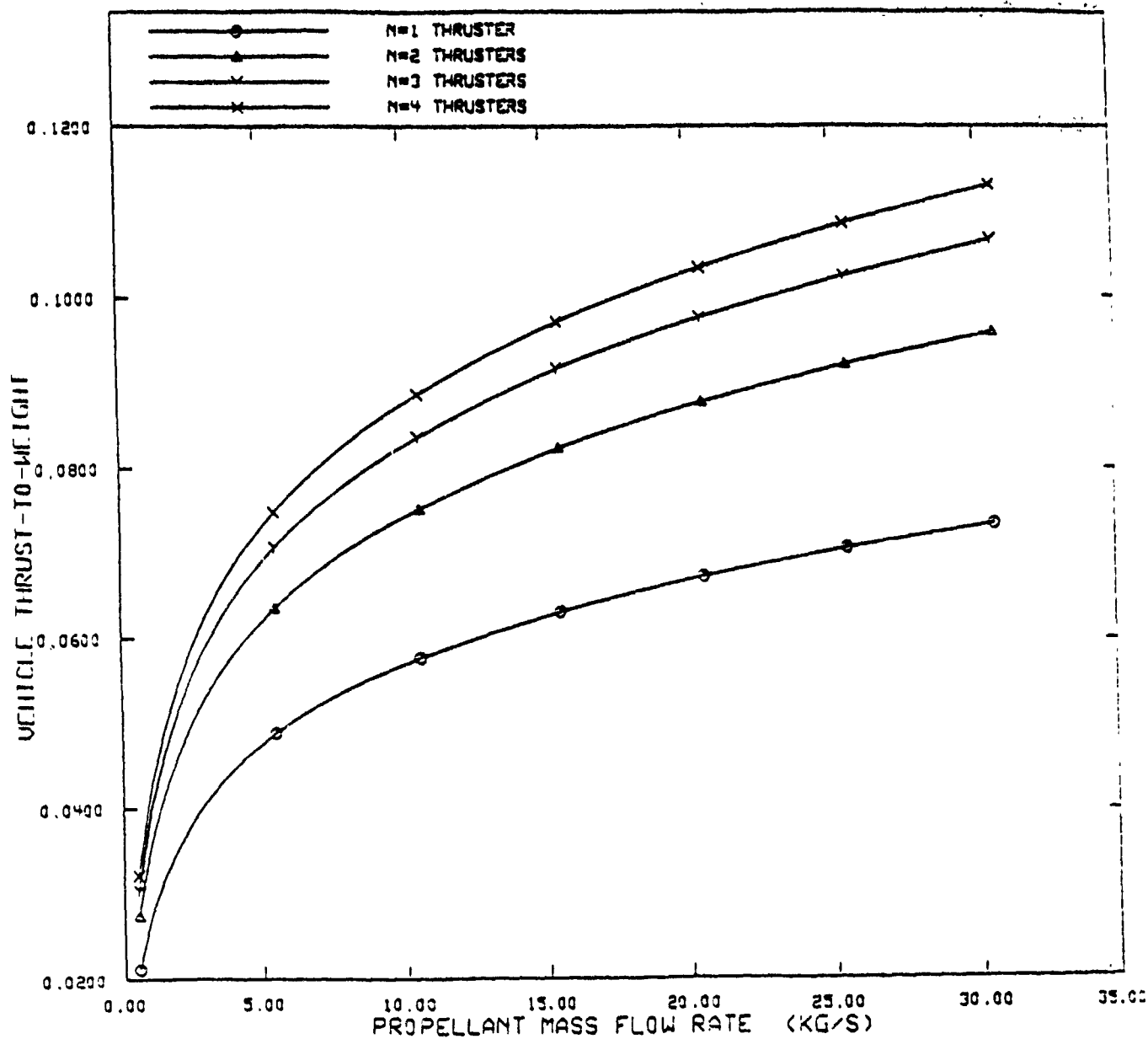


Figure 44. Vehicle F/W vs. Propellant Mass Flow Rate for $I=20$ MA and $\Delta v = 10\text{km/s}$ ($I^{8/3}$ Scaling)

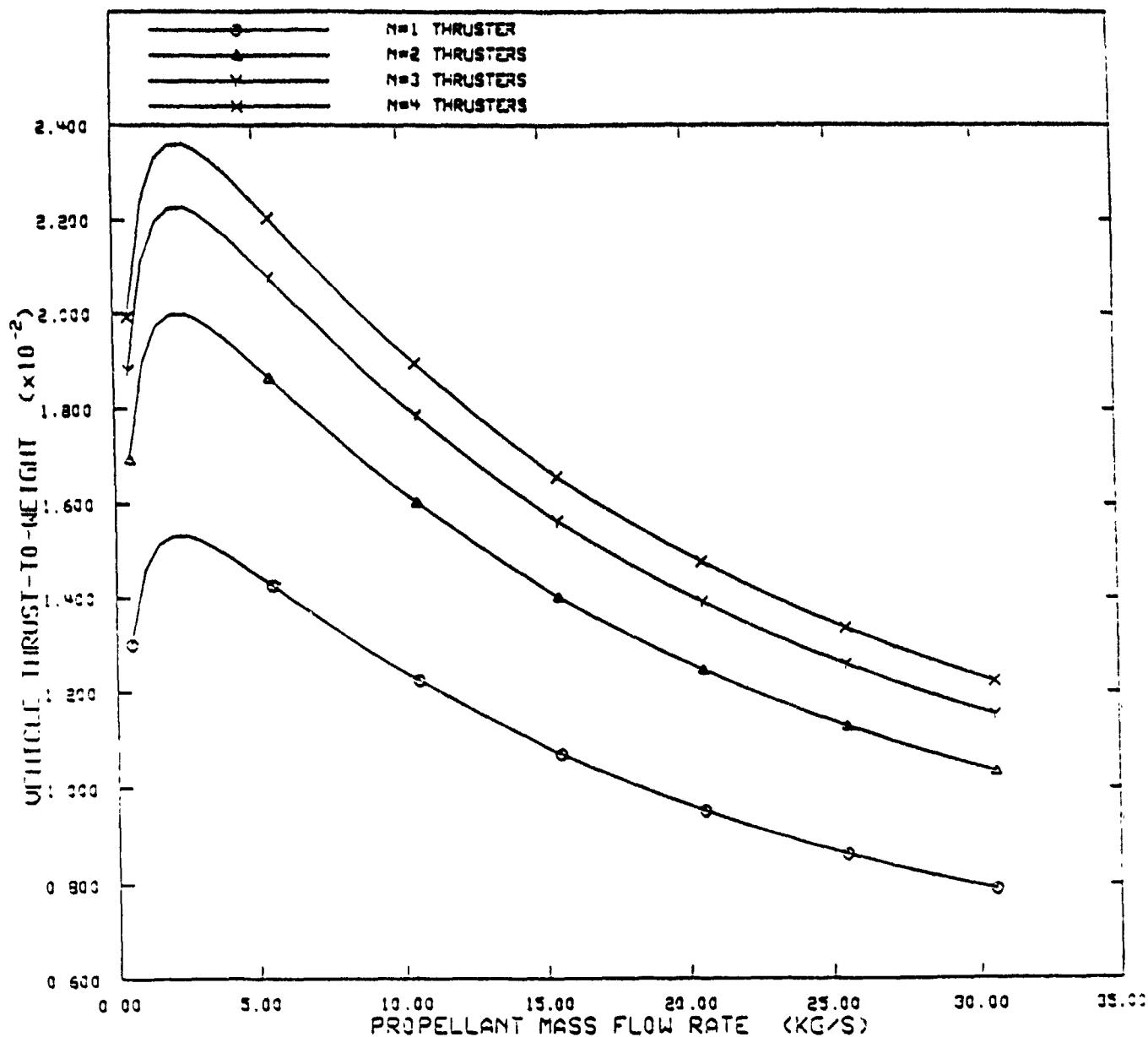


Figure 45. Vehicle F/W vs. Propellant Mass Flow Rate for I=20 MA and $\Delta v = 40\text{km/s}$ ($I^{8/3}$ Scaling)

APPENDIX B

CODE FOR EVALUATION OF DPF PROPULSION WITH NON-POLARIZED AND SPIN-POLARIZED FUELS

How to use the code:

This is a simple direction for how to use the DPF fusion propulsion code with $D-^3He$ fuel.

1. There are four major programs, all of them are for impulsive operation:
 - a) `impsq.f` : I^2 scaling, unpolarized fuel
 - b) `spimpsq.f` : I^2 scaling, spin-polarized fuel
 - c) `imp83.f` : $I^{8/3}$ scaling, unpolarized fuel
 - d) `spimp83.f` : $I^{8/3}$ scaling, spin-polarized fuel
2. Input file : `test.dat`
3. Compile the program as usual, i.e., '`f77 impsq.f`' or '`fort impsq.f`'
4. Use '`a.out`' to get the output files. Each program produces four output files:
 - a) `Test.out` : a file lists all the information you need
 - b) `tw.out` : used to plot thrust-to-weight ratio vs. propellant mass flow rate graph with `genplot`
 - c) `isp.out` : I_{sp} vs. propellant mass flow rate
 - d) `twisp.out` : thrust-to-weight ratio vs. I_{sp}
5. The program `imp3d.f` is just for reference. It can be used to create 3-D plot with `PLOT3D`. One thing should be noticed: modify it before you use to avoid any possible error.
6. Whenever you rerun the program, remember to remove all four output files first.


```

C *****
C *****
C ***** THE DENSE PLASMA FOCUS : A FUSION PROPULSION SCENARIO *****
C *****
C *****
C

```

```

C PROGRAMMER : CHRISTOPHER L. LEAKEAS
C SCHOOL OF NUCLEAR ENGINEERING
C PURDUE UNIVERSITY
C WEST LAFAYETTE, IN 47907

```

```

C WRITTEN AT : ASTRONAUTICS LABORATORY
C AL (AFSC) /LSVF
C EDWARDS AFB, CA 93523-5000

```

```

C MODIFIER : MEI-YU WANG

```

```

C THIS PROGRAM WILL CALCULATE THE PARAMETERS NECESSARY IN THE OPERATION
C OF A DENSE PLASMA FOCUS FOR USE AS A SPACE THRUSTER.
C

```

PROGRAM FOCUS

```

REAL ADMSFLW, AVMASS, BPNCH, BOLTZ, CPH2, CPELEC, CPHION, CAP
REAL CONST, CYCREFL, DFRACT, DSCHRG, DHE1, DHE2, DHE3, DHE4
REAL DDN1, DDN2, DDN3, DDN4, DDP1, DDP2, DDP3, DDP4
REAL ENERGY, ELECTHR, ELECTEN, F, FRACT, FSNPLW, FPNCH
REAL GRAV, HIONTHR, HEFRACT, IMAXSQ, IMAX, ISP, IVOL
REAL IMAGNET, IMOPT, KT, KTOPT, LANODE, LPNCH, LIMIT
REAL MCAP, MPROP, MPROSTR, MMAGNET, MPAYLD, MFUEL, MFUELSY
REAL MSHIELD, MSFLW, MTOT, MUNOT, MH2, NFTHRST, PNCHRAD, PVOL
REAL PNCHTIM, PABSW, PI2R, PIN, PI, PMAGNET, PROPTHR, QDOTREM
REAL QLEFT, RHOI, RA, RC, RHOCU, REPRATE, SIGVDHE
REAL SIGVDDN, SIGVDDP, SPECEN, TBURN, TOTHRST, TFP, TPLOSS
REAL TEMP, TDELTA, TPFDE, TPFDDN, TPFDDP, TAVG, TPBREM, TPCYC
REAL THICK, TDISTON, TSTAGH, TSTAGE, TTHRTH, TTHRE, VOLT, VRUN
REAL VHIONEX, VHIONTH, VELECTH, VELECEX, WDE, WDDN, WDDP, WASTE
REAL X, XSECTAR, VEX, MIN, VMAX, WNOT

```

```

C DECLARE ARRAYS FOR ITERATIONS

```

```

REAL DELTAP(1000), DNP(1001), HENP(1001), NPNCH(1001)
REAL PFDHE(1000), PFDON(1000), PFDDP(1000), PFTCT(1000)
REAL PBREM(1000), PCYC(1000), PLOSS(1000), RRDHE(1000)
REAL RRDDN(1000), RRDDP(1000)

```

```

INTEGER I, J, K, ITERS, NUMTHR

```

```

C CLEAR ALL ARRAYS

```

```

DO 100 I = 1, 1000

```

```

    DNP(I) = 0
    NPNCH(I) = 0
    HENP(I) = 0
    RRDHE(I) = 0
    RRDDN(I) = 0
    RRDDP(I) = 0
    PFDHE(I) = 0
    PFDON(I) = 0
    PFDDP(I) = 0
    PFTOT(I) = 0
    PBREM(I) = 0
    PCYC(I) = 0

```

PLOSS(I) = 0
 DELTAP(I) = 0

100 CONTINUE

```

C
C
C   IMAXSQ = MAXIMUM CURRENT SQUARED (AMPS)
C   IMOPT  = ASSUMED VALUE OF MAXIMUM ATTAINABLE CURRENT (AMPS)
C   KTOPT  = CORRESPONDING PLASMA TEMPERATURE ASSUMING T GOES AS I**2 (KEV)
C   CONST  = CONSTANT OF PROPORTIONALITY BETWEEN TEMP AND CURRENT (KEV/A**2)
C   BOLTZ  = BOLTZMANN'S CONSTANT (J/K)
C   RHOI   = INITIAL FILL GAS DENSITY (KG/M**3)
C   VRUN   = PLASMA SHEATH RUNDOWN VELOCITY AT THE END OF THE ANODE (M/S)
C   RA     = ANODE RADIUS (M)
C   RC     = CATHODE RADIUS (M)
C   LANODE = ANODE LENGTH (M)
C   PNCHRAD = RADIUS OF PINCH (M)
C   LPNCH  = PINCH LENGTH (M)
C   FSNPLW = SNOWFLOW EFFICIENCY FACTOR, FRACTION OF INITIAL FILL GAS
C           WHICH IS ENTRAINED IN THE RUNDOWN.
C   FPNCH  = PINCH EFFICIENCY FACTOR, FRACTION OF GAS IN RUNDOWN WHICH
C           IS TRAPPED INSIDE THE PINCH.
C   F      = TOTAL EFFICIENCY = FSNPLW*FPNCH
C   DFRACT = PERCENTAGE OF DEUTERIUM IN FILL GAS
C   HEFRAC = PERCENTAGE OF HELIUM IN FILL GAS
C   AVMASS = AVERAGE MASS OF PARTICLES TRAPPED IN PINCH (KG)
C   ITERS  = NUMBER OF ITERATIONS PERFORMED DURING EACH PINCH
C   NPINCH(I) = PINCH NUMBER DENSITY FOR Ith ITERATION (M**3)
C   REPRATE = NUMBER OF FIRINGS PER UNIT TIME (S**-1)
C   PNCHTIM = DURATION OF PINCH FORMATION (S)
C   KT     = ENERGY OF PARTICLES IN PINCH (KEV)
C   IVOL   = INITIAL VOLUME BETWEEN ANODE AND CATHODE (M**3)
C   PNCHTIM = DURATION OF STABLE PINCH PHASE (S)
C   PVOL   = FINAL VOLUME OF PINCH (M**3)
C   PFDHE(I) = FUSION POWER FROM D-HE3 REACTION FOR Ith ITERATION (W)
C   PFDDN(I) = FUSION POWER FROM DDN REACTION FOR Ith ITERATION (W)
C   PFDDP(I) = FUSION POWER FROM DDP REACTION FOR Ith ITERATION (W)
C   PFTOT(I) = TOTAL FUSION POWER FOR Ith ITERATION [PFDHE+PFDDN+PFDDP (W)]
C   TPFDEHE = TOTAL FUSION POWER FROM DHe3 REACTION (W)
C   TPFDDN  = TOTAL FUSION POWER FOR DDn REACTION (W)
C   TPFDDP  = TOTAL FUSION POWER FOR DDp REACTION (W)
C   TFP     = TOTAL FUSION POWER (W)
C   PBREM(I) = RADIATIVE LOSSES DUE TO BREMSSTRAHLUNG RADIATION (W)
C   PCYC(I)  = RADIATIVE LOSSES DUE TO CYCLOTRON RADIATION (W)
C   CYCREFL  = FRACTION OF CYCLOTRON RADIATION RETAINED BY PLASMA
C   PIN     = POWER NECESSARY FOR THE OPERATION OF THE FOCUS (W)
C   BPNCH   = MAGNETIC FIELD IN PINCH (DETERMINES PCYC) (T)
C   PLOSS(I) = TOTAL POWER LOST OR REQUIRED TO OPERATE DEVICE (W)
C   DELTAP(I) = NET POWER INCREASE OR DECEREASE (W)
C   TPBEREM = TOTAL BREMSSTRAHLUNG RADIATION (W)
C   TPCYC   = TOTAL CYCLOTRON RADIATION GENERATED (W)
C   TPLOSS  = TOTAL RADIATIVE POWER LOSSES (W)
C   TDELTAP = TOTAL NET CHANGE IN POWER (W)
C   WCAP    = INITIAL ENERGY STORED IN CAPACITOR BANKS (J)
C   VOLT    = CHARGING POTENTIAL OF CAPACITOR BANKS (V)
C   CAP     = INITIAL EXTERNAL CAPACITANCE (CAPACITOR BANK) (F)
C   LINIT   = INITIAL INDUCTANCE OF EXTERNAL CIRCUIT (H)
C   LDOT    = TIME RATE OF CHANGE OF COAXIAL INDUCTANCE (H/S)
C   IDOT    = RATE OF CHANGE OF CURRENT (A/S)
C   A1-A4   = CURVE FIT VALUES TO FIND REACTION RATE PARAMETERS
C   SIGVDHE = REACTION RATE PARAMETER FOR D-HE3 (M**3/S)
C   SIGVDDN = REACTION RATE PARAMETER FOR DDN (M**3/S)
C   SIGVDDP = REACTION RATE PARAMETER FOR DDP (M**3/S)
C   WDHE    = ENERGY RELEASED PER D-HE3 REACTION (J)
C   WDDN    = ENERGY RELEASED PER DDN REACTION (J)

```

```

C      WDDP = ENERGY RELEASED PER DDP REACTION (J)
C      DNP(I) = NUMBER DENSITY OF DEUTERIUM IN PINCH (M**-3)
C      HENP(I) = NUMBER DENSITY OF HELIUM IN PINCH (M**-3)
C      RRDHE(I) = REACTION RATE FOR D-HE3 REACTION (M**-3S**-1)
C      RRDDN(I) = REACTION RATE FOR DDN REACTION (M**-3S**-1)
C      RRDDP(I) = REACTION RATE FOR DDP REACTION (M**-3S**-1)
C      DSCHRG = TIME FOR FILL GAS TO BE DISCHARGED (S)
C      YSECTAR = CROSS SECTIONAL AREA OF FOCUS DEVICE (M**2)
C      NFTHRST = THRUST DUE TO EXPELLED (NON-PINCH) GASES (N)
C      FRACT = FRACTION OF ESCAPING CYCLOTRON RADIATION ABSORBED
C              IN THE WALLS OF THE MIXING CHAMBER AND ELECTRODES
C      PABSW = CYCLOTRON POWER ABSORBED IN THE WALLS & ELECTRODES (MW)
C      RHOCU = ELECTRICAL RESISTIVITY OF COPPER (OHM M)
C      PI2R = POWER GENERATED DUE TO OHMIC HEATING IN THE ELECTRODES (MW)
C      MH2 = MASS OF DIATOMIC HYDROGEN MOLECULE (KG)
C      WASTE = WASTE HEAT DUE TO OHMIC HEATING AND RADIATION ABSORBED (MW)
C      MSFLW = COOLANT MASS FLOW RATE REQUIRED TO COOL WASTE HEAT AND
C              KEEP TURBINE INLET TEMPERATURE LESS THAN 2000 K (KG/S)
C      ADMSFLW = ANY ADDITIONAL HYDROGEN USED FOR PROPELLANT (KG/S)
C      ENERGY = ELECTRICAL ENERGY PRODUCED BY TURBINE AT 20% EFFICIENCY (MW)
C      TAVG = MASS AVERAGED TEMPERATURE OF COOLANT FROM TURBINE AND ANY
C              ADDITIONAL PROPELLANT FLOW (K)
C
C      ISP = SPECIFIC IMPULSE (S)
C      MUNOT = PERMITTIVITY OF FREE SPACE (H/M)
C      GRAV = ACCELERATION OF GRAVITY AT EARTH'S SURFACE (M/S**2)
C      TOTRST = TOTAL OF ALL THRUSTS (N), (LBF)

```

```

C *****:*****
C *****  DEFINE VALUES OF ALL CONSTANTS *****
C *****

```

```

DATA MUNOT,PI,GRAV/1.257E-6,3.1415,9.8/

DATA CYCREFL,DSCHRG/0.6,1.0E-7/

DATA DHE1,DHE2,DHE3,DHE4/0.35715,-3.32451,10.11363,-25.66533/

DATA DDN1,DDN2,DDN3,DDN4/0.29811,-2.08296,5.70135,-22.0878/

DATA DDP1,DDP2,DDP3,DDP4/0.30795,-2.12009,5.68718,-22.03746/

DATA WDHE,WDDN,WDDP,IMAGNET/2.93E-12,5.24E-13,6.46E-13,3.18E5/

DATA MH2,BOLTZ,RHOCU,FRACT/3.34E-27,1.38E-23,1.673E-8,0.2/

DATA CPH2,CPELEC,CPHION,TDISION/4157,1.517E7,8267,5000/

```

```

C *****
C *****  OPEN INPUT AND OUTPUT FILES *****
C *****

```

```

OPEN (UNIT=1,FILE='test.dat',STATUS='OLD')
OPEN (UNIT=2,FILE='test.out',STATUS='NEW')
OPEN (UNIT=13,FILE='twisp.out',STATUS='NEW')
OPEN (UNIT=14,FILE='tw.out',STATUS='NEW')
C OPEN (UNIT=15,FILE='isp.out',STATUS='NEW')

```

```

READ(1,*)
READ(1,*) RA
READ(1,*)

```

```

READ(1,*) RC
READ(1,*)
READ(1,*) LANODE
READ(1,*)
READ(1,*) RHOI
READ(1,*)
READ(1,*) VOLT
READ(1,*)
READ(1,*) CAP
READ(1,*)
READ(1,*) LINIT
READ(1,*)
READ(1,*) SPECEN
READ(1,*)
READ(1,*) FSNPLW
READ(1,*)
READ(1,*) FPNCH
READ(1,*)
READ(1,*) LPNCH
READ(1,*)
READ(1,*) PNCHRAD
READ(1,*)
READ(1,*) DFRACT
READ(1,*)
READ(1,*) HEFRACT
READ(1,*)
READ(1,*) REPRATE
READ(1,*)
READ(1,*) PNCSTIM
READ(1,*)
READ(1,*) ITERS
READ(1,*)
READ(1,*) DELTAV
READ(1,*)
READ(1,*) NUMTHR

```

```

CLOSE (UNIT=1)

```

```

C *****
C ***** CALCULATE FOCUS PARAMETERS *****
C *****
C

```

```

MIN=1.0E7
DO 77 IMOPT=MIN,1.5E7,5.0E6
    K=0
    DO 88 ADMSFLW=0.0,30.0,0.5

```

```

XSECTAR = PI*(RC**2 - RA**2)

```

```

IVOL = XSECTAR*LANODE

```

```

PVOL = PI*PNCHRAD**2*LPNCH

```

```

F = FSNPLW * FPNCH

```

```

AVMASS = HEFRACT*5.0E-27 + DFRACT*3.34E-27

```

```

C ***** MAXIMUM CURRENT *****

```

```

C GIVEN BY DOLAN, VOL 2

```

```

IMAXSQ = 2.704*SQRT((CAP*VOLT**3)/(MUNOT*LINIT*LOG(RC/RA)))*
& ((RA**2*RHOI/MUNOT)**0.25) -

```

IMAX = SQRT(IMAXSQ)

C ***** PLASMA TEMPERATURE *****

C
: ASSUME THAT PLASMA TEMPERATURE SCALES AS I SQUARED
C ASSUME MAXIMUM ATTAINABLE CURRENT IS IMOPT

KT = MUNOT*IMAXSQ*AVMASS*LPNCH/(78.96*F*REOI*LANODE*
& (RC**2 - RA**2)*1.6E-16)

CONST = KT/IMAXSQ

KTOPT = CONST*IMOPT**2

C ***** RUNDOWN VELOCITY *****

C
C THE RUNDOWN VELOCITY IS CALCULATED USING THE MOMENTUM EQUATION
C

VRUN = SQRT(MUNOT*IMOPT**2/(78.96*RA**2*REOI))

C ***** INITIAL PINCH NUMBER DENSITIES *****

C
C NPNCH(1) = F*REOI*LANODE*(RC**2-RA**2)/(AVMASS*PNCHRAD**2
& *LPNCH)

DNP(1) = DFRACT*NPNCH(1)

HENP(1) = HEFRACT*NPNCH(1)

C *****
C ***** CALCULATE REACTION RATES *****
C *****

X = LOG10(KTOPT)

SIGVDHE = 1.0E-6*(10**((DHE1*(X**3)+DHE2*(X**2)
& +DHE3*X+DHE4))*1.5

SIGVDDN = 1.0E-6*(10**((DDN1*(X**3)+DDN2*(X**2)
& +DDN3*X+DDN4)))

SIGVDDP = 1.0E-6*(10**((DDP1*(X**3)+DDP2*(X**2)
& +DDP3*X+DDP4)))

DO 99 I=1,ITERS

RRDHE(I) = DNP(I)*(HENP(I)*SIGVDHE)
RRDDN(I) = 0.5*DNP(I)*(DNP(I)*SIGVDDN)
RRDDP(I) = 0.5*DNP(I)*(DNP(I)*SIGVDDP)

C
C ***** DETERMINE CHARGED FUSION POWER FROM PINCH *****

PFDDHE(I)=RRDHE(I)*WDHE*PVOL*REPRATE*PNCHTIM*(1.0/ITERS)*1.0E-6
PFDDN(I)=RRDDN(I)*WDDN*PVOL*REPRATE*PNCHTIM*(1.0/ITERS)*1.0E-6
PFDDP(I)=0.25*RRDDN(I)*WDDN*PVOL*REPRATE*PNCHTIM*1.0E-6
& *(1.0/ITERS)

PFTOT(I)=PFDDHE(I)+PFDDN(I)+PFDDP(I)

```

C ***** 1. DETERMINE NET POWER CHANGE *****
C
C
      VMAX=VOLT*((IMOPT+IMAGNET)/JMAX)
      PIN = VMAX * IMOPT * REPRATE * DSCHRG * 1.0E-6

C BPNCH IS THE MAGNETIC FIELD AT THE SURFACE OF THE PINCH
C WHICH IS RESPONSIBLE FOR THE CYCLOTRON RADIATION EMITTED

      BPNCH = MUNOT*F*IMOPT/(2*PI*PNCHRAD)

C POWER LOSS IS THE STEADY STATE LOSS (PER UNIT VOLUME) TIMES THE
C PLASMA VOLUME TIMES THE TIME PER PINCH TIMES THE NUMBER OF PINCHES
C PER SECOND.

      PCYC(I)=6.21E-17/(8*PI)*MUNOT**2*(F*IMOPT)**2*LPNCH*NPNCH(I)*
&      KTOPT*(1+KTOPT/146)*REPRATE*PNCHTIM*(1.0/ITERS)*1.0E-6

      PBREM(I)=5.35E-37*(F**2)*NPNCH(I)*(DNP(I)+(4*HENP(I)))
&      *(SQRT(KTOPT))*PVOL*REPRATE*PNCHTIM*(1.0/ITERS)
&      *1.0E-06

C ASSUME THAT CYCREFL % OF CYCLOTRON RADIATION IS RETAINED IN PLASMA

      PLOSS(I) = PBREM(I) + (1-CYCREFL)*PCYC(I)

      DELTAP(I) = PFTOT(I) - PLOSS(I)

C
C ***** DETERMINE THE THRUST FROM EXPELLED FILL GASES *****
C ***** ASSUMING GASES ARE EXPELLED FROM THE DEVICE IN 1E-7 S *****

      NFTHRST = RHOI*VRUN**2*XSECTAR*REPRATE*DSCHRG

      DNP(I+1)=DNP(I)-(RRDHE(I)+2*RRDDN(I)+2*RRDDP(I))*PNCHTIM
&      *(1.0/ITERS)

      HENP(I+1)=HFNP(I)-RRDHE(I)*PNCHTIM*(1.0/ITERS)

      NPNCH(I+1) = DNP(I+1) + HENP(I+1)

99  CONTINUE

      TFP = 0
      TPLOSS = 0
      TDELTAP = 0
      TFPDHE = 0
      TPFDDN = 0
      TPFDDP = 0
      TPBREM = 0
      TPCYC = 0

C
C TOTAL ELEMENTS IN ALL ARRAYS
C

      DO 200 J = 1,ITERS

      TFP = TFP + PFTOT(J)

```

```

TPLOSS = TPLOSS + PLOSS(J)
TDELTA2 = TDELTA2 + DELTA2(J)
TPFDHE = TPFDHE + PFDHE(J)
TPFDDN = TPFDDN + PFDN(J)
TPFDDP = TPFDDP + PFDN(J)
TPBREM = TPBREM + PBREM(J)
TPCYC = TPCYC + PCYC(J)

```

200 CONTINUE

C ***** CYCLOTRON RADIATION ABSORBED IN WALL AND ELECTRODES *****

PABSW = FRACT * (1-CYCREFL)*TPCYC

C ***** TOTAL POWER DISSIPATED IN ELECTRODES BY OHMIC HEATING *****

PI2R = IMOPT**2*RHOCU*LANODE*(1/(PI*RA**2)+1/(PI*(RC**2
& -RA**2)))*1.0E-6*DSCHRG*REPRATE

C ***** POWER TO BE REMOVED FROM MAGNET (MW) *****

PMAGNET = 0.01

C ***** TOTAL POWER TO BE REMOVED FROM THE WALLS AND ELECTRODES *****

C ***** AND MAGNET *****

WASTE = PI2R + PABSW + PMAGNET

C ** NEED TO KEEP INLET TEMPERATURE TO TURBINE BELOW ABOUT 2000K *****

C *****MASS FLOW REQUIRED TO DO SO IS GIVEN BY *****

MSFLW = WASTE*61.14/(2000 - 20)

C ***** ASSUME TURBINE TO BE 20% EFFICIENT *****

C ELECTRICAL POWER GENERATED IS 20% OF WASTE HEAT

ENERGY = 0.2*WASTE

C *** ASSUME TURBINE EXIT TEMPERATURE IS ABOUT 700K, WHERE IT CAN

C BE MIXED WITH ADDITIONAL MASS FLOW AT 20K *****

TAVG = (MSFLW*700 + ADMSFLW*20)/(ADMSFLW+MSFLW)

C **** ASSUME GAS ABSORBS MOST FUSION POWER PRODUCED, MIXES UNIFORMLY.

C AND EXITS AT A UNIFORM TEMPERATURE OF TOUT *****

C

C ASSUME GAS ABSORBS HEAT UP TO 5000K AS H2 WITH GAMMA=1.40

C THE HEAT REMOVED FROM THE SYSTEM IN DOING SO IS:

C *****

QDOTREM=(ADMSFLW+MSFLW)*CPH2*(TDISION-TAVG)

C *****

TEMP=TAVG+1.0E6*TDELTA2/(CPH2*(ADMSFLW+MSFLW))

IF (TEMP.LT. TDISION) THEN

GOTO 88

ENDIF

C THIS LEAVES A TOTAL OF QLEFT TO BE ABSORBED BY A COMPLETELY

C DISSOCIATED AND IONIZED COMBINATION OF AN ELECTRON GAS

C AND A GAS OF HYDROGEN IONS.

```

C *****
      QLEFT=1.0E6*TDELTA2-QDOTREM
C *****

C   NOW THE POWER IS ABSORBED BY AN ELECTRON GAS AND A HYDROGEN
C   ION GAS. THE CONSTANT VOLUME HEAT CAPACITY OF A FREE
C   MONATOMIC GAS CAN BE FOUND USING FERMI-DIRAC STATISTICS TO BE
C    $CV=(N/2)*R$ , WHERE R IS THE UNIVERSAL GAS CONSTANT AND N IS THE
C   NUMBER OF DEGREES OF FREEDOM OF EACH PARTICLE, IN OUR CASE, 3.

C   ***** R = 8.3143 J/mol K *****

C   ASSUMING AN IDEAL GAS,  $CP = CV + R$ 
C   ie.  $CP = (5/2)*R = 20.786 \text{ J/mol K}$ 
C   1 MOLE OF ELECTRONS IS  $5.48E-7 \text{ KG}$ 
C   1 MOLE OF  $H^+$  IONS IS  $1.006E-3 \text{ KG}$ 
C    $CPELEC = 1.517E7 \text{ J/KG K}$ 
C    $CPHION = 8267 \text{ J/KG K}$ 
C
C   QLEFT = MDOT*(CPELEC+CPHION)*DELTAT
C   AFTER ABSORPTION OF THIS ENERGY, THE PLASMA IS ASSUMED TO
C   COME TO THERMAL EQUILIBRIUM AT STAGNATION CONDITIONS, ie.  $V=0$ .

C *****
      TSTAGH=TDISION + QLEFT/((ADMSFLW+MSFLW)*(CPHION*0.999455))
      TSTAGE=TDISION + QLEFT/((ADMSFLW+MSFLW)*(CPELEC*0.000545))
C *****

C   ASSUME THAT THE FLOW NOW ENTERS A MERIDIONAL MAGNETIC NOZZLE
C   WITH ONE COIL AT THE THROAT OF THE NOZZLE.
C   THE SPECS FOR SUCH A NOZZLE ARE GIVEN IN THE AL REPORT
C   "CHARACTERIZATION OF PLASMA FLOW THROUGH MAGNETIC NOZZLES".

C   ACCORDING TO THE SPECS,  $TSTAG/TTHR = 1.35$ 
C   AND  $VEXIT/VTHROAT = 2.0$ 

C *****
      TTHRTH = TSTAGH/1.35
      TTHRTE = TSTAGE/1.35

C *****

C   FROM CONSERVATION OF ENERGY:  $CP*DELTAT=(1/2)*VTHROAT^2$ 
C   THERMAL ENERGY IS CONVERTED TO ENTHALPY OF THE PLASMA

C *****
      VHIONTH=SQRT(2*CPHION*(TSTAGH-TTHRTH))
      VELECTH=SQRT(2*CPELEC*(TSTAGE-TTHRTE))
C *****

C   FLOW EXITS TWICE AS FAST BECAUSE OF EXPANSION
C   THROUGH THE NOZZLE.
C
      VHIONEX = 2.0*VHIONTH
      VELECEX = 2.0*VELECTH

C   RESULTING THRUST FROM PLASMA

C *****
      ELECTER = 5.45E-4*(ADMSFLW+MSFLW)*VELECEX
      HIONTHR = 0.999455*(ADMSFLW+MSFLW)*VHIONEX

```


PROPTER = ELECTER + HICNTER

TOTERST = (NFTERST + PROPTER)

ISP=TOTERST/(GRAV*(REOI*IVOL*REPRATE*(1-F)+ADMSFLW+MSFLW))

VEX=ISP*GRAV

C *****

C

C ***** ESTIMATE MASSES FOR MARS MISSION *****

C

C ASSUME FIXED PAYLOAD MASS OF ABOUT 100 METRIC TONS

C *****

MPAYLD = 1.0E5

C *****

C DETERMINE THE NECESSARY CAPACITOR MASS USING INPUTTED
C SPECIFIC ENERGY

C

C ELECTRIC ENERGY FROM CAPACITOR BANKS

C

C *****

WNOT=0.5*CAP*VOLT**2

ELECTEN = WNOT*((IMOPT+IMAGNET)/IMAX)**2.0

C *****

C NEED ELECTEN IN kJ AND SPECEN IN kJ/kg

C *****

MCAP = NUMTER*ELECTEN/1000/SPECEN

C *****

C MASS OF MAGNET TO BE USED AT THE CENTER OF THE MAGNETIC NOZZLE
C ASSUME A FIELD OF 2 TESLA IS NEEDED AT THE TEROAT WHICH HAS
C A RADIUS OF 10 CM. THE COPPER MAGNET WILL THUS HAVE AN INNER RADIUS
C OF 10 CM AND AN OUTER RADIUS CHOSEN AS 50 CM IN ORDER TO
C MINIMIZE RESISTANCE. THE MAGNET WILL BE PULSED 100 TIMES PER
C SECOND AND EACH PULSE WILL LAST ABOUT 10**-4 SECONDS. THE LENGTH
C OF THE MAGNET WAS CHOSEN TO BE 1 CM.

C *****

MMAGNET = 67.55*NUMTER

C *****

C POWER DISSIPATED IN THE MAGNET IS I**2*R*PNCETIM*REPRATE
C OR ABOUT 10 KW. NOTE THAT THESE NUMBERS GIVE ENERGY DENSITIES
C IN THE MAGNET WHICH ARE MUCH LESS THAN THE MAXIMUM TOLERABLE
C ENERGY DENSITY AT WHICH COPPER BEGINS TO MELT.

C

C ***** CALCULATE THE AMOUNT OF PROPELLANT NEEDED FROM THE
C MISSION DELTA V AND THE EXHAUST VELOCITY USING THE
C ROCKET EQUATION.

C AS A FIRST APPROX. TO THE INITIAL MASS, CONSIDER ONLY
C PAYLOAD, CAPACITORS, AND MAGNET MASSES. THIS MAKES THE
C CALCULATION CONSIDERABLY EASIER AND INTRODUCES ONLY A

```

C      MPROP=(EXP (DELTAV/VEX) -1) * (MPAYLD+MCAP+MMAGNET)

      MPROSTR=0.15*MPROP

J      ***** TOTAL BURN TIME *****

      TBURN = MPROP/(ADMSFLW+MSFLW)

C      MASS OF DEUTERIUM AND HELIUM 3 FUEL

C      *****
      MFUEL = NUMTHR*RHOI*IVOL*REPRATE*TBURN

      MFUELSY = 0.1*MFUEL
C      *****

C
C      CALCULATE MASS OF SHIELD NECESSARY TO KEEP NEUTRON FLUENCE
C      BELOW 10**13 FOR A MISSION THAT IS DAYS LONG
C
C      LITHIUM HYDRIDE SHIELD THICKNESS IS IN METERS

C      ASSUME SHIELD IS 1 METER FROM NEUTRON SOURCE AND SUBTENDS
C      AN ANGLE SUCH THAT ABOUT 12.5% OF ALL NEUTRONS RELEASED
C      IN THE DDn REACTION HIT THE SHIELD

C      *****
      THICK = 0.1*LOG(0.125*RRDDN(ITER+1)*PNCHTIM*REPRATE*PVOL
&          *TBURN/(86400*(4*PI*1.157E12)))
C      *****

C      ASSUME SHIELD HAS A CROSS SECTIONAL AREA OF ONE METER
C      MASS = DENSITY*AREA*THICKNESS (DENSITY OF LIH IS
C      APPROXIMATELY 725 KG/M**3)

C      *****
      MSHIELD = NUMTHR*725.0*PI*THICK
C      *****

C      ***** TOTAL MASS CALCULATION (IN KG) *****
C

      MTOT = MPAYLD+MCAP+MPROP+MPROSTR+MFUEL+MFUELSY
&          +MSHIELD+MMAGNET

      WRITE(13,*) ISP,NUMTHR*TOTHRST/(GRAV*MTOT)
      WRITE(14,*) MSFLW+ADMSFLW,NUMTHR*TOTHRST/(GRAV*MTOT)
C      WRITE(15,*) MSFLW+ADMSFLW,ISP
      K=K+1
      88  CONTINUE
      PRINT*,K
      77  CONTINUE

C      ***** WRITE RESULTS TO OUTPUT FILE  IMP.OUT *****

999  WRITE(2,*) 'INITIAL FILL GAS DENSITY'
      WRITE(2,*) RHOI
      WRITE(2,*) 'MAXIMUM CURRENT IN AMPS'
      WRITE(2,*) IMAX

```

```

WRITE(2,*) 'PLASMA PINCH TEMPERATURE IN KEV'
WRITE(2,*) KT
WRITE(2,*) 'AT A CURRENT OF (MA)'
WRITE(2,*) IMOPT
WRITE(2,*) 'PLASMA PINCH TEMPERATURE IN KEV'
WRITE(2,*) KTOPT
WRITE(2,*) 'RUNDOWN VELOCITY AT THE END OF THE ANODE IN M/S'
WRITE(2,*) VRUN
WRITE(2,*)
WRITE(2,*) 'INITIAL AND FINAL D NUMBER DENSITY IN M**-3'
WRITE(2,*) DNP(1),DNP(ITER+1)
WRITE(2,*) 'INITIAL AND FINAL HE NUMBER DENSITY IN M**-3'
WRITE(2,*) HENP(1),HENP(ITER+1)
WRITE(2,*) 'FRACTION OF DEUTERIUM BURNED'
WRITE(2,*) 1-(DNP(ITER+1)/DNP(1))
WRITE(2,*) 'FRACTION OF HELIUM-3 BURNED'
WRITE(2,*) 1-(HENP(ITER+1)/HENP(1))
WRITE(2,*)
WRITE(2,*) 'REACTION RATE PARAMETERS FOR DHe3, DDn, AND DDp '
WRITE(2,*) 'IN M**3/S'
WRITE(2,*) SIGVDHE
WRITE(2,*) SIGVDDN
WRITE(2,*) SIGVDDP
WRITE(2,*)

WRITE(2,*) 'INITIAL AND FINAL REACTION RATES FOR DHe3, DDn,
& AND DDp IN M**-3S**-1'

WRITE(2,*) RRDHE(1),RRDHE(ITER)
WRITE(2,*) RRDDN(1),RRDDN(ITER)
WRITE(2,*) RRDDP(1),RRDDP(ITER)
WRITE(2,*)
WRITE(2,*) 'CHARGED PARTICLE FUSION POWER FROM DHe3, DDn, AND
&DDp IN MEGAWATTS'

WRITE(2,*) TPFDDHE,TPFDDN,TPFDDP
WRITE(2,*) 'TOTAL FUSION POWER IN MEGAWATTS'
WRITE(2,*) TFP
WRITE(2,*) 'POWER NEEDED TO OPERATE FOCUS IN MEGAWATTS'
WRITE(2,*) PIN
WRITE(2,*) 'BREMSSTRAHLUNG AND CYCLOTRON LOSSES IN MEGAWATTS'
WRITE(2,*) TPBREM,(1-CYCREFL)*TPCYC
WRITE(2,*) 'TOTAL POWER LOSSES IN MEGAWATTS'
WRITE(2,*) TPLOSS
WRITE(2,*)

IF (TDELTAP-PIN .LT. 0) THEN
  WRITE(2,*) 'NET DECREASE IN POWER IN MEGAWATTS'
  WRITE(2,*) TDELTAP-PIN
ELSEIF (TDELTAP-PIN .GT. 0) THEN
  WRITE(2,*) 'NET INCREASE IN POWER IN MEGAWATTS'
  WRITE(2,*) TDELTAP-PIN-PMAGNET
ELSE
  WRITE(2,*) 'THERE IS NO NET CHANGE IN REACTOR POWER'
ENDIF

WRITE(2,*)
WRITE(2,*) 'TOTAL ELECTRICAL POWER PRODUCED IN MEGAWATTS'
WRITE(2,*) ENERGY
WRITE(2,*) 'TOTAL MASS FLOW RATE IN KG/S'
WRITE(2,*) ADMSFLW+MSFLW
WRITE(2,*) 'ION STAGNATION TEMPERATURE IN K,eV'
WRITE(2,*) TSTAGH,TSTAGH/12000
WRITE(2,*) 'ELECTRON STAGNATION TEMPERATURE IN K,eV'
WRITE(2,*) TSTAGE,TSTAGE/12000
WRITE(2,*) 'ION AND ELECTRON EXIT VELOCITIES IN M/S'

```

```

WRITE(2,*) VHIONEX,VELECEX
WRITE(2,*) 'FINAL PROPELLANT THRUST IN N'
WRITE(2,*) PROPTHR
WRITE(2,*) 'TOTAL BURN TIME IN S,DAYS'
WRITE(2,*) TBURN,TBURN/86400

WRITE(2,*)
WRITE(2,*) '***** SYSTEM MASSES IN KG'
WRITE(2,*) 'PAYLOAD MASS:',MPAYLD
WRITE(2,*) 'PROPELLANT MASS:',MPROP
WRITE(2,*) 'PROPELLANT SYSTEM AND STRUCTURE:',MPROSTR
WRITE(2,*) 'FUEL MASS:',MFUEL
WRITE(2,*) 'FUEL SYSTEM MASS:',MFUELSY
WRITE(2,*) 'ELECTRIC ENERGY FROM CAPACITORS (J)',ELECTEN
WRITE(2,*) 'CAPACITOR MASS:',MCAPI
WRITE(2,*) 'SHIELD MASS:',MSHIELD
WRITE(2,*) 'MAGNET MASS:',MMAGNET
WRITE(2,*) '***** TOTAL MASS:',MTOT
WRITE(2,*)
WRITE(2,*) 'TOTAL THRUST IN NEWTONS,LBF'
WRITE(2,*) NUMTHR*TOTHRST,NUMTHR*TOTHRST/4.4482
WRITE(2,*)
WRITE(2,*) 'THRUST TO WEIGHT RATIO'
WRITE(2,*) NUMTHR*TOTHRST/(MTOT*GRAV)
WRITE(2,*) 'SPECIFIC IMPULSE IN SECONDS'
WRITE(2,*) ISP
WRITE(2,*) '*****'
WRITE(2,*)

CLOSE(UNIT=2)
CLOSE(UNIT=13)
CLOSE(UNIT=14)
CLOSE(UNIT=15)
CLOSE(UNIT=16)
CLOSE(UNIT=17)

```

END

